CHAPTER 5

Results

CHAPTER 5

5 Results

5.1 Extraction yield of medicinal plants

The percent yield of all medicinal plants included in this study was recorded as shown in Table 7.

Table 7 Plant name, part used and percent yield of PHE

S. No	Taxonomical name	Common name	Part used	% Yield (w/w)
1.	*Terminaliachebula* Retz. (TC)	Haritaki	Fruit	34.03±0.006
2.	*Terminaliabellerica*Roxb. (TB)	Bibhitaki	Fruit	21.35±0.006
3.	*Andrographispaniculata*Nees. (AP)	Chiretta	Whole Herb	8.73±0.012
4.	*Berberisaristata*DC. (BA)	DaruHaridra	Stem	2.48±0.012
5.	*Nyctanthesarbostratis*L. (NA)	Harsingar	leaf	7.63±0.012
6.	*Premnaintegrifolia* L. (PI)	Agnimatha	leaf	6.98±0.012
7.	*Emblica officinalis* Gaertn. (EO)	Amla	Fruit	8.21±0.015
8.	*Citrullus colocynthis* L. (CC)	Indrayan	Root	4.47±0.017
9.	*Cyperus rotundus* L. (CR)	Mustak	Root	7.97±0.013
10.	*Picrorhiza kurroa* Royle (PR)	Kutaki	Rhizome	12.94±0.023
11.	*Tinospora cordifolia*(TCg)	Giloy	Stem	1.47±0.011

Result of % Yield is represented by mean ±SE

5.2Phytochemical investigation of extracts

5.2.1Preliminary phytochemical study

The presence of various categories of phytochemicals such as carbohydrates (Molish test and Benedict test), alkaloids (Mayer test and Wagner test), glycosides (Modified Borntrager test and Legal test), flavonoids (Shinoda test and Lead acetate test), phytosterols (Salkowski test and Liebermann-Burchard test), tannins (Gelatin test and Ferric chloride test), and saponins (Foam test) was identified in the preliminary qualitative tests of all the extracts and all four PHE combinations.

5.2.2 Determination of total phenolic content

Total phenolic content (TPC) was found as GAE by referring to a standard curve with the equation y = 0.004x and an R^2 value of 0.976 (Fig. 5A). The phenolic contentand total

phenolic content of all extracts and different PHE combinations, as well as gallic acid used as a standard in the present research, were recorded. PHE2 has shown the highest phenolic content and TPC, among others, which are found to be 584.33± 0.04 mg/g and 29.22 mg/g GAE (Fig.5B and Fig. 7).

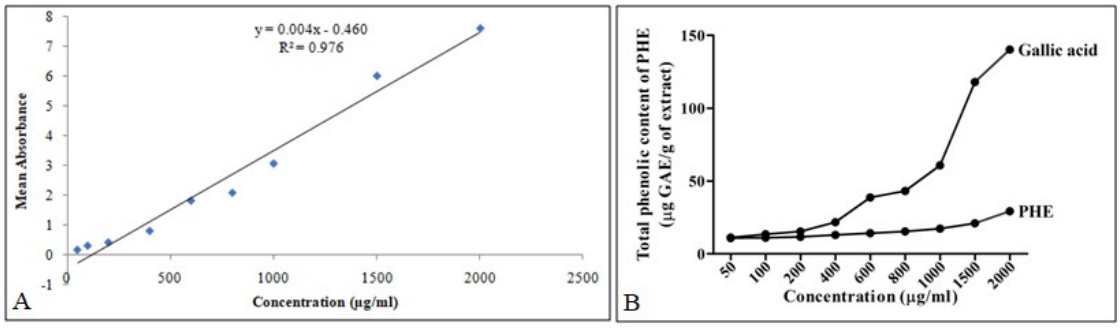

Figure 5 Total phenolic content, **A**) Standard gallic acid, R^2 values represented mean data set of n = 3 and **B**) PHE

5.2.3 Determination of total flavonoid content

The total flavonoid content (TFC) was estimated using the colorimetric method. This was written as RE by using a standard curve with the equation y = 0.004x andan R^2 = 0.975 (Fig.6A). Flavonoid and TFC of all extracts and different PHE combinations, as well as rutin used as standardsin the present research, were recorded. PHE2 has shown the highest flavonoid and TFC, among others. Thus, the results of flavonoid content and TFC are about (280.75±0.01 mg/g, 14.04 mg/g) RE in PHE2 (Fig.6B and Fig. 8).

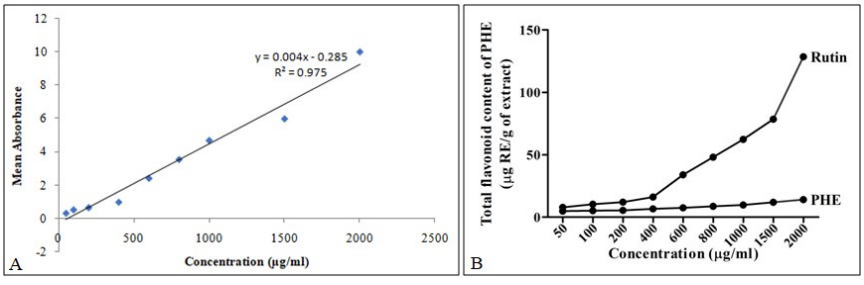

Figure 6 Total flavonoid content, **A**)Standard rutin, R^2 values represented mean data set of n = 3 and **B**) PHE

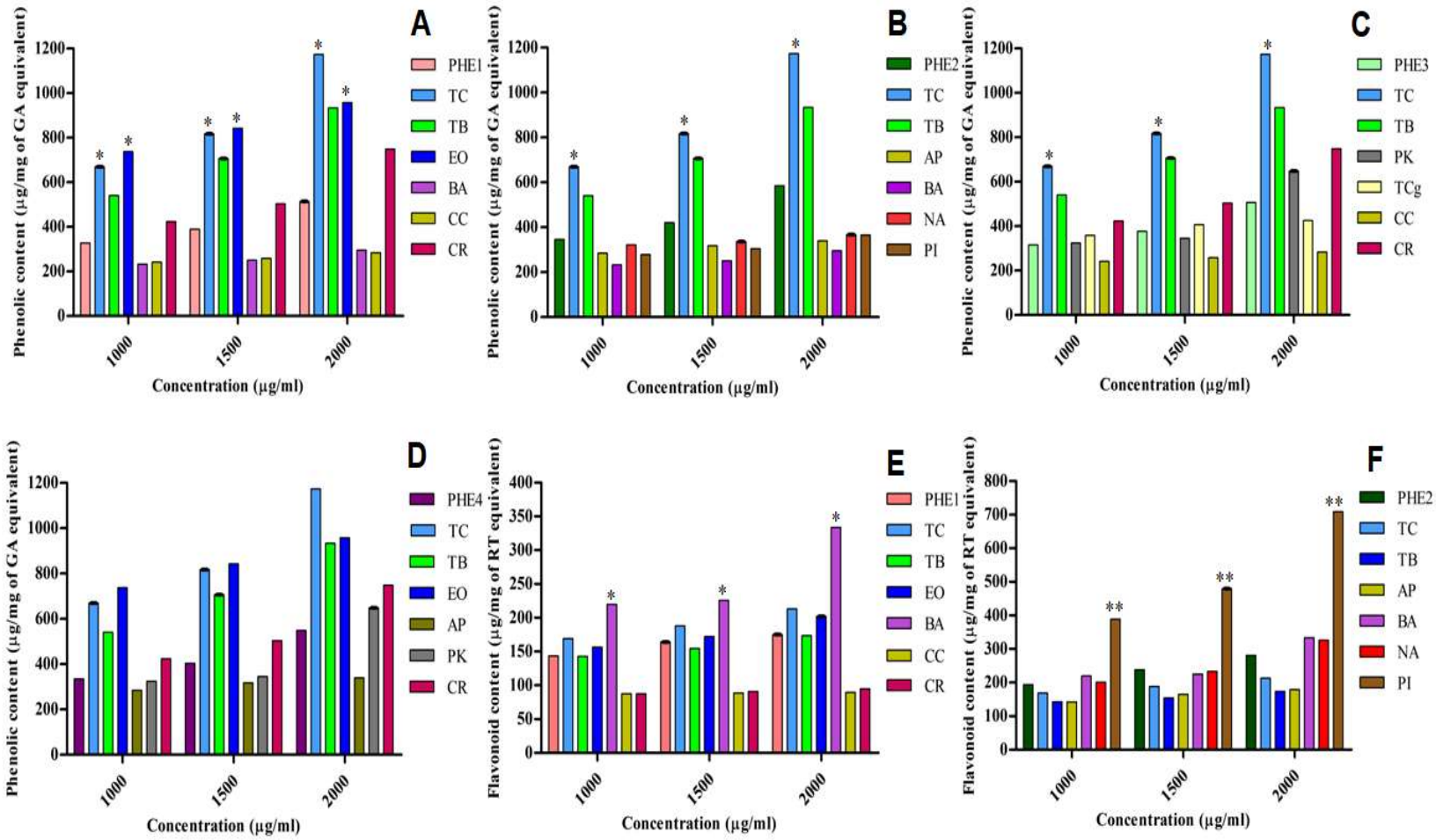

Figure 7 Determination of phytochemical present in the PHE with ingredient plant extract. **A-D)** Phenol content, **E-F)** Flavonoid content (One – way analysis of variance with Tukey Post hock test, significant * $p < 0.05$, ** $p < 0.001$)

5.2.4 Antioxidant capacity of extracts

The DPPH assay approach relies just on free radical scavenging activity by antioxidant capacity, which results in a decreasing absorbance at 517 nm as the concentration of antioxidants increases. Various concentrations of extract were taken (50, 100, 200, 400, 600, 800, 1000, 1500, and 2000 µg/ml), and demonstrated the antioxidant capacity of all the extracts and different PHE combinations, as well as the ascorbic acid used as a standard in this research. PHE2 has shown the highest antioxidant capacity among others and is comparable to that of standard ascorbic acid (Fig. 8 and Table 8).

5.2.5 Comprehensive study of phenol, flavonoid contents and Antioxidant potential of PHE

Results demonstrated that the phenolic, flavonoid, TPC, TFC, and antioxidant capacitiesof all the PHE combinations showed the highest potential of PHE2 (Fig. 9).

Table 8 Antioxidant potential of all formulation and standard in the study

Concentration(µg/ml)	DPPH radical scavenging capacity of medicinal plants and Standard				
	PHE1	**PHE2**	**PHE3**	**PHE4**	**Ascorbic acid**
50	14.51±0.089	17.31±0.082	12.27±0.011	16.01±0.011	24.35±0.008
100	24.61±0.005	27.23±0.114	23.65±0.006	26.86±0.015	32.22±0.007
200	35.59±0.003	39.53±0.098	34.96±0.005	38.65±0.021	39.66±0.005
400	47.31±0.005	53.76±0.103	45.83±0.002	49.48±0.019	50.34±0.008
600	60.87±0.038	69.71±0.050	59.06±0.001	61.97±0.006	80.23±0.015
800	73.95±0.013	83.97±0.040	71.40±0.022	75.01±0.009	88.79±0.029
1000	86.36±0.016	97.01±0.017	84.63±0.004	94.17±0.008	93.41±0.003
1500	92.52±0.008	98.45±0.006	90.53±0.004	97.71±0.002	95.44±0.003
2000	96.86±0.014	98.89±0.010	96.27±0.007	98.04±0.002	98.52±0.002
EC_{50}(µg/ml)	426.43	392.14	565.24	461.16	310.51

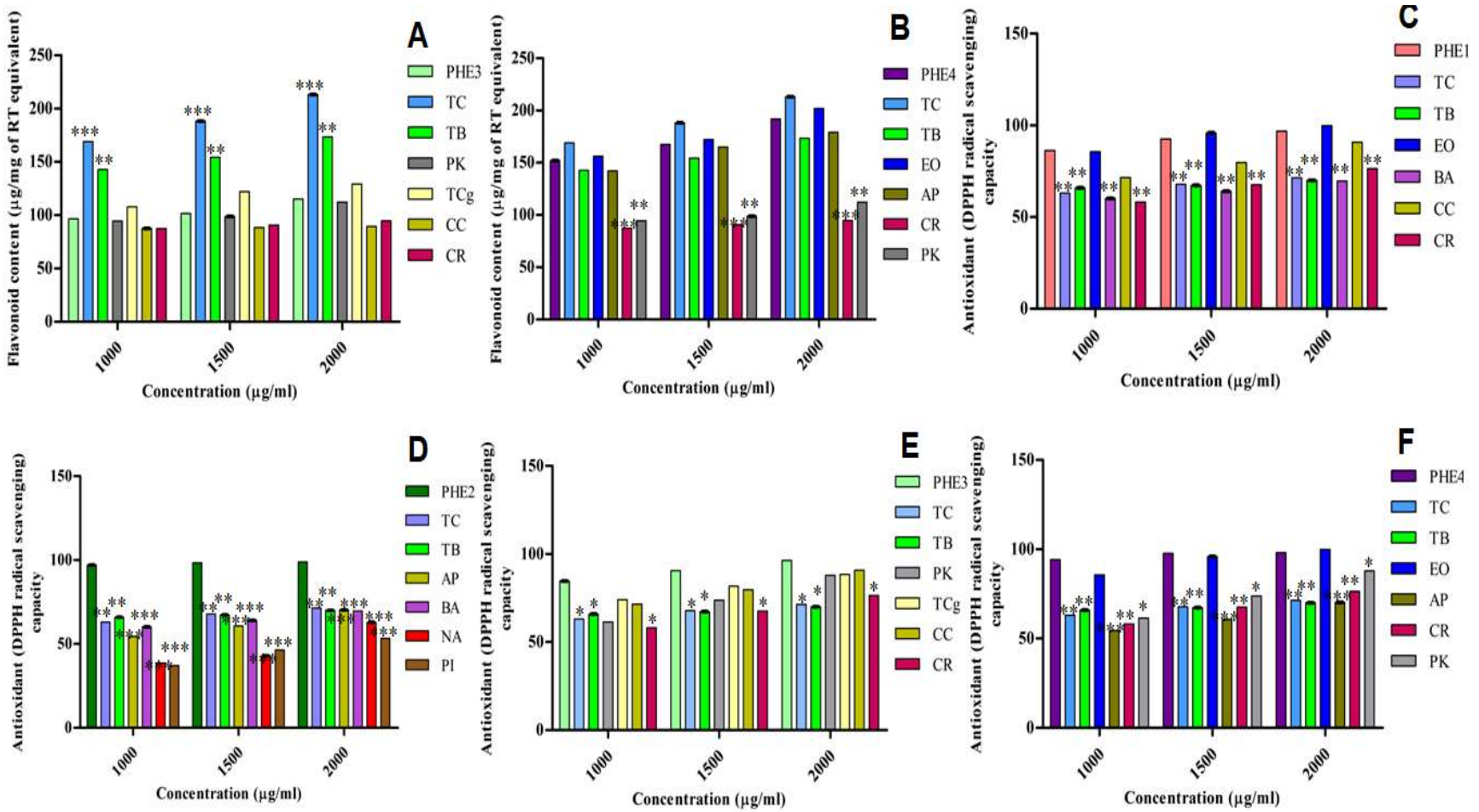

Figure 8 Determination of phytochemical present in the PHE with ingredient plant extract along with antioxidant potential. **A-B**) Flavonoid content, **C-F**) Antioxidant potential. (One – way analysis of variance with Tukey Post hock test, significant * $p < 0.05$, ** $p < 0.001$, *** $p < 0.0001$)

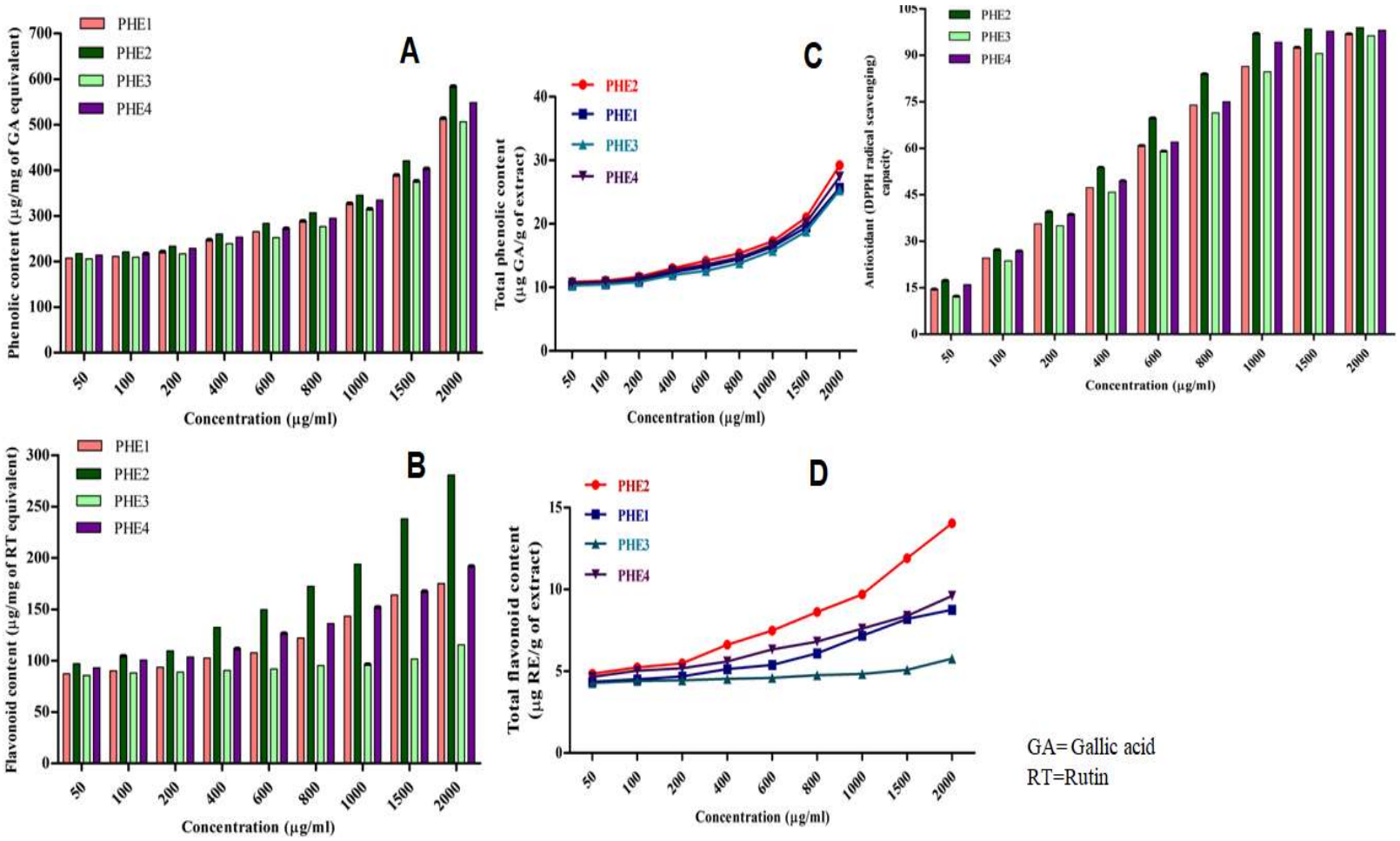

Figure 9 Determination of phytochemical present in the PHE. **A**) Phenol content, **B**) Flavonoid content, **C**) Total phenolic content, **D**) Total flavonoid content, and **E**) Antioxidant potential. (One – way analysis of variance with Tukey Post hock test)

5.3Heavy metals determination of PHE through ICP-MS

The detected levels of Pb, Ni, Hg, Cd, and As (mg/kg) in the PHE sample are found below the reference limit in the sample; meanwhile, As and Cd were found below the quantification limit (BQL), i.e., less than the LOQ/LOD limit (0.2mg/kg) in the sample (Table 9). With the help of an established calibration curve, the total mean concentrations found are displayed in Table 10.The following is a list of the decreasing order of the mean heavy metal levels found in the PHE sample: Pb > Ni > Hg > As > Cd.

Table 9 Concentration of heavy metals (Pb, Cd, As, Hg and Ni by ICP-MS) determination of PHE

Description	Analyte	Wt. of sample (gm)	Volume make up (ml)	Concentration from calibration curve (ppb)	Concentration of analyte (mg/kg)	Mean±SD	Reference
Dark green-thick paste	Arsenic (**As**)	0.4980	50	0.738	0.074*	0.074±0.055	<5.0
	Cadmium (**Cd**)	0.4980	50	0.443	0.044*	0.044±0.039	<0.30
	Mercury (**Hg**)	0.4980	50	2.271	0.228	0.228±0.021	<0.50
	Nickel (**Ni**)	0.4980	50	10.141	1.018	1.018±0.220	<1.683
	Lead (**Pb**)	0.4980	50	18.355	1.843	1.843±0.535	<10.0

* = BQL means Below Quantification Limit (which is 0.2 mg/kg)

Table 10 Mean data of heavy metals Pb, Cd, As, Hg and Ni in ICP-MS determination of PHE

Analyte	Mass	Intensity	RSD	Conc. from calibration curve (ppb)	SD	RSD	Blank intensity
Arsenic (**As**)	75	208.3	7.1	0.738	0.055	7.4	8
Cadmium (**Cd**)	111	428.3	8.6	0.443	0.039	8.8	7
Mercury (**Hg**)	202	4457.4	0.8	2.271	0.021	0.9	469
Nickel (**Ni**)	60	12682.0	2.0	10.141	0.220	2.2	1189
Lead (**Pb**)	208	165536.1	2.9	18.355	0.535	2.9	288

5.4*In vitro* anti-inflammatory activity of PHE

5.4.1Membrane stabilization assay

There are a variety of external pressures that might disrupt the stability of the membrane, resulting in its destabilization. The hemolysis procedure will ensure this instability, which can be avoided by the anti-inflammatory ingredients in the PHE. The change in absorbance of the hemoglobin content present in the resulting supernatant can be used to determine whether the

hemolytic activity is having an inhibitory action, as shown in Table 11. The entrapment efficiency of hemolysis induced by various quantities of PHE was calculated. A concentration of 91.449 µg/ml was determined to be the IC_{50}, where 100 µg/ml exhibited the highest amount of inhibition (54.911±0.017 percent). The hemolysis of the membrane is reduced as the quantity of the drug increases, but the stabilization or preservation of the membrane is increased. As a result, the anti-inflammatory action of the extracts proved concentration-dependent. The IC_{50} of aspirin (standard) is 89.451µg/ml.

Table 11*In vitro* anti-inflammatory study of PHE

Concentration(µg/ml)	Membrane stabilization		Protein denaturation	
	% inhibition PHE	% inhibition Aspirin	% inhibition PHE	% inhibition Aspirin
20	16.071±0.080	17.015±0.039	40.990±0.032	41.395±0.017
40	22.061±0.024	22.521±0.056	51.784±0.027	53.227±0.017
60	32.885±0.015	33.168±0.036	60.516±0.031	61.427±0.046
80	44.983±0.023	45.101±0.030	80.777±0.060	81.106±0.066
100	54.911±0.017	56.986±0.032	94.849±0.038	95.305±0.020
IC_{50} (µg/ml)	91.449	89.451	36.940	35.723

5.4.2. Inhibition of albumin denaturation

This is dependent on the extract's means to protect the protein from denaturation as a result of intrinsic and extrinsic factors. The amount of protein degradation decreases as the proportion of the extract is increased, demonstrating that the extract has the capacity to safeguard the protein from the conformational change during the experiment.The change in absorbance observed in Table 11 in the finished supernatant can be interpreted as evidence of protein denaturation inhibition activity on the enzyme.The percentage inhibition of protein denaturation induced by different concentration ranges of PHE was calculated. The concentration at which the IC_{50} was observed to be 36.940µg/ml was determined. When it came to inhibiting heat-induced albumin denaturation, the PHE proved to be effective. At 100

µg/ml, the highest level of inhibition (94.849±0.038 percent) was observed. The IC_{50} of aspirin (standard) is 35.723µg/ml.

5.5. *In vitro* anti-diabetic activity of PHE

5.5.1. α- Amylase inhibition assay

The IC_{50} values were determined by evaluating the plot of % α-amylase inhibition as a result of the concentration of extract (Fig.10). PHE inhibited α-amylase with a maximum of 78.56 ±0.10 at 140 µg/ml and an IC_{50} of 93.27 µg/ml. Acarbose, the conventional positive control, inhibited α-amylase the most (98.03±0.01) at 140 µg/ml, resulting in an IC_{50} of 67.24 µg/ml (Table 12).

Table 12α-Amylase inhibitory activities of PHE

Conc. (µg/ml)	α-Amylase inhibition activity (%)	
	PHE	**Acarbose**
20	11.28±0.10	15.07±0.03
40	21.41±0.14	31.64±0.14
60	30.39±0.17	43.00±0.01
80	40.55±0.25	62.02±0.07
100	52.76±0.19	75.76±0.14
120	63.95±0.15	87.13±0.01
140	78.56±0.10	98.03±0.01
IC50	93.27	67.24

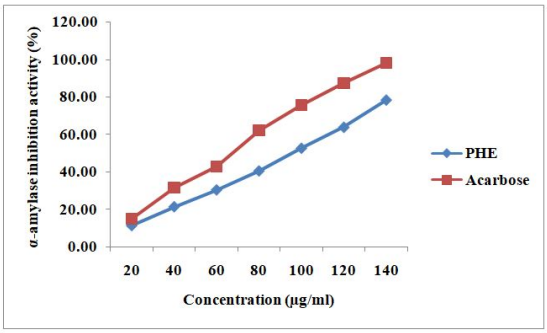

Figure10α-Amylase inhibitory activities of PHE

5.5.2. α- Glucosidase inhibition assay

As shown in Figure11, acarbose, as a reference drug, had a higher inhibitory activity for α-glucosidase compared to PHE. In the present study, PHE showed its maximal α-glucosidase inhibitory activity at 74.84±0.01% at 140µg/ml with an IC_{50} of 85.09µg/ml and acarbose at 93.94% at 140µg/ml with an IC_{50} of 69.13µg/ml, as shown in Table 13.

Table 13α-Glucosidase inhibitory activities of PHE

Concentration (µg/ml)	α-Glucosidase inhibition activity (%)	
	PHE	**Acarbose**
20	22.80±0.01	14.37±0.13
40	28.82±0.04	30.36±0.25
60	35.04±0.03	44.17±0.14
80	46.87±0.04	60.62±0.11
100	57.81±0.03	73.43±0.08
120	67.69±0.01	84.80±0.07
140	74.84±0.01	93.94±0.06
IC_{50}	85.09	69.13

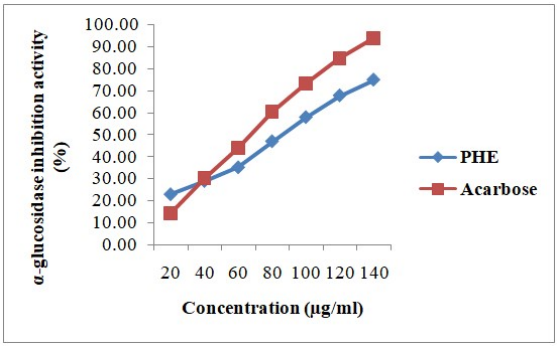

Figure11α-Glucosidase inhibitory activities of PHE

Moreover, the IC_{50} of *in vitro* studies (anti-inflammatory and anti-diabetic) of PHE was calculated comprehensively, as tabulated in Table 14 and Fig.12.

Table 14 Determination of IC_{50} for the PHE

			Determination of IC_{50}				
S.No.	Activity	*In Vitro* Assay	PHE1	PHE2	PHE3	PHE4	Aspirin
1.	Anti-inflammatory	Membrane Stabilization	111.27±0.05	91.45±0.01	115.77±0.06	106.65±0.04	89.45±0.01
		Albumin Denaturation	52.65±0.06	36.94±0.05	55.73±0.04	49.76±0.05	35.72±0.03
	Activity	*In Vitro* Assay	PHE1	PHE2	PHE3	PHE4	Acarbose
2.	Anti-diabetic	α-Glucosidase Inhibition	100.96±0.11	85.09±0.03	111.31±0.06	100.05±0.06	69.13±0.14
		α-Amylase Inhibition	107.88±0.07	93.27±0.19	131.41±0.12	97.04±0.08	67.24±0.07

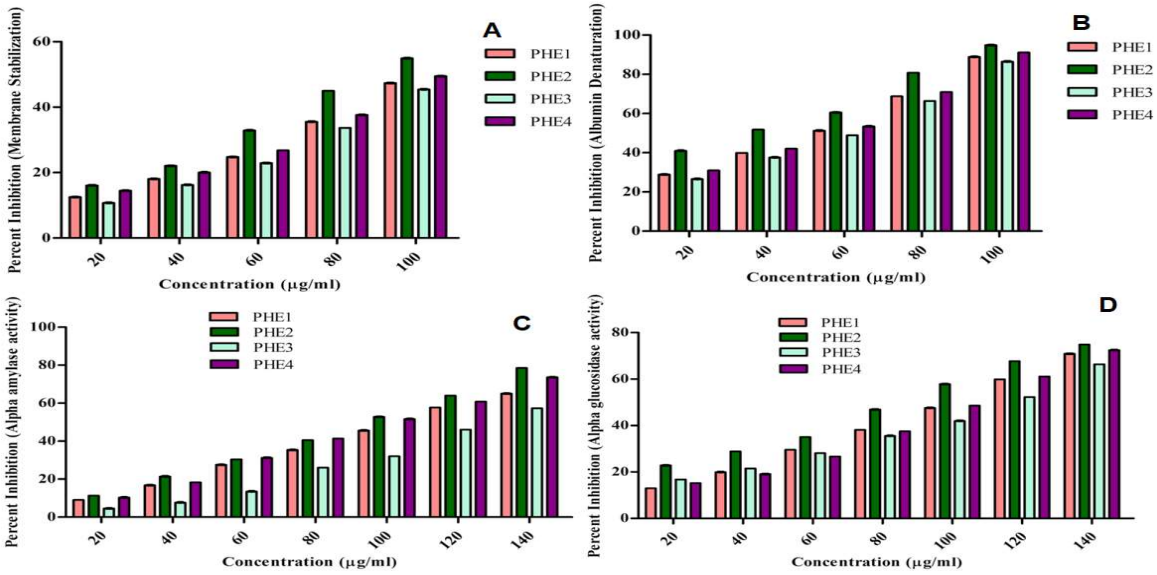

Figure 12 Comprehensive study of anti-inflammatory and anti-diabetic activity in the PHE. **A**) Membrane stabilization, **B**) Albumin denaturation, **C**) Alpha amylase inhibition activity, **D**) Alpha glucosidase inhibition activity. (One – way analysis of variance with Tukey Post hock test)

5.6Anti-hyperglycemic activity through oral glucose tolerance test (OGTT)

Glucose loading produced hyperglycemia after 30 min of administration in all groups, with a maximum increase achieved with the control (Fig. 13). Unlike the standard and PHE, which significantly reduced FBG ($p < 0.05$), no appreciable effect was observed with the DMR after 30 min of glucose loading. The effect of all treatment doses started to become apparent as time went by, and a significant decline was noted at 60, 90, and 120 minutes by all, which was maintained by alltreatment doses until the end of the experiment (Fig. 13).

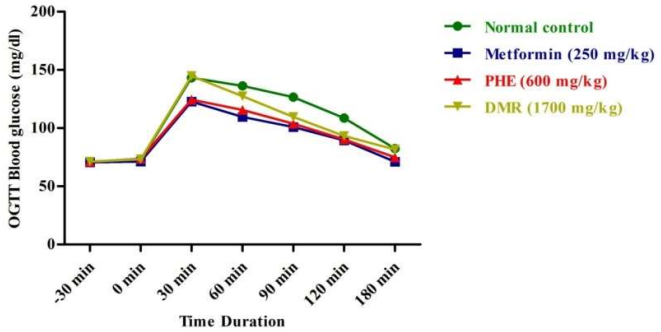

Figure13 Antihyperglycemic activity (OGTT) of PHE. (One – way analysis of variance with Tukey Post hock test), Dabur Madhu Rakshak (DMR)

5.7Phytochemical investigation of PHE

5.7.1Bioactive contents from GC-MS

The metabolites were detected after correlating the spectrum configurations acquired with those of a mass spectral registry that was commonly accessible (NIST and Wiley libraries). The combined results of GC-MS fingerprinting of the PHE showed the presence of 35 peaks, and out of those, 22 phytoconstituents were classified (Fig.14). These are assigned to a variety of chemical classifications, and it has been claimed that the majority of them have significant bioactivity (antioxidant, anti-inflammatory, etc.). Table 15 lists the phytoconstituents that were detected with their respective peak numbers, retention times (RT), peak areas (percentage of total peak area), etc. The major phytoconstituents detected include isopropyl linoleate (20.55%), 9-Octadecenoic acid, 12-hydroxy-, methyl ester, [R-(Z)]-(17.21%), 2-Buten-1-ol, 2-ethyl-4-(2,2,3-trimethyl-3-cyclopenten-1-yl (17.22%), 13-Hexyloxacyclotridec-10-en-2-one (14.13%), Phytol (5.72%), 6-Octadecenoic acid, methyl ester, (Z)- (5.23%), 1,2,5,6-Tetrahydrobenzonitrile (4.26%), Hexadecanoic acid, methyl ester (1.87%), cis-9-Hexadecenal (1.86%), 9,12-Octadecadienoic acid, methyl ester (1.69%), Neophytadiene (1.47%), Methyl stearate (1.21%), 1,2-Benzenedicarboxylic acid, dibutyl ester (1.36%), 1-Glyceryl ricinoleate (1.08%), and the bioactivity reported is depicted in Table 15. 2-Buten-1-ol, 2-ethyl-4-(2,2,3-trimethyl-3-cyclopenten-1-yl) (17.22%), 1,2,5,6-Tetrahydrobenzonitrile (4.26%), 4-Piperidinamine, 2,2,6,6-tetramethyl-(0.07%), and Undecanoic acid, 5-chloro-, chloromethyl ester (0.41%) arethe first time reported in the ingredient plants used for PHE. Alpha Aocospiro A (ATA), the bioactive compound of PHE was a novel compound in the PHE (Fig. 15), which contains numerous biological activities in literature and was predicted for antidiabetic activity in bioinformatic study in futher research.

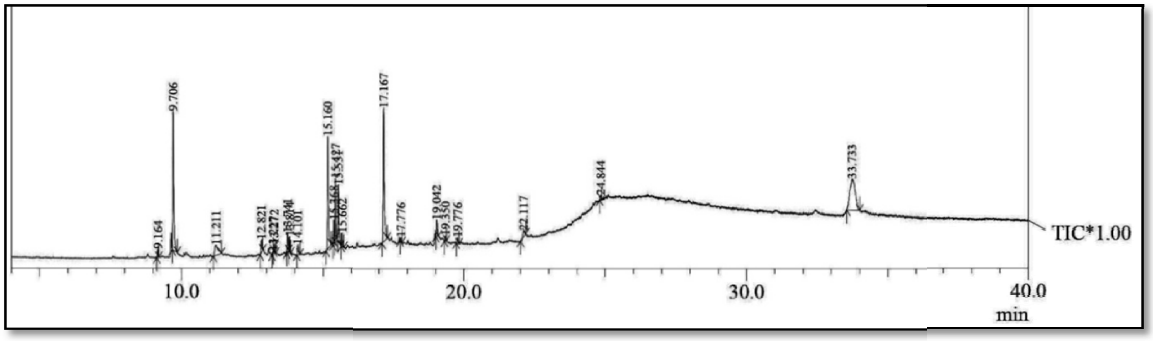

Figure14GC-MS chromatogram of PHE

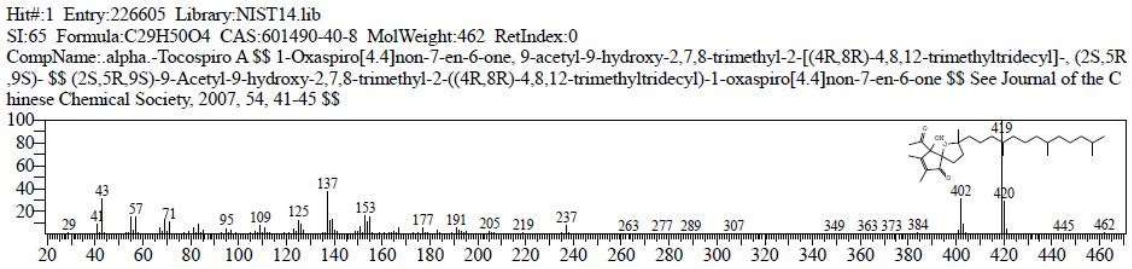

Figure15 GC-MS mass peak chromatogram of Alpha-Tocospiro A

5.7.2Bioactive contents fromUPLC-Q-TOF-MS/MS

Thephytochemical fingerprint by UPLC-Q-TOF-MS/MS study of PHE confirms the presence of 22 flavonoids (Table 16) from positive and negative modes of total ion chromatograms (Fig. 16) and also 22 flavonoids from mass peak chromatograms in good proportion on the basis of peak percentage area (Table 17).Different types of phytocomponents, including terpenoids, phenyl propanoids, alkaloids, amino acids, tannin and others, were identified in PHE. The mass data chromatogram with the structure of compounds of the identified flavonoids on the basis of prominent peaks at different retention times and m/z ratios was considered for the identification of flavonoids in the PHE in both positive (Fig. 17) and negative (Fig. 18) modes. The result revealed that 22 prominent flavonoids like quercetin-3-glucuronide (476.1272), saponarin (327.0284), kaempferide (301.0164), acacetin (284.2160), puerarin (297.0563), homoorientin (352.9668), isorhamnetin derivatives (476.0864),

neodiosmin (609.0165), vitexin (429.9127), luteolin (284.7090), and others were identified in good proportion as well as listed with their name, exact mass, formula, class, and sub-class at different RT in Table 17. The therapeutic values of the 3 common identified flavonoids in [M+H]+ and [M-H]- modes of the UPLC-Q-TOF-MS/MS study areshown in Fig. 19.

Table 15GC-MS fingerprint of PHE

Peak	RT	Area	Area%	Peak name	MF	Chemical structures	Bioactivity
1	9.164	104084	0.77	Phenol, 2,4-bis(1,1-dimethylethyl)-	$C_{14}H_{22}O$	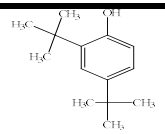	Antibacterial, antimicrobial, anti-inflammatory, antioxidant, antifungal, anticancer
2	9.706	2330268	17.22	2-Buten-1-ol, 2-ethyl-4-(2,2,3-trimethyl-3-cyclopenten-1-yl	$C_{14}H_{24}O$	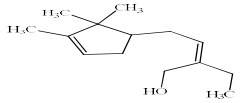	NR
3	11.211	575885	4.26	1,2,5,6-Tetrahydrobenzonitrile	C_7H_9N		NR
4	12.821	199217	1.47	Neophytadiene	$C_{20}H_{38}$	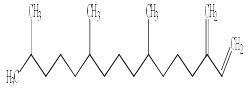	Anti bacterial, anti-inflammatory, antimicrobial, analgesic, anti-oxidant spectrum and antipyretic activities
5	13.227	9887	0.07	4-Piperidinamine, 2,2,6,6-tetramethyl-	$C_9H_{20}N_2$	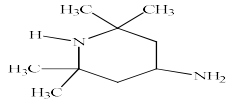	NR
6	13.272	90901	0.67	3,7,11,15-Tetramethyl-2-hexadecen-1-ol	$C_{20}H_{40}O$	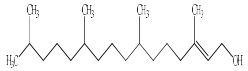	Antimicrobial, Anti-inflammatory, anticancer, anti-arthritic, diuretic, flavouring and cytotoxic
7	13.741	253696	1.87	Hexadecanoic acid, methyl ester	$C_{17}H_{34}O_2$		potent antimicrobial activity, antibacterial, antioxidant, antitumor,immunostimulant
8	13.814	156337	1.16	Benzenepropanoic acid, 3,5-bis(1,1-dimethylethyl)-4-hydroxy-, methyl ester	$C_{18}H_{28}O_3$	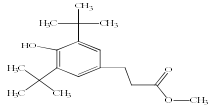	Antifungal, Antioxidant activities
9	14.101	184106	1.36	1,2-Benzenedicarboxylic acid, dibutyl ester	$C_{16}H_{22}O_4$ or $C_6H_4(COOC_4H_9)_2$	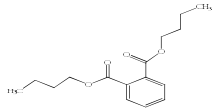	Indirect Additives
10	15.160	1912528	14.13	13-Hexyloxacyclotridec-10-en-2-one	$C_{18}H_{32}O_2$	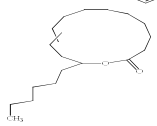	Anti-acne; antibacterial; antimalarials, antiparasitic agents, Antitumor and antimicrobial

Table 15 Conti.....

11	15.368	228733	1.69	9,12-Octadecadienoic acid, methyl ester	$C_{19}H_{34}O_2$	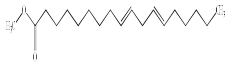	Anti inflammatory, nematicide, insectifuge, hypocholesterolemic, cancer preventive, hepatoprotective, antihistaminic, antiacne, antiarthritic, Antioxidant
12	15.427	708011	5.23	6-Octadecenoic acid, methyl ester, (Z)-	$C_{19}H_{36}O_2$		Inhibit production of uric acid, increase aromatic amino acid decarboxylase activity
13	15.531	773778	5.72	Phytol	$C_{20}H_{40}O$	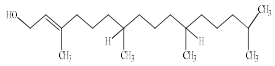	Anti microbial, anti-inflammatory, anticancer, diuretic, anti-inflammatory, antioxidant
14	15.662	163471	1.21	Methyl stearate	$C_{19}H_{38}O_2$	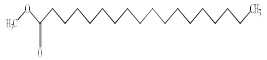	Antidiarrheal, cytotoxic, antiproliferative Activities, Antioxidant, antifungal
15	17.167	2328586	17.21	9-Octadecenoic acid, 12-hydroxy-, methyl ester, [R-(Z)]-	$C_{19}H_{36}O_3$	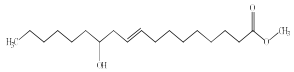	Antiparasitic; antineoplastic & antiallergic agents; containing insect repellants
16	17.776	56021	0.41	Undecanoic acid, 5-chloro-, chloromethyl ester	$C_{12}H_{22}Cl_2O_2$	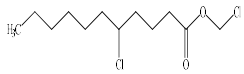	NR
17	19.042	251062	1.86	cis-9-Hexadecenal	$C_{16}H_{30}O$	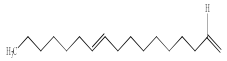	Antimicrobial
18	19.350	77873	0.58	15-Hydroxypentadecanoic acid	$C_{15}H_{30}O_3$	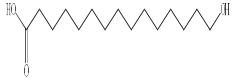	Inhibit production of uric acid, increase aromatic amino acid decarboxylase activity, also helpful in Parkinson's disease treatment
19	19.776	112625	0.83	Dioctyl phthalate	$C_{24}H_{38}O_4$	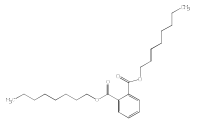	Antiabortive; anti-acne; antibacterial & antiparasitic agents
20	22.117	146462	1.08	1-Glyceryl ricinoleate	$C_{21}H_{40}O_5$	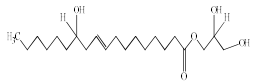	NR
21	24.844	87144	0.64	Alpha-Tocospiro A	$C_{29}H_{50}O_4$	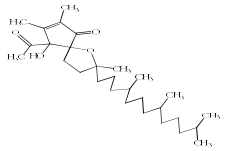	Antioxidant
22	33.733	2781198	20.55	Isopropyl linoleate	$C_{21}H_{38}O_2$		Antioxidant

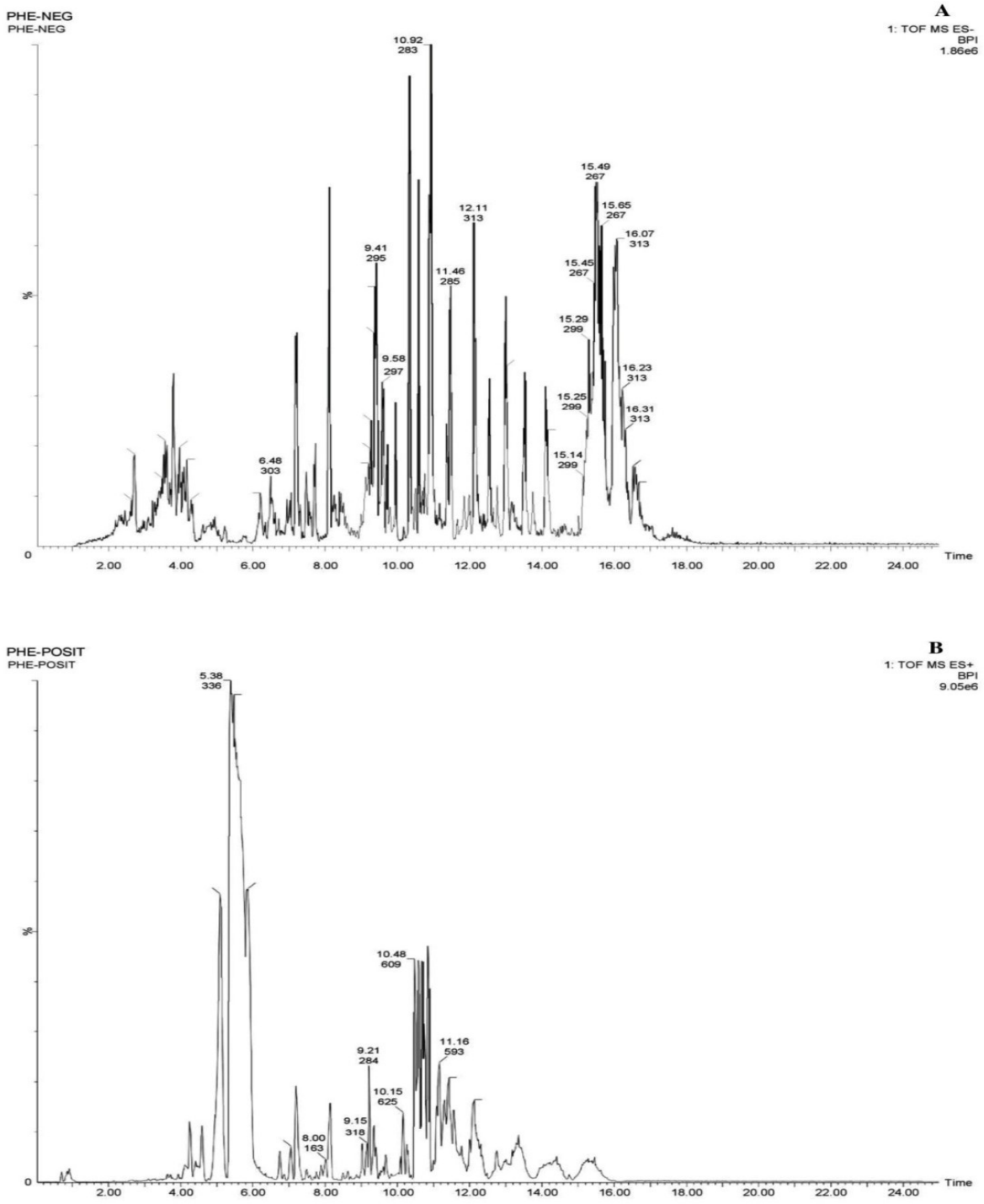

Figure 16 Total ion chromatogram of PHE byUPLC-Q-TOF-MS/MS

Table 16 Phytochemical analysis of PHE byUPLC-Q-TOF-MS/MS

Name	Peak	Rt	Peak %	Exact mass	Formula	Class	Subclass	M/Z	Mode
(+-)-Taxifolin	303	6.48	6.033	304.058	C15H12O7	Flavonoid	Dihydroflavonol	303.25	$[M-H]^-$
Puerarin	295	9.41	2.593	416.38	C21H20O9	Flavonoid	Isoflavone	415.10293	$[M-H]^-$
Homoorientin	297	9.58	0.016	448.38	C21H20O11	Flavonoid	Flavone	447.09276	$[M-H]^-$
Kaempferide	299	15.14	15.782	300.28	C16H12O6	Flavonoid	Flavonol	299.05559	$[M-H]^-$
Neodiosmin	299	15.25	7.322	608.56	C28H32O15	Flavonoid	Flavone	607.16631	$[M-H]^-$
Rutin	299	15.29	1.972	610.153	C27H30O16	Flavonoid	Flavonol	609.57	$[M-H]^-$
Apigenin-7-O-glucoside	267	15.45	1.270	432.105	C21H20O10	Flavonoid	Flavone	431.4	$[M-H]^-$
Formononetin	267	15.49	6.545	268.28	C16H12O4	Flavonoid	Isoflavone	267.06576	$[M-H]^-$
Ononin	267	15.65	0.001	430.4	C22H22O9	Flavonoid	Isoflavone	429.11858	$[M-H]^-$
Isorhamnetin-3-Galactoside-6"-Rhamnoside	313	16.07	0.498	624.169	C28H32O16	Flavonoid	Flavonol	623.6	$[M-H]^-$
Isorhamnetin-3-O-glucoside	313	16.23	0.910	478.111	C22H22O12	Flavonoid	Flavonol	477.43	$[M-H]^-$
Isorhamnetin-3-O-rutinoside	313	16.31	0.876	624.169	C28H32O16	Flavonoid	Flavonol	623.59	$[M-H]^-$
Quercetin-3-Galactoside-6"-Rhamnoside-3"'-Rhamnoside	313	12.11	0.429	770.226	C34H42O20	Flavonoid	Flavonol	769.77	$[M-H]^-$
Hesperetin	283	10.92	3.288	302.28	C16H14O6	Flavonoid	Flavonone	301.07123	$[M-H]^-$
Kaempferol	285	11.46	0.001	286.24	C15H10O6	Flavonoid	Flavonol	285.03994	$[M-H]^-$
Saponarin	336	5.38	0.236	594.158	C27H30O15	Flavonoid	Flavone	595.47	$[M+H]^+$
Eriodictyol	163	8.00	1.748	288.27	C15H12O6	Flavonoid	Flavanone	289.07119	$[M+H]^+$
Gossypin	318	9.15	0.802	480.09	C21H20O13	Flavonoid	Flavonol	481.39	$[M+H]^+$
Vitexin	284	9.21	0.246	432.38	C21H20O10	Flavonoid	Flavone	433.11344	$[M+H]^+$
Peonidin-3,5-O-di-beta-glucopyranoside	625	10.15	23.342	625.176	C28H33O16	Flavonoid	Anthocyanin	625.56	$[M+H]^+$
Diosmin	609	10.48	3.033	608.174	C28H32O15	Flavonoid	Flavone	609.53	$[M+H]^+$
Fortunellin	593	11.16	23.059	592.179	C28H32O14	Flavonoid	Flavone	593.5	$[M+H]^+$

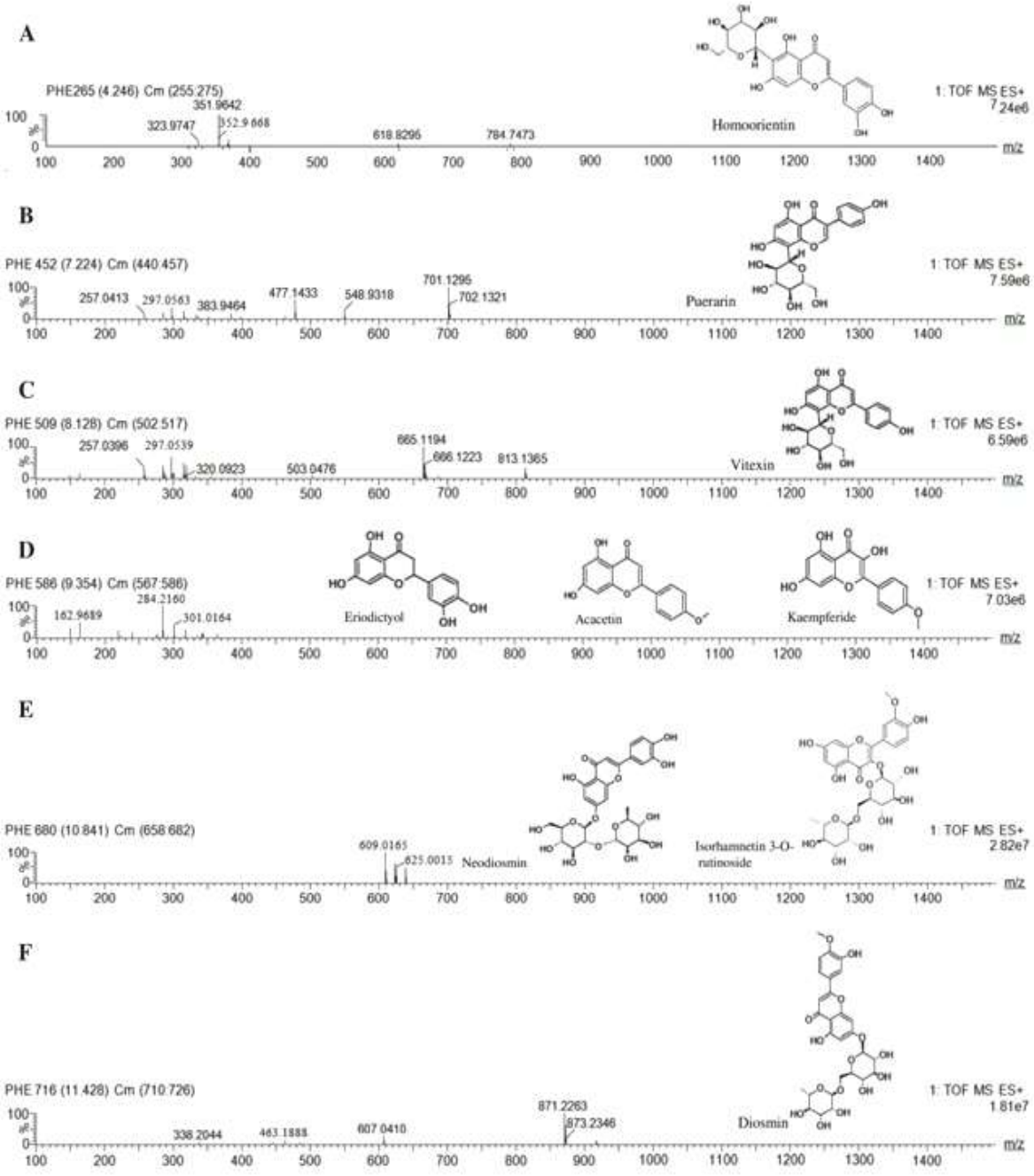

Figure17 Mass data of the flavonoids identified in the UPLC-Q-TOF-MS/MS study of PHE. In positive mode **A**) Homoorientin; **B**) Puerarin; **C**) Vitexin; **D**) Eriodictyol, Acacetin, and Kaempferide; **E**) Neodiosmin and isorhamnetin-3-O-rutinoside; **F**) Diosmin

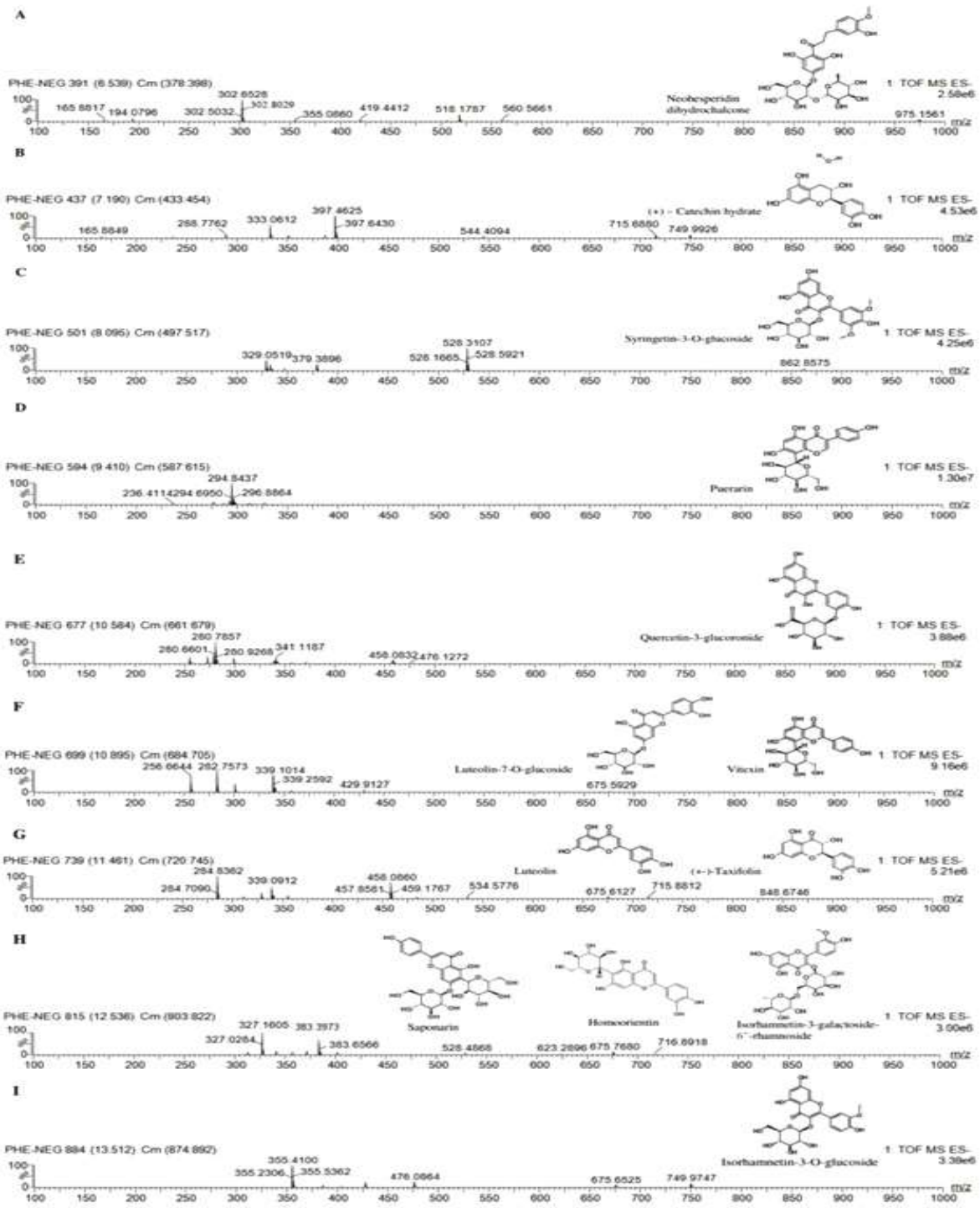

Figure18 Mass data of the flavonoids identified in the UPLC-Q-TOF-MS/MS study of PHE. In negative mode **A**) Neohesperidin dihydrochalcone; **B**) (+)-Catechin hydrate; **C**) syringetin-3-O-glucoside; **D**) Puerarin; **E**) Quercetin-3-Glucuronide; **F**) Luteolin-7-O-glucoside and Vitexin; **G**) Luteolin and (+-)-Taxifolin; **H**) Saponarin, Homoorientin, and Isorhamnetin-3-Galactoside-6''-Rhamnoside; **I**) Isorhamnetin-3-O-glucoside

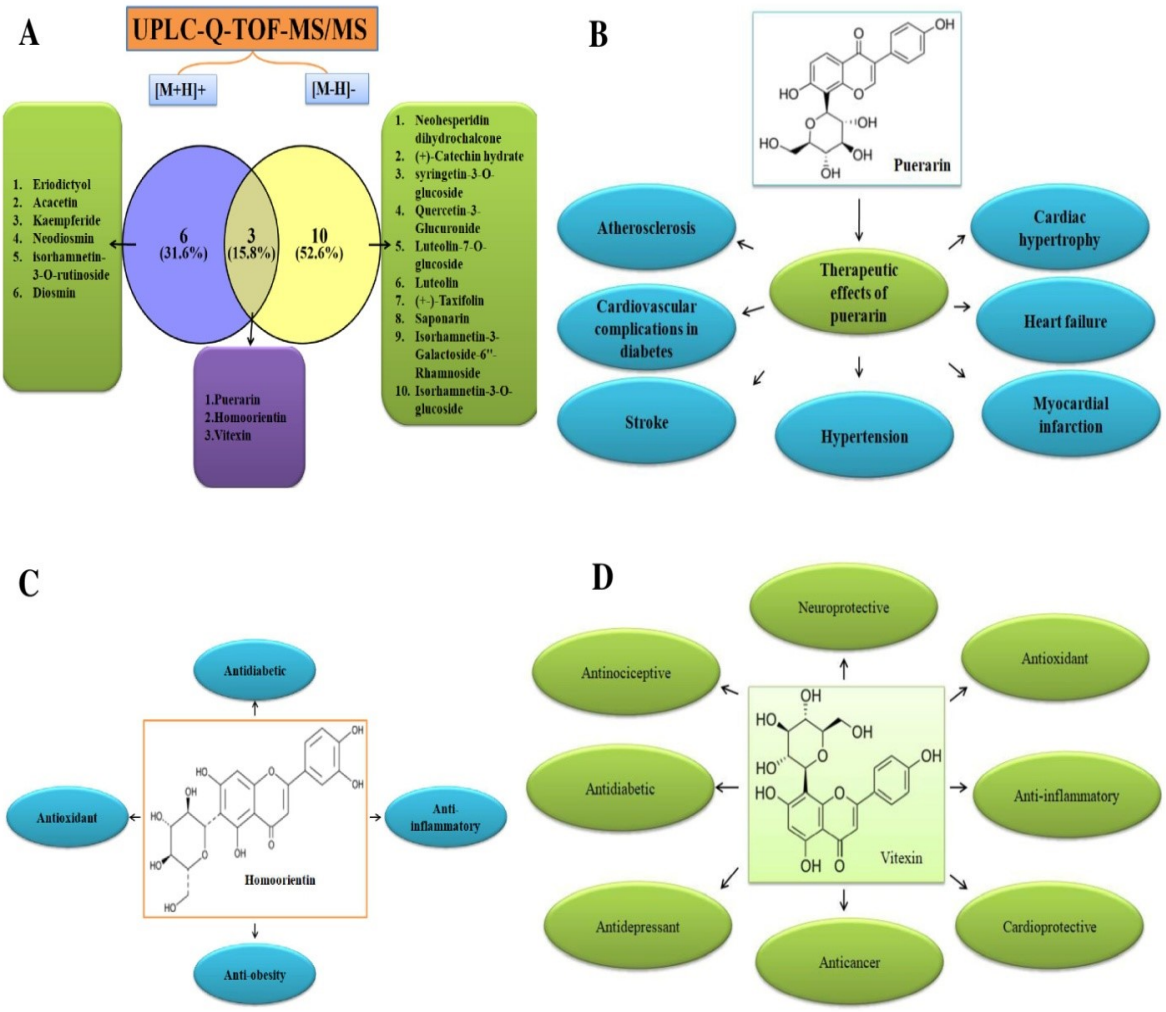

Figure19 Schematic diagram flavonoids identified in the PHE with their therapeutic values. **A**) Prevalent common bioactive flavonoids of PHE from UPLC-Q-TOF-MS/MS analysis;**B**) Puerarin;**C**) Homoorientin; and **D**) Vitexin

Table 17 Flavonoids identified in UPLC-Q-TOF-MS/MS study of PHE

Name	Peak	Rt	Peak %	Exact mass	Formula	Class	Subclass	m/z	Mode
Homoorientin	352.9668	4.246	0.9238	448.1	C21H20O11	Flavonoid	Flavone	449.41	$[M+H]^+$
Puerarin	297.0563	7.224	0.1183	416.38	C21H20O9	Flavonoid	Isoflavone	417.11853	$[M+H]^+$
Vitexin	297.0539	8.128	0.0503	432.38	C21H20O10	Flavonoid	Flavone	433.11344	$[M+H]^+$
Eriodictyol	162.9689	9.354	0.0200	288.27	C15H12O6	Flavonoid	Flavanone	289.07119	$[M+H]^+$
Acacetin	284.2160	9.354	0.6375	284.068	C16H12O5	Flavonoid	Flavone	285.27	$[M+H]^+$
Kaempferide	301.0164	9.354	0.0400	300.28	C16H12O6	Flavonoid	Flavonol	301.07119	$[M+H]^+$
Neodiosmin	609.0165	10.841	18.1122	608.174	C28H32O15	Flavonoid	Flavone	609.5	$[M+H]^+$
Isorhamnetin-3-O-rutinoside	625.0015	10.841	3.0642	624.169	C28H32O16	Flavonoid	Flavonol	625.55	$[M+H]^+$
Diosmin	463.1888	11.428	3.9737	608.174	C28H32O15	Flavonoid	Flavone	609.53	$[M+H]^+$
Neohesperidin dihydrochalcone	302.8029	6.539	0.84160	612.205	C28H36O15	Flavonoid	Flavanone	611.57	$[M-H]^-$
(+)-Catechin hydrate	288.7762	7.190	0.01153	290.27	C15H14O6	Flavonoid	Flavonol	289.07123	$[M-H]^-$
Syringetin-3-O-glucoside	329.0519	8.095	0.02346	508.121	C23H24O13	Flavonoid	Flavonol	507.43	$[M-H]^-$
Puerarin	294.8437	9.410	0.04956	416.38	C21H20O9	Flavonoid	Isoflavone	415.10293	$[M-H]^-$
Quercetin-3-Glucuronide	476.1272	10.584	5.48716	478.074	C21H18O13	Flavonoid	Flavonol	447.4	$[M-H]^-$
Luteolin-7-O-glucoside	282.7573	10.895	3.78509	448.1	C21H20O11	Flavonoid	Flavone	447.41	$[M-H]^-$
Vitexin	429.9127	10.895	8.62802	432.105	C21H20O10	Flavonoid	Flavone	431.36	$[M-H]^-$
Luteolin	284.7090	11.461	10.66232	286.047	C15H10O6	Flavonoid	Flavone	285.24	$[M-H]^-$
(+-)-Taxifolin	284.8362	11.461	0.59157	304.058	C15H12O7	Flavonoid	Flavonol	303.25	$[M-H]^-$
Saponarin	327.0284	12.536	0.00008	594.52	C27H30O15	Flavonoid	Flavone	609.14558	$[M-H]^-$
Homoorientin	327.1605	12.536	0.41373	448.1	C21H20O11	Flavonoid	Flavone	447.4	$[M-H]^-$
Isorhamnetin-3-Galactoside-6"-Rhamnoside	623.2896	12.536	7.23812	624.169	C28H32O16	Flavonoid	Flavonol	623.6	$[M-H]^-$
Isorhamnetin-3-O-glucoside	476.0864	13.512	15.74018	478.111	C22H22O12	Flavonoid	Flavonol	477.43	$[M-H]^-$

5.7.3 Bioactive components and UHPLC-HRMS metabolite profile of PHE

Through early qualitative tests and GC-MS analyses, it was determined that PHE exhibited synergistic antioxidant capacity as well as strong in vitro anti-inflammatory activity because of the presence of several bioactive components in PHE from our study [82]. Therefore, PHE can be utilized as a complementary therapy for the treatment of inflammatory conditions and metabolic diseases like diabetes. After that, we further analyze several biomarker compounds of the ingredient medicinal plants and PHE through UHPLC-HRMS analysis. In the next step, the regulation of gut bacteria as well asthe production of SCFAs in diabetic rats through PHE treatment, we were able to extend the results of prior work on PHE.

Metabolic profiling led to the identification of numerous phytochemicals in PHE, including phenolic acids, organic acids, flavonoids, triterpenes, fatty acids, sesquiterpenes, coumarins, lignans, and sugars (Table 18). Annotation sources included predicted composition, mzCloud search, chemSpider search, and massList search (Arita Lab 6549 Flavonoid Structure Database). The UHPLC-HRMS metabolite fingerprint revealed numerous bioactive compounds present in it. Out of 1759 screening checks, flavonoids were identified in 361 checks, with 9.9% calculated on the basis of the total peak percent area (Table 18). Biomarker compounds like chebulic acid (0.368%), gallic acid (0.759%), ellagic acid (0.469%), andrographolide (1.304%), berberine (6.442%), kaempferol (0.069%), quercetin (0.020%), apigenin (0.040%), and other bioactive compounds like luteolin (0.034%), oxyberberine (0.141%), rutin (0.017%), genistein (0.022%), ferulic acid (0.148%), hesperidin (0.336%), and isorhamnetin (0.015%) were identified in good proportion from PHE shown in Table 18.The total metabolite profile of PHE was expressed in a total ion chromatogram at the various retention times (RT) for bioactive compounds obtained in both the negative and positive modes of analysis (Fig. 20). In this study, MS chromatograms with MS1 and MS2

peaks of well-known biomarker compounds like chebulic acid (Fig. 21), gallic acid (Fig. 22), andrographolide (Fig. 23), and berberine (Fig. 24) were of particular interest.

The identified biomarker compounds in PHE, like chebulic acid, gallic acid, ellagic acid, andrographolide, berberine, kaempferol, quercetin, apigenin, luteolin, rutin, ferulic acid, hesperidin, and other bioactive compounds,were also identified in different proportions from all 6 ingredient medicinal plants in PHE, as shown in Tables19-24.The total metabolite profile of all 6 extracts was also expressed in a total ion chromatogram at various retention times (RT) for several bioactive compounds obtained in both negative and positive modes of analysis (Figs. 25-30).A comprehensive study of the anti-diabetic bioactive component of PHE derived from ingredient medicinal plants was observed, with a diversity of biomarker compounds present for biological activity (Fig. 31).

Table 18UHPLC-HRAMSS-based metabolic profile of PHE

S.No.	Name	Class	Formula	Delta Mass [ppm]	Calc. MW	RT [min]	Area (Max.)	Analysis mode	Total area (Max.)	% Peak area
1.	Apigenin	Flavonoid	C15 H10 O5	-0.15	270.05278	7.557	7355758.293	$[M+H]^+$	101074411.5	0.040
2.	Quercetin	Flavonoid	C15 H10 O7	0.99	302.04295	8.152	15164818.59	[M-H]–	50213415.32	0.020
3.	Isorhamnetin	Flavonoid	C16 H12 O7	1.83	316.05888	9.261	19192967.03	[M-H]–	37837315.92	0.015
4.	Rutin	Flavonoid	C27 H30 O16	0.62	610.15376	7.099	42467443.3	[M-H]–	42467443.3	0.017
5.	kaempferol	Flavonoid	C15 H10 O6	-3.7	286.04668	7.617	142942886	$[M+H]^+$	173637148.4	0.069
6.	luteolin	Flavonoid	C15 H10 O6	1.19	286.04808	8.335	63825716.6	[M-H]–	86306012.36	0.034
7.	4,5-Dicaffeoylquinic acid	Flavonoid	C25 H24 O12	1.21	516.1274	7.449	576214331.4	[M-H]–	665837043.5	0.263
8.	Berberine	Alkaloid	C20 H17 N O4	-3.34	335.11464	7.143	16301382253.26	$[M+H]^+$	16301382253.26	6.442
9.	Oleic acid	Fatty acid	C18 H34 O2	1.05	282.25618	10.539	16173960.66	[M-H]–	16173960.66	0.006
10.	Gallic acid	Phenolic acid	C7 H6 O5	2.63	170.02197	0.809	1413661605	[M-H]–	1920874649.13	0.759
11.	Ellagic acid	Polyphenolic	C14 H6 O8	-4.65	302.00486	5.847	140450767.8	$[M+H]^+$	1186917742.19	0.469
12.	chebulagic acid	Polyphenolic	C41 H30 O27	1.51	954.09889	7.08	23928784.69	[M-H]–	23928784.69	0.009
13.	Chebulic acid	Polyphenolic	C14 H12 O11	1.78	356.0386	0.815	820533485.7	[M-H]–	930040462.09	0.368
14.	corilagin	Polyphenolic	C27 H22 O18	2.35	634.08211	5.849	926420516.75	[M-H]–	926420516.75	0.366
15.	Ferulic acid	Phenolic acid	C10 H10 O4	1.79	194.05826	6.789	5134686.163	[M-H]–	374402311.51	0.148
16.	Isoferulic acid	Phenolic acid	C10 H10 O4	1.79	194.05826	7.297	83016372.58	[M-H]–	83016372.58	0.033
17.	Caffeic acid	Phenolic acid	C9 H8 O4	2.41	180.04269	5.603	406465710	[M-H]–	606844362.27	0.240
18.	D-(-)-Quinic acid	Organic acid	C7 H12 O6	1.88	192.06375	1.394	109974461.1	[M-H]–	398186317.96	0.157
19.	Andrographolide	Terpenoid	C20 H30 O5	-3.76	350.20801	8.207	2755145165	$[M+H]^+$	3298603769.56	1.304
20.	Oleanolic acid	Triterpenoid	C30 H48 O3	-4.47	456.35831	10.943	191713483.1	$[M+H]^+$	219583459.90	0.087
21.	Cinnamic acid	Organic acid	C9 H8 O2	-4.59	148.05175	0.821	75495782.62	$[M+H]^+$	515806247.65	0.204
22.	Chlorogenic acid	Phenolic acid	C16 H18 O9	-4.87	354.09336	5.397	612034050.1	$[M+H]^+$	1415255105	0.559
23.	Piperine	Alkaloid	C17 H19 N O3	-3.97	285.13536	9.767	420124923.1	$[M+H]^+$	420124923.1	0.166
24.	D-(+)-Proline	Amino acid	C5 H9 N O2	-4.05	115.06286	0.807	389505804.7	$[M+H]^+$	502547802.7	0.199
25.	Nootkatone	Sesquiterpenoid	C15 H22 O	-4.28	218.16613	10.44	313515259.1	$[M+H]^+$	313515259.1	0.124
26.	D-(+)-Pyroglutamic Acid	Amino acid	C5 H7 N O3	-4.41	129.04202	0.967	284199211.4	$[M+H]^+$	449591931	0.178
27.	Citric acid	Organic acid	C6 H8 O7	3.04	192.02759	0.963	403417142.1	[M-H]–	791891786	0.313

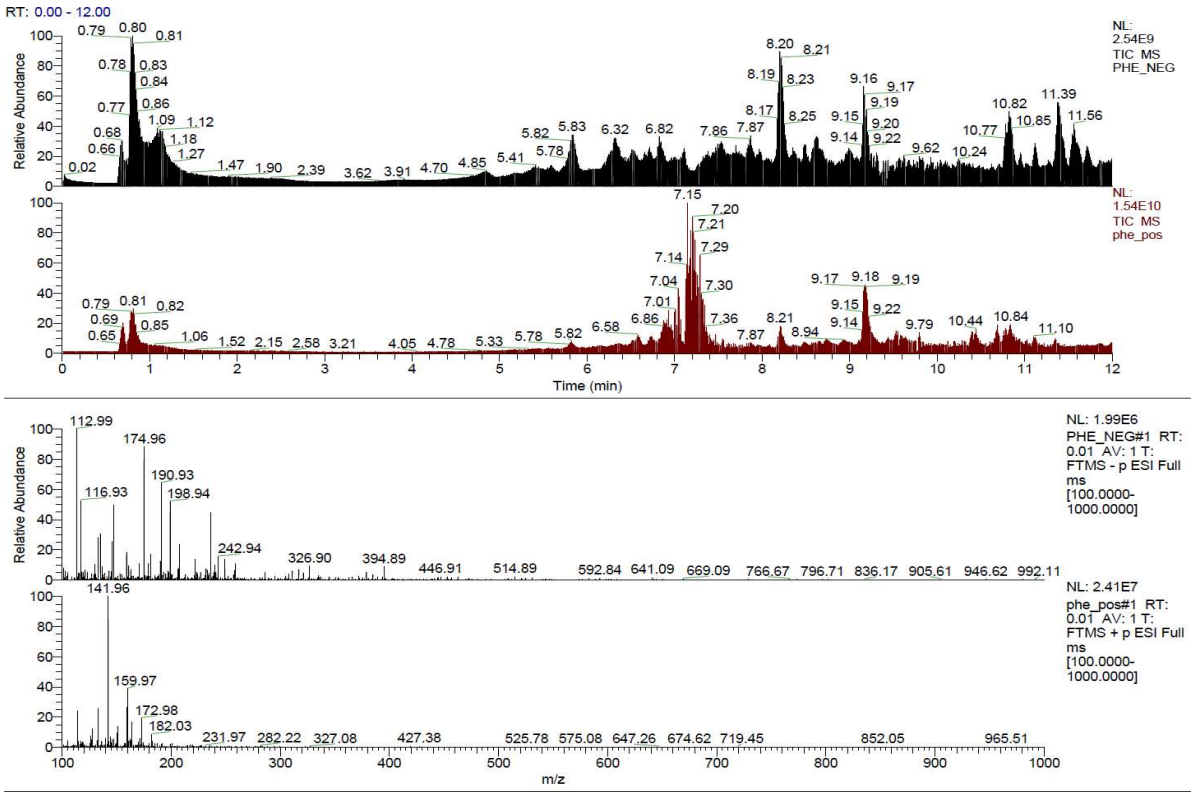

Figure20 Total ion chromatogram of whole metabolites from PHE with relative abundance

Structure	Name	RT [min]	Formula	Molecular Weight	Group Areas
	Chebulic acid	0.82	C14 H12 O11	n/a	n/a

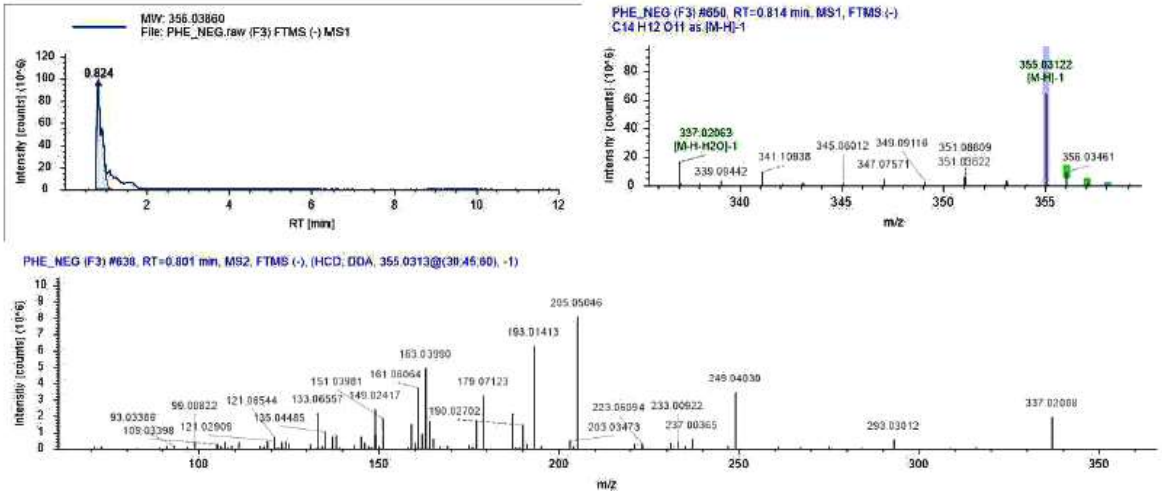

Figure 21 Chebulic acid (C14H12O11) in full scan MS of negative ionisation mode of PHE with raw, MS1 and MS2Chromatograms

Structure	Name	RT [min]	Formula	Molecular Weight	Group Areas
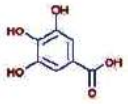	Gallic acid	5.82	C7 H6 O5	n/a	n/a

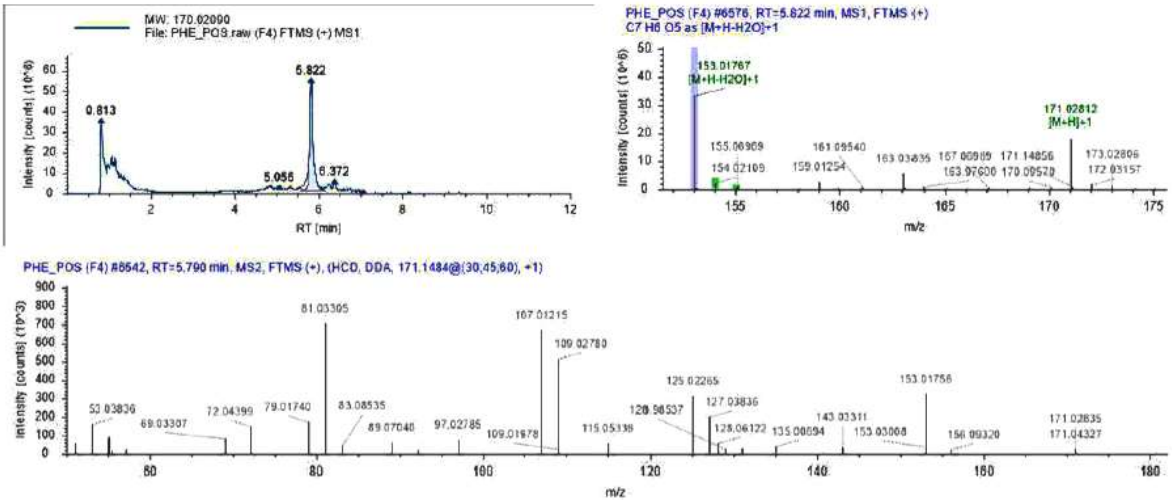

Figure 22 Gallic acid (C7H6O5) in full scan MS of negative ionisation mode of PHE with raw, MS1 and MS2Chromatograms

Structure	Name	RT [min]	Formula	Molecular Weight	Group Areas
	Andrographolide	8.21	C20 H30 O5	n/a	n/a

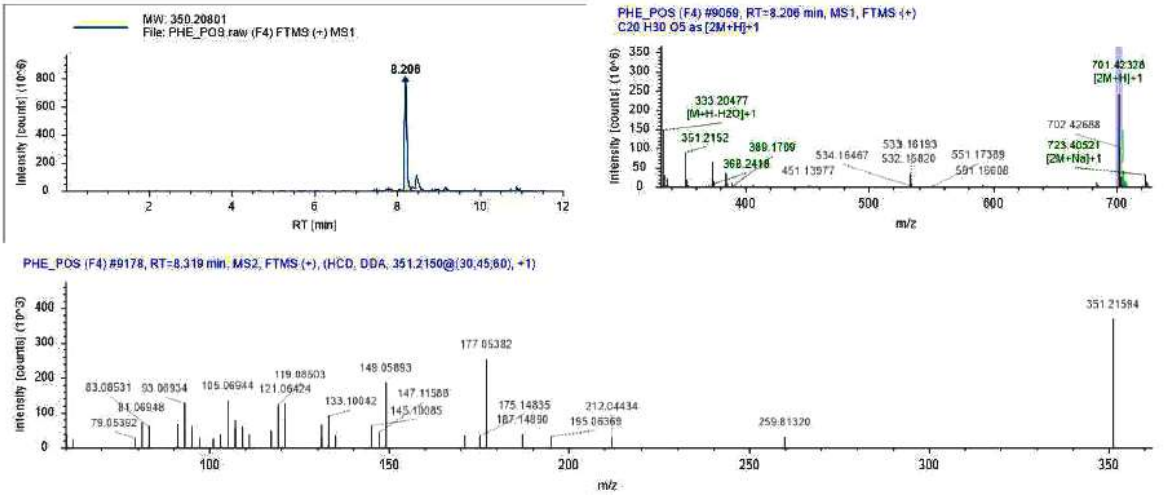

Figure 23 Andrographolide (C20H30O5) in full scan MS of positive ionisation mode of PHE with raw, MS1 and MS2Chromatograms

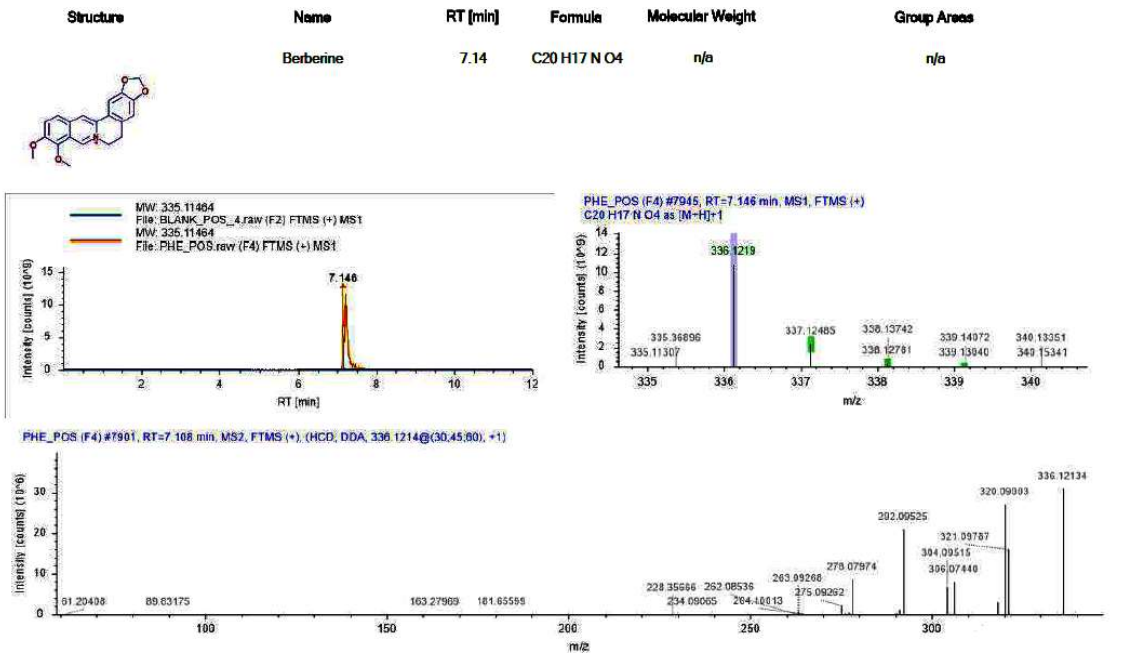

Figure 24 Berberine (C20H17NO4) in full scan MS of positive ionisation mode of PHE with raw, MS1 and MS2Chromatograms

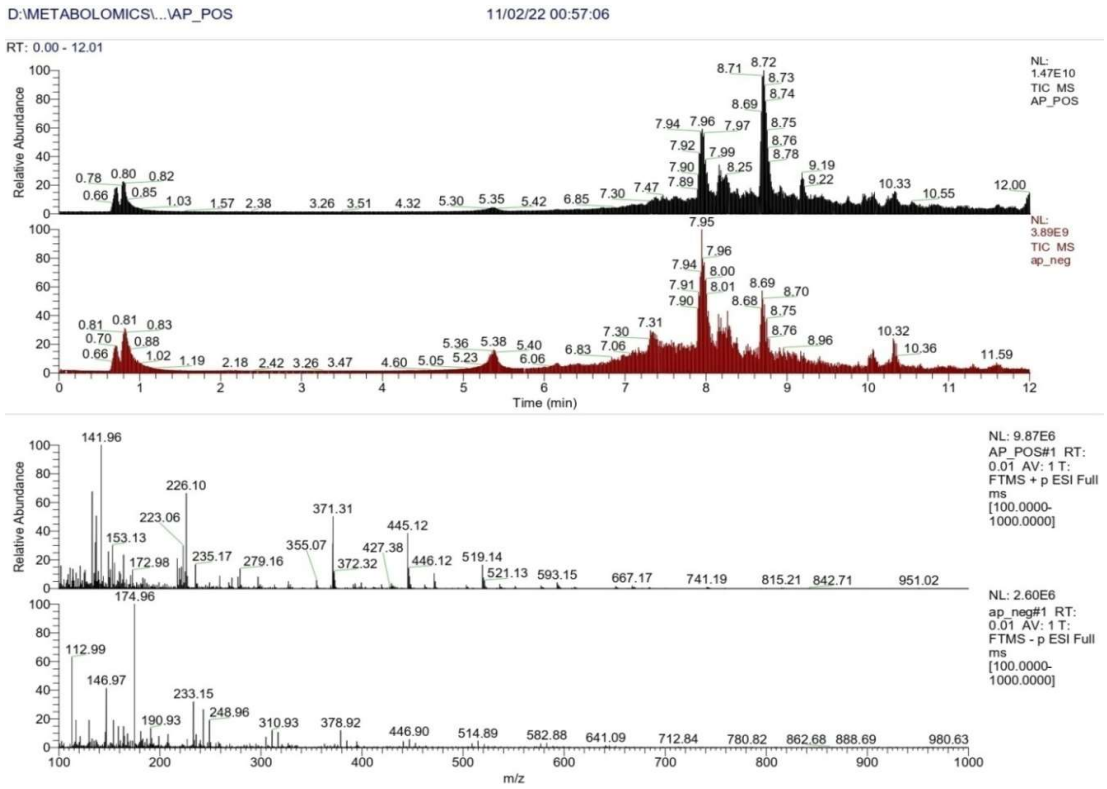

Figure25 Total ion chromatogram of whole metabolites from whole herb extract of *Andrographis paniculata*

Table 19UHPLC-HRAMSS-based metabolic profile of whole herb extract of *Andrographis paniculata*

S.No.	Name	Class	Formula	Delta Mass [ppm]	Calc. MW	RT [min]	Area (Max.)	Analysis mode	Total area (Max.)	% Peak area
1.	Andrographolide	Terpenoid	C20 H30 O5	-4.1	350.20789	8.044	1.605E+10	$[M-H]^-$	16050346532	8.484
2.	3-O-β-D-Glucopyranosylandrographolide	Terpenoid glucoside	C26 H40 O10	-1.28	512.26149	7.382	89005096.6	$[M+H]^+$	482758529	0.255
3.	Neochlorogenic acid	Polyphenolic	C16 H18 O9	-3.82	354.09373	7.422	81171094.5	$[M-H]^-$	81171094.46	0.043
4.	D-(+)-Proline	Amino acid	C5 H9 N O2	-3.4	115.06294	0.896	87234058.7	$[M+H]^+$	87234058.74	0.046
5.	13(S)-HOTrE	Fatty acid	C18 H30 O3	-3.25	294.21854	10.144	2523308162	$[M-H]^-$	2674436655	1.414
6.	9S,13R-12-Oxophytodienoic acid	Prostaglandin like acid	C18 H28 O3	-3.26	292.20289	8.885	250823922	$[M+H]^+$	826529975	0.437
7.	Nootkatone	Sesquiterpenoid	C15 H22 O	-2.95	218.16642	9.847	2450536040	$[M+H]^+$	2814874311	1.488
8.	(15Z)-9,12,13-Trihydroxy-15-octadecenoic acid	Fatty acid	C18 H34 O5	-3.08	330.23961	8.701	12613088.3	$[M+H]^+$	1217797778	0.644
9.	Eicosatetraynoic acid	Fatty acid	C20 H24 O2	-3.09	296.17671	8.038	5320348627	$[M+H]^+$	7579497333	4.006
10.	Citric acid	Organic acid	C6 H8 O7	-2.05	192.02661	1.077	177199259	$[M-H]^-$	543035918	0.287
11.	11-Aminoundecanoic acid	Amine derivative of fatty acid	C11 H23 N O2	-4.3	201.17201	0.898	306224417	$[M+H]^+$	306224416.7	0.162
12.	Apigenin 7-O-glucuronide	Flavonoid	C21 H18 O11	-4.16	446.08306	7.451	499953221	$[M+H]^+$	1826629833	0.966
13.	Luteolin	Flavonoid	C15 H10 O6	-4.05	286.04658	8.165	321379876	$[M-H]^-$	321379876.3	0.170
14.	Apigenin	Flavonoid	C15 H10 O5	-1.17	270.05251	7.451	20537483.8	$[M+H]^+$	306643942.1	0.162
15.	Kaempferol	Flavonoid	C15 H10 O6	-1.13	286.04741	7.18	27293530	$[M+H]^+$	27293529.95	0.014
16.	4,5-Dicaffeoylquinic acid	Flavonoid	C25 H24 O12	-4.79	516.1243	7.28	2205409239	$[M-H]^-$	4544455278	2.402
17.	Berberine	Alkaloid	C20 H17 N O4	-3.79	335.11449	7.216	146254274	$[M+H]^+$	623842647	0.330
18.	Gallic acid	Phenolic acid	C7 H6 O5	-2.12	170.02116	0.905	16299411	$[M-H]^-$	93679295	0.050
19.	Ferulic acid	Phenolic acid	C10 H10 O4	-3.75	194.05718	6.898	10230632.4	$[M+H]^+$	141304371	0.075
20.	Caffeic acid	Phenolic acid	C9 H8 O4	-2.44	180.04182	5.641	199446497	$[M-H]^-$	199446496.6	0.105
21.	D-(-)-Quinic acid	Organic acid	C7 H12 O6	-3.35	192.06274	0.91	1295784939	$[M-H]^-$	1995202647	1.055
22.	DL-Malic acid	Organic acid	C4 H6 O5	-3.72	134.02103	0.945	1777339815	$[M-H]^-$	1777339815	0.939
23.	16-Hydroxyhexadecanoic acid	Fatty acid	C16 H32 O3	-4.57	272.2339	10.341	24726324.8	$[M-H]^-$	353307132	0.187
24.	(-)-Caryophyllene oxide	Sesquiterpenoid	C15 H24 O	-3.21	220.18201	9.373	144137550	$[M+H]^+$	435653700	0.230
25.	Chlorogenic acid	Phenolic acid	C16 H18 O9	-4.21	354.09359	5.188	451771751	$[M-H]^-$	3996893709	2.113

Table 20UHPLC-HRAMSS-based metabolic profile of leaf extract of *Premna integrifolia*

S.No.	Name	Class	Formula	Delta Mass [ppm]	Calc. MW	RT [min]	Area (Max.)	Analysis mode	Total area (Max.)	% Peak area
1.	D-(+)-Proline	Amino acid	C5 H9 N O2	-3.52	115.06292	1.208	42068037.8	$[M+H]^+$	42068037.85	0.039
2.	4-Oxoproline	Amino acid derivative	C5 H7 N O3	-3.34	129.04216	1.235	22921622.1	$[M-H]^-$	31299651	0.029
3.	4-Undecylbenzenesulfonic acid	Arenesulfonic acid	C17 H28 O3 S	-4.3	312.17457	12.307	11506942.2	$[M-H]^-$	11506942.19	0.011
4.	9-Oxo-10(E),12(E)-octadecadienoic acid	Fatty acid	C18 H30 O3	-2.82	294.21867	10.703	3795131435	$[M+H]^+$	3795131435	3.486
5.	(+/-)13-HODE	Fatty acid	C18 H32 O3	-3.89	296.23399	10.712	1877800258	$[M-H]^-$	1877800258	1.725
6.	13(S)-HOTrE	Fatty acid	C18 H30 O3	-3.2	294.21855	9.379	615702444	$[M+H]^+$	3658669721	3.361
7.	9S,13R-12-Oxophytodienoic acid	Prostaglandin like acid	C18 H28 O3	-3.77	292.20274	9.179	1880317534	$[M+H]^+$	2062663597	1.895
8.	(15Z)-9,12,13-Trihydroxy-15-octadecenoic acid	Fatty acid	C18 H34 O5	-4.65	330.23909	9.975	28913737.6	$[M+H]^+$	28913737.58	0.027
9.	3,5-Dimethoxybenzoic acid	Benzoic acid derivative	C9 H10 O4	-3.18	182.05733	6.967	19698568.7	$[M+H]^+$	19698568.65	0.018
10.	5-Hydroxymethyl-2-furaldehyde	Organic	C6 H6 O3	-2.42	126.03139	7.179	23226298.2	$[M+H]^+$	1544967115	1.419
11.	L(-)-Pipecolinic acid	Carboxylic acid	C6 H11 N O2	-3.34	129.07855	1.22	25824462.5	$[M+H]^+$	25824462.5	0.024
12.	11-Aminoundecanoic acid	Amine derivative of fatty acid	C11 H23 N O2	-3.77	201.17212	1.211	316045315	$[M+H]^+$	316045315	0.290
13.	Isoferulic acid	Phenolic acid	C10 H10 O4	-3.93	194.05715	7.299	8326380.19	$[M+H]^+$	8326380.194	0.008
14.	D-(-)-Quinic acid	Organic acid	C7 H12 O6	-2.41	192.06293	1.198	5307589.96	$[M-H]^-$	5307589.963	0.005
15.	DL-Malic acid	Organic acid	C4 H6 O5	-3.04	134.02112	1.202	3745677.67	$[M-H]^-$	31177840	0.029
16.	9-Oxononanoic acid	Fatty acid	C9 H16 O3	-3.14	172.1094	10.42	6375198.52	$[M-H]^-$	6375198.515	0.006
17.	α-Eleostearic acid	Fatty acid	C18 H30 O2	-3.78	278.22353	10.718	4154954229	$[M+H]^+$	4154954229	3.816
18.	p-cymene	Monoterpene	C10 H14	-3.23	134.10912	7.509	39060879.2	$[M+H]^+$	39060879.2	0.036
19.	6-Phenyl-1-hexanol	Fatty alcohol	C12 H18 O	-3.17	178.1352	9.915	27569921.5	$[M+H]^+$	159193696	0.146
20.	16-Hydroxyhexadecanoic acid	Fatty acid	C16 H32 O3	-3.91	272.23408	12.006	681303153	$[M-H]^-$	681303152.6	0.626
21.	16-Oxohexadecanoic acid	Fatty acid	C16 H30 O3	-3.5	270.21855	11.086	3304797.38	$[M-H]^-$	81795090	0.075
22.	2,3-Dihydro-1-benzofuran-2-carboxylic acid	Carboxylic acid	C9 H8 O3	-2.03	164.04701	6.673	32681240.1	$[M-H]^-$	83676544	0.077
23.	(-)-Caryophyllene oxide	Sesquiterpenoid	C15 H24 O	-3.34	220.18198	8.746	28943222	$[M+H]^+$	37377791	0.034
24.	Cinnamic acid	Organic acid	C9 H8 O2	-3.49	148.05191	10.894	139137415	$[M+H]^+$	139137415.4	0.128

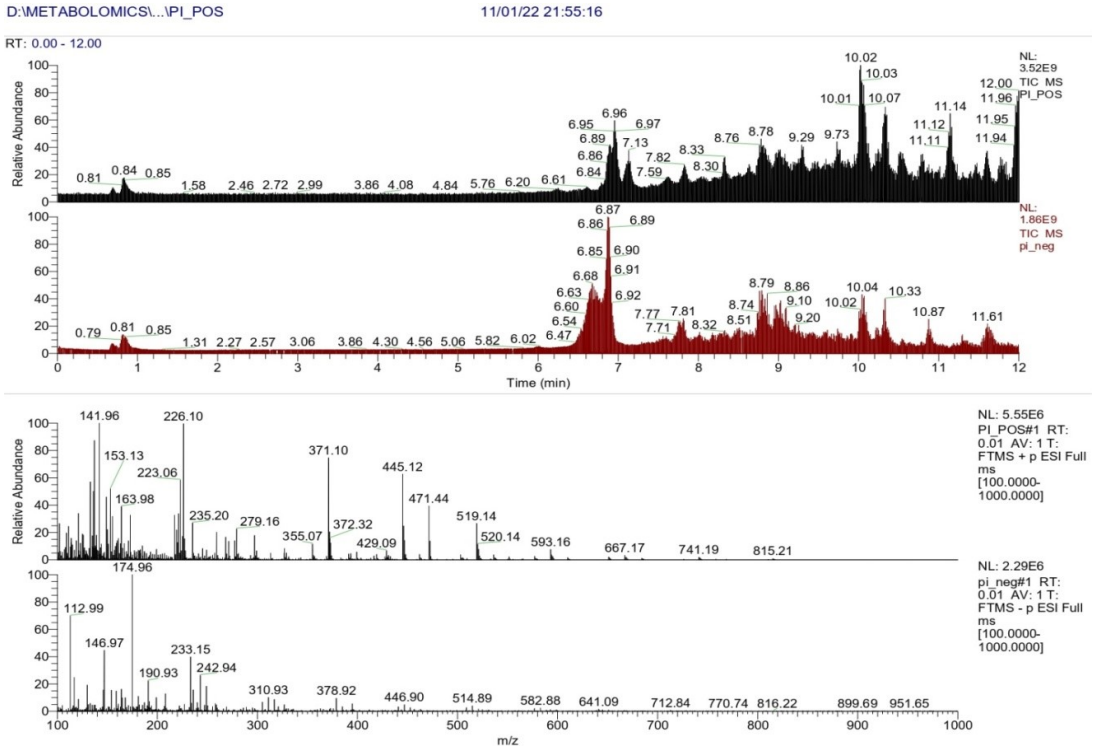

Figure26 Total ion chromatogram of whole metabolites from leaf extract of *Premna integrifolia*

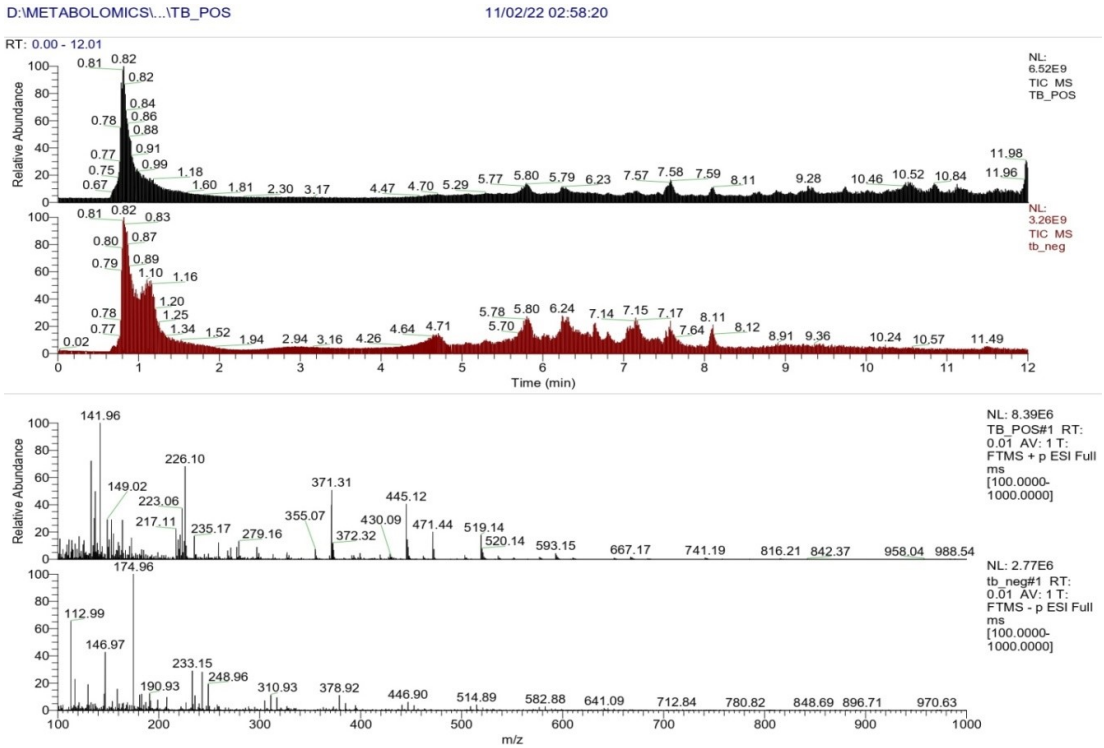

Figure27 Total ion chromatogram of whole metabolites from fruit extract of *Terminaliabellerica*

Table 21UHPLC-HRAMSS-based metabolic profile of fruit extract of *Terminaliabellerica*

S.No.	Name	Class	Formula	Delta Mass [ppm]	Calc. MW	RT [min]	Area (Max.)	Analysis mode	Total area (Max.)	% Peak area
1.	D-(+)-Proline	Amino acid	C5 H9 N O2	-3.57	115.06292	0.813	1889816165	$[M+H]^+$	2063761002	1.858
2.	4-Oxoproline	Amino acid derivative	C5 H7 N O3	-4.14	129.04206	0.842	78323015.9	$[M-H]^-$	78323015.87	0.071
3.	9S,13R-12-Oxophytodienoic acid	Prostaglandin like acid	C18 H28 O3	-3.97	292.20268	8.807	46661006	$[M+H]^+$	46661006.03	0.042
4.	Nootkatone	Sesquiterpenoid	C15 H22 O	-4.1	218.16617	9.746	80725002.1	$[M+H]^+$	80725002.06	0.073
5.	1,2,3,6-Tetra-O-galloyl-β-D-glucose	Gallotannin	C34 H28 O22	-4.25	788.10387	0.841	297200025	$[M-H]^-$	357239291	0.322
6.	5-Hydroxymethyl-2-furaldehyde	Organic	C6 H6 O3	-3.81	126.03121	1.097	1015865187	$[M+H]^+$	3475444159	3.130
7.	Hydroxy-1,4-benzoquinone	Organic	C6 H4 O3	-3.89	124.01556	1.128	1.5016E+10	$[M-H]^-$	15055410773	13.557
8.	D-(+)-Pyroglutamic Acid	Amino acid	C5 H7 N O3	-3.92	129.04209	0.969	486511357	$[M+H]^+$	486511356.9	0.438
9.	Citric acid	Organic acid	C6 H8 O7	-2.21	192.02658	0.966	528940898	$[M-H]^-$	579590941.5	0.522
10.	L(-)-Pipecolinic acid	Carboxylic acid derivative	C6 H11 N O2	-3.17	129.07857	0.832	637631329	$[M+H]^+$	1240728624	1.117
11.	11-Aminoundecanoic acid	Amine derivative of fatty acid	C11 H23 N O2	-4.45	201.17198	0.819	892552908	$[M+H]^+$	892552908.3	0.804
12.	Quercetin-3β-D-glucoside	Flavonoid	C21 H20 O12	-4.54	464.09337	7.166	9492505.37	$[M+H]^+$	9492505.366	0.009
13.	Berberine	Alkaloid	C20 H17 N O4	-4.33	335.11431	7.218	47285694.6	$[M+H]^+$	47285694.55	0.043
14.	Oleic acid alkyne	Fatty acid	C18 H30 O2	-3.69	278.22355	11.599	197620820	$[M-H]^-$	197620820.4	0.178
15.	Gallic acid	Phenolic acid	C7 H6 O5	-2.84	170.02104	0.826	6926858937	$[M-H]^-$	7610598299	6.853
16.	Chebulic acid	Polyphenolic	C14 H12 O11	-3.54	356.0367	0.812	22007108.6	$[M+H]^+$	22007108.6	0.020
17.	Corilagin	Polyphenolic	C27 H22 O18	-2.94	634.07875	5.64	176696897	$[M-H]^-$	2101325136	1.892
18.	D-(-)-Mannitol	Sugar	C6 H14 O6	-3.92	182.07832	0.783	50252557.7	$[M-H]^-$	50252557.66	0.045
19.	D-(-)-Quinic acid	Organic acid	C7 H12 O6	-3.4	192.06273	0.873	338472040	$[M-H]^-$	338472039.9	0.305
20.	DL-Malic acid	Organic acid	C4 H6 O5	-3.38	134.02107	1.176	145432551	$[M-H]^-$	2736712375	2.464
21.	2-Isopropylmalic acid	Hydroxy fatty acid	C7 H12 O5	-3.26	176.0679	4.802	56767682	$[M-H]^-$	214786312	0.193
22.	9,10-Dihydroxystearic acid	Fatty acid	C18 H36 O4	-4.78	316.25985	10.165	89297457.6	$[M+H]^+$	89297457.61	0.080
23.	16-Hydroxyhexadecanoic acid	Fatty acid	C16 H32 O3	-4.91	272.23381	10.327	5274341.02	$[M-H]^-$	27789476.2	0.025
24.	5-Formylfurfural	Organic	C6 H4 O3	-2.99	124.01567	1.585	68143459.5	$[M+H]^+$	68143459.48	0.061
25.	(-)-Caryophyllene oxide	Sesquiterpenoid	C15 H24 O	-3.7	220.1819	9.527	31383483.2	$[M+H]^+$	31383483.2	0.028
26.	Piperine	Alkaloid	C17 H19 N O3	-4.27	285.13528	9.176	205811495	$[M+H]^+$	205811494.5	0.185

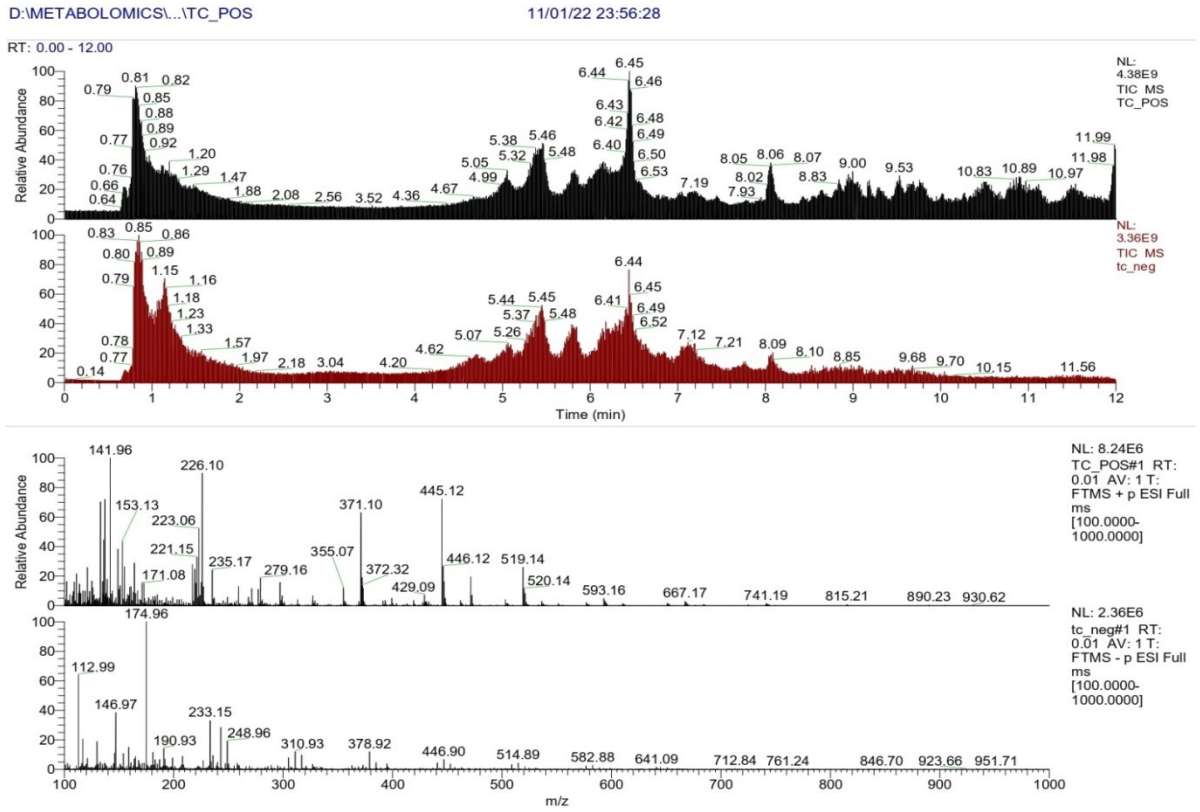

Figure28 Total ion chromatogram of whole metabolites from fruit extract of *Terminaliachebula*

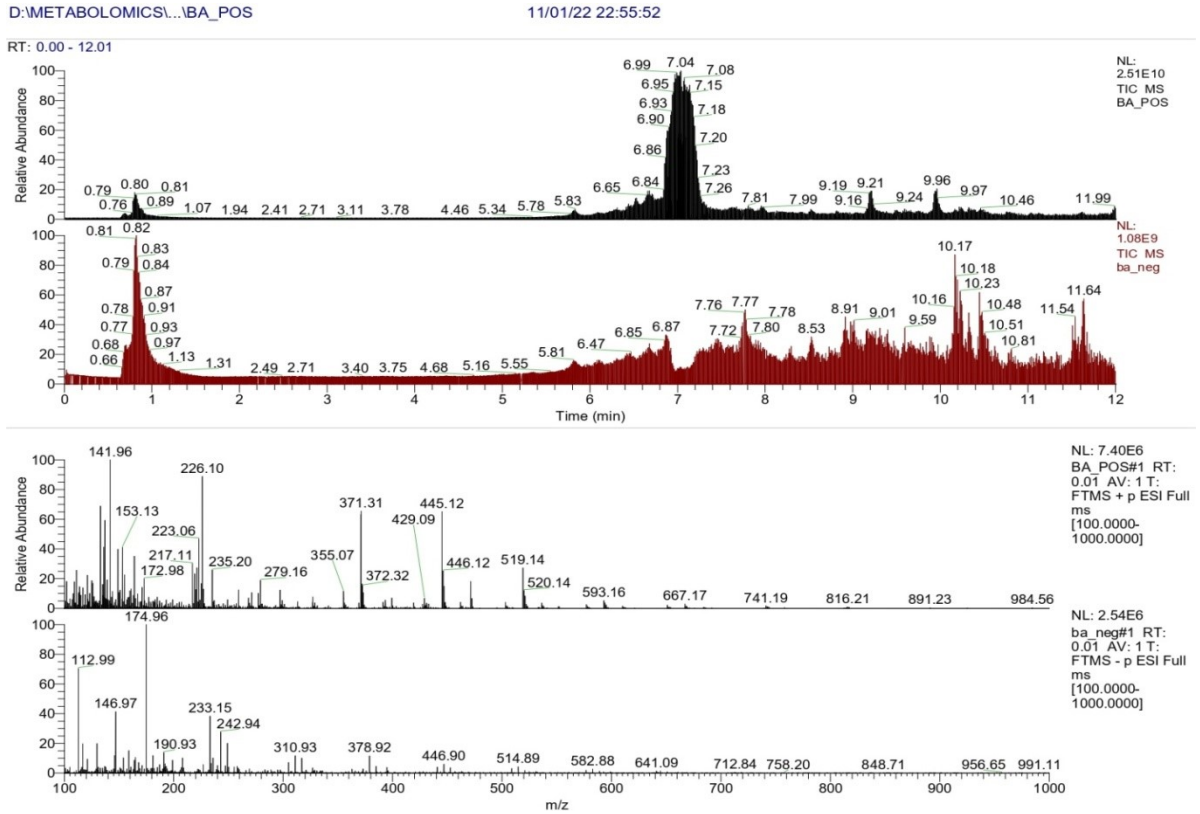

Figure29 Total ion chromatogram of whole metabolites from stemextract of *Berberisaristata*

Table 22UHPLC-HRAMSS-based metabolic profile of fruit extract of *Terminaliachebula*

S.No.	Name	Class	Formula	Delta Mass [ppm]	Calc. MW	RT [min]	Area (Max.)	Analysis mode	Total area (Max.)	% Peak area
1.	D-(+)-Proline	Amino acid	C5 H9 N O2	-3.01	115.06298	0.805	785272182	$[M+H]^+$	887908805	0.471
2.	Nootkatone	Sesquiterpenoid	C15 H22 O	-3.15	218.16638	9.753	63400672	$[M+H]^+$	63400671.97	0.034
3.	1,2,3,6-Tetra-O-galloyl-β-D-glucose	Gallotannin	C34 H28 O22	-3.64	788.10436	0.82	100576657	[M-H]–	1046803220	0.555
4.	2-(E)-O-feruloyl-D-galactarate(2-)	Dicarboxylic acid	C16 H16 O11	-2.6	384.06826	4.993	9256263365	$[M+H]^+$	30399344526	16.131
5.	5-Hydroxymethyl-2-furaldehyde	Organic	C6 H6 O3	-3.35	126.03127	1.084	1463964643	$[M+H]^+$	4253517773	2.257
6.	Hydroxy-1,4-benzoquinone	Organic	C6 H4 O3	-2.67	124.01571	1.133	8958006616	[M-H]–	8972802873	4.761
7.	D-(+)-Pyroglutamic Acid	Amino acid	C5 H7 N O3	-1.17	129.04244	0.891	126169843	$[M+H]^+$	152246087.5	0.081
8.	Citric acid	Organic acid	C6 H8 O7	-2.21	192.02658	0.845	160797731	[M-H]–	300228832	0.159
9.	11-Aminoundecanoic acid	Amine derivative of fatty acid	C11 H23 N O2	-4	201.17208	0.81	606207201	$[M+H]^+$	606207201.3	0.322
10.	Quercetin-3β-D-glucoside	Flavonoid	C21 H20 O12	-3.29	464.09395	7.151	8277715.88	$[M+H]^+$	8277715.881	0.004
11.	Rutin	Flavonoid	C27 H30 O16	-3.43	610.15129	7.129	21017307.9	$[M+H]^+$	21017307.92	0.011
12.	Kaempferol	Flavonoid	C15 H10 O6	-4.46	286.04646	8.076	14214024.6	$[M+H]^+$	14214024.62	0.008
13.	Berberine	Alkaloid	C20 H17 N O4	-2.24	335.11501	7.076	151440192	$[M+H]^+$	151440192.2	0.080
14.	Oleic acid alkyne	Fatty acid	C18 H30 O2	-3.35	278.22365	11.6	87837311.2	[M-H]–	87837311.17	0.047
15.	Gallic acid	Phenolic acid	C7 H6 O5	-1.96	170.02119	0.835	6137077901	[M-H]–	11341636625	6.018
16.	Ellagic acid	Polyphenolic	C14 H6 O8	-2.71	302.00545	7.001	355157999	$[M+H]^+$	6902402360	3.663
17.	Chebulic acid	Polyphenolic	C14 H12 O11	-4.12	356.03649	0.901	3077494908	[M-H]–	3077494908	1.633
18.	corilagin	Polyphenolic	C27 H22 O18	-3.04	634.07869	5.788	1844876852	[M-H]–	1844876852	0.979
19.	D-(-)-Mannitol	Sugar	C6 H14 O6	-2.49	182.07858	0.808	259978349	[M-H]–	259978348.8	0.138
20.	6-O-Galloyl-glucose	Phenolic	C13 H16 O10	-4.2	332.07295	0.858	849573029	[M-H]–	849573029.4	0.451
21.	5-GALLOYLSHIKIMIC ACID	Phenolic	C14 H14 O9	-4.36	326.06236	0.835	303393042	[M-H]–	1782244859	0.946
22.	D-(-)-Quinic acid	Organic acid	C7 H12 O6	-2.47	192.06291	0.836	1390591539	[M-H]–	1390591539	0.738
23.	DL-Malic acid	Organic acid	C4 H6 O5	-4.08	134.02098	0.886	357352922	[M-H]–	357352922.2	0.190
24.	16-Hydroxyhexadecanoic acid	Fatty acid	C16 H32 O3	-3.79	272.23411	10.335	6748943.9	[M-H]–	30796742.78	0.016
25.	Cinnamic acid	Organic acid	C9 H8 O2	-2.9	148.052	8.546	11375088.1	[M-H]–	81441526.05	0.043
26.	Piperine	Alkaloid	C17 H19 N O3	-3.04	285.13563	9.179	1638449828	$[M+H]^+$	1638449828	0.869

Table 23UHPLC-HRAMSS-based metabolic profile of stemextract of *Berberisaristata*

S.No.	Name	Class	Formula	Delta Mass [ppm]	Calc. MW	RT [min]	Area (Max.)	Analysis mode	Total area (Max.)	% Peak area
1.	9-Oxo-10(E),12(E)-octadecadienoic acid	Fatty acid	C18 H30 O3	-3.24	294.21854	10.334	4512640835	$[M+H]^+$	4512640835	2.653
2.	13(S)-HOTrE	Fatty acid	C18 H30 O3	-2.79	294.21867	10.458	1477616191	$[M+H]^+$	1481167016	0.871
3.	3,5-Dimethoxybenzoic acid	Benzoic acid derivative	C9 H10 O4	-1.95	182.05755	6.096	237241240	$[M-H]^-$	1579529754	0.929
4.	Protopine	Alkaloid	C20 H19 N O5	-2.95	353.12528	0.808	501126087	$[M+H]^+$	1595323802	0.938
5.	Glaucine	Alkaloid	C21 H25 N O4	-3.51	355.17711	0.821	552603426	$[M+H]^+$	2678793633	1.575
6.	2-Furoic acid	Organic	C5 H4 O3	-2.57	112.01576	1.151	327937037	$[M+H]^+$	327937037.4	0.193
7.	N-Methylhernagine	Alkaloid	C20 H23 N O4	-2.87	341.16173	0.814	2229090278	$[M+H]^+$	9076018133	5.335
8.	11-Aminoundecanoic acid	Amine derivative of fatty acid	C11 H23 N O2	-3.69	201.17214	0.8	509870064	$[M+H]^+$	509870063.7	0.300
9.	Quercetin	Flavonoid	C15 H10 O7	-4.57	302.04127	7.799	16448066.4	$[M-H]^-$	16448066.36	0.010
10.	Kaempferol	Flavonoid	C15 H10 O6	-4.89	286.04634	7.884	11042018.4	$[M-H]^-$	11042018.38	0.006
11.	Berberine	Alkaloid	C20 H18 N O4	1.72	336.12416	6.798	678311088	$[M+H]^+$	678311087.6	0.399
12.	Gallic acid	Phenolic acid	C7 H6 O5	-2.84	170.02104	1.153	30610935.9	$[M-H]^-$	30610935.9	0.018
13.	Ferulic acid	Phenolic acid	C10 H10 O4	-3.22	194.05728	6.688	109866768	$[M+H]^+$	318320952	0.187
14.	Isoferulic acid	Phenolic acid	C10 H10 O4	-2.93	194.05734	7.226	485771757	$[M-H]^-$	543795304	0.320
15.	Caffeic acid	Phenolic acid	C9 H8 O4	-1.74	180.04194	5.553	26977138.8	$[M-H]^-$	26977138.79	0.016
16.	D-(-)-Quinic acid	Organic acid	C7 H12 O6	-2.81	192.06285	0.881	9226923.26	$[M-H]^-$	9226923.258	0.005
17.	DL-Malic acid	Organic acid	C4 H6 O5	-3.22	134.02109	0.87	389108666	$[M-H]^-$	389108665.6	0.229
18.	α-Eleostearic acid	Fatty acid	C18 H30 O2	-3.67	278.22356	11.849	729641476	$[M+H]^+$	729641475.9	0.429
19.	3-oxopalmitic acid	Fatty acid	C16 H30 O3	-4.06	270.2184	10.199	7715071.03	$[M-H]^-$	171554933	0.101
20.	16-Hydroxyhexadecanoic acid	Fatty acid	C16 H32 O3	-2.55	272.23445	10.236	31498074.9	$[M-H]^-$	189372335	0.111
21.	16-Oxohexadecanoic acid	Fatty acid	C16 H30 O3	-4.06	270.2184	11.113	7903817.05	$[M-H]^-$	7903817.05	0.005
22.	Oleanolic acid	Triterpenoid	C30 H48 O3	-3.49	456.35875	11.397	16881332.8	$[M+H]^+$	16881332.84	0.010
23.	Piperine	Alkaloid	C17 H19 N O3	-3.44	285.13551	9.17	1911706101	$[M+H]^+$	1911706101	1.124
24.	Syringic acid	Phenolic	C9 H10 O5	-3.37	198.05216	5.636	102570379	$[M+H]^+$	376053686	0.221
25.	Fraxetin	Coumarin	C10 H8 O5	-2.94	208.03656	5.806	180854257	$[M+H]^+$	208421085	0.123

Table 24UHPLC-HRAMSS-based metabolic profile of leaf extract of *Nyctanthesarbor-tristis*

S.No.	Name	Class	Formula	Delta Mass [ppm]	Calc. MW	RT [min]	Area (Max.)	Analysis mode	Total area (Max.)	% Peak area
1.	9-Oxo-10(E),12(E)-octadecadienoic acid	Fatty acid	C18 H30 O3	-3.82	294.21837	10.328	233975085	$[M+H]^+$	233975084.6	0.188
2.	13(S)-HOTrE	Fatty acid	C18 H30 O3	-4.19	294.21826	10.073	1492195931	$[M-H]^-$	1492195931	1.197
3.	9S,13R-12-Oxophytodienoic acid	Prostaglandin like acid	C18 H28 O3	-3	292.20297	8.794	276260685	$[M+H]^+$	945264514	0.758
4.	Nootkatone	Sesquiterpenoid	C15 H22 O	-3.81	218.16623	9.756	228430162	$[M+H]^+$	228430162	0.183
5.	5-Hydroxymethyl-2-furaldehyde	Organic	C6 H6 O3	-2.92	126.03133	7.164	59734452	$[M+H]^+$	59734452.05	0.048
6.	D-(+)-Pyroglutamic Acid	Amino acid	C5 H7 N O3	-3.96	129.04208	0.887	157775630	$[M+H]^+$	157775630.3	0.127
7.	Citric acid	Organic acid	C6 H8 O7	-3.16	192.0264	0.929	416352897	$[M-H]^-$	416352896.8	0.334
8.	11-Aminoundecanoic acid	Amine derivative of fatty acid	C11 H23 N O2	-3.54	201.17217	0.806	1136635022	$[M+H]^+$	1136635022	0.912
9.	Luteolin	Flavonoid	C15 H10 O6	-4.55	286.04644	8.336	28648869.1	$[M-H]^-$	28648869.06	0.023
10.	Quercetin	Flavonoid	C15 H10 O7	-3.34	302.04164	7.04	151463003	$[M+H]^+$	463686334	0.372
11.	Isorhamnetin	Flavonoid	C16 H12 O7	-4.05	316.05702	7.535	88425493	$[M+H]^+$	88425493.02	0.071
12.	Kaempferol	Flavonoid	C15 H10 O6	-3.17	286.04683	6.943	227816299	$[M+H]^+$	1406049502	1.128
13.	Berberine	Alkaloid	C20 H17 N O4	-2.97	335.11476	7.209	319839632	$[M+H]^+$	319839632.4	0.257
14.	Oleic acid alkyne	Fatty acid	C18 H30 O2	-4.34	278.22337	10.623	6692643.79	$[M-H]^-$	30119526.3	0.024
15.	Gallic acid	Phenolic acid	C7 H6 O5	-2.57	170.02109	0.825	10918498	$[M-H]^-$	50635871.2	0.041
16.	D-(-)-Mannitol	Sugar	C6 H14 O6	-4.52	182.07822	0.794	2306616770	$[M-H]^-$	2454332326	1.969
17.	Ferulic acid	Phenolic acid	C10 H10 O4	-4.18	194.0571	7.361	54293870.8	$[M-H]^-$	254061558	0.204
18.	Caffeic acid	Phenolic acid	C9 H8 O4	-2.68	180.04178	4.862	84761657.3	$[M-H]^-$	648192621	0.520
19.	DL-Malic acid	Organic acid	C4 H6 O5	-4.17	134.02096	0.866	1561540294	$[M-H]^-$	1561540294	1.253
20.	9,10-Dihydroxystearic acid	Fatty acid	C18 H36 O4	-3.46	316.26026	11.525	33832765.3	$[M+H]^+$	33832765.34	0.027
21.	Acetophenone	Aromatic ketone	C8 H8 O	-2.5	120.05721	6.639	25668021	$[M+H]^+$	188812129	0.151
22.	16-Hydroxyhexadecanoic acid	Fatty acid	C16 H32 O3	-4.01	272.23405	11.298	16532523.1	$[M-H]^-$	541419160	0.434
23.	16-Oxohexadecanoic acid	Fatty acid	C16 H30 O3	-3.61	270.21852	10.911	22415716.7	$[M-H]^-$	52500577.6	0.042
24.	Oleanolic acid	Triterpenoid	C30 H48 O3	-4.36	456.35835	9.299	60666490.7	$[M+H]^+$	1604660639	1.287
25.	Citral	Monoterpene	C10 H16 O	-2.51	152.11973	7.218	159336311	$[M+H]^+$	159336311.4	0.128

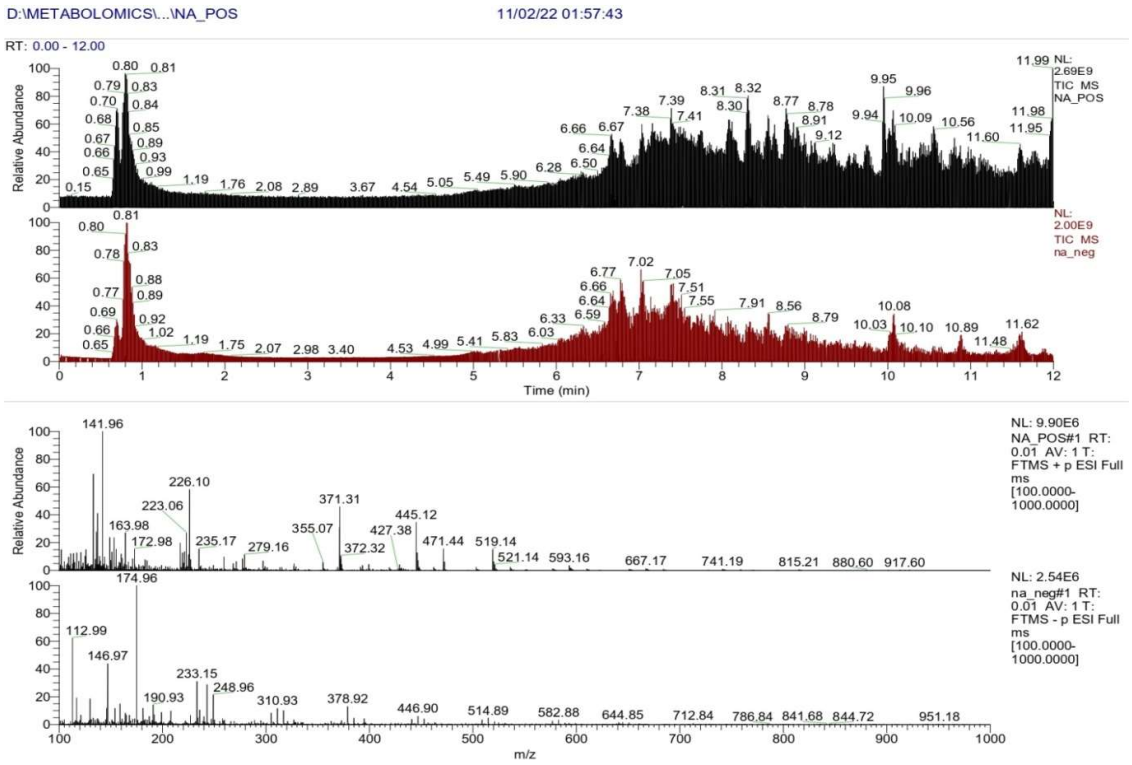

Figure30 Total ion chromatogram of whole metabolites from leaf extract of *Nyctanthesarbor-tristis*

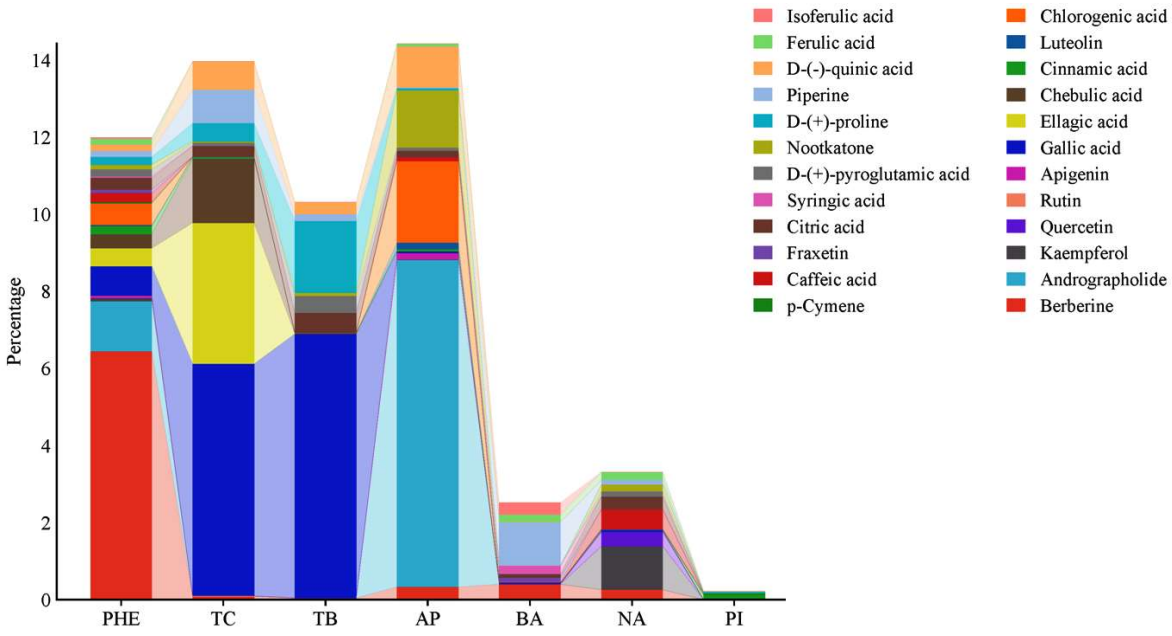

Figure31 Stack bars with fill of anti-diabetic bioactive contents of PHE

5.7.4Characterization and quantification of polyphenols

The TLC technique was modified so that it could provide a more accurate measurement of the PHE fingerprint. A strong, well-defined peak was seen at retention factors (Rf) = 0.97 for quercetin and Rf = 0.34 for rutin. Kaempferol has a distinct peak at 0.75 Rf in a different mobile phase and experiment. Spots with clear resolution were obtained after 20 minutes of saturation at room temperature in both experiments. Acomparison of the PHE chromatogram to the standard was done for the identification of kaempferol, quercetin, and rutin in PHE (Figs. 33-35). On the basis of the area under the curve and standard plot, the percentage concentration of identified constituents was estimated as kaempferol (0.12%), quercetin (0.10%), and rutin (0.31%) in the PHE chromatograms (Figs. 32, 33, and 34, respectively). The developed TLC plates were observed without derivatization at 254 nm and 366 nm under UV light. Figures 35A and 35B show the results of kaempferol standard chromatography and PHE chromatography on a TLC plate at 254 and366 nm, respectively. Figures 35C and 35D show the results for quercetin, rutin, and PHE at 254 and 366 nm, respectively.

5.7.4.1Method validation

The linear function of standard concentration (200 and 1000 ng/µL) was plotted for the calibration curve; 0.98, 0.994, and 0.997 are the correlation coefficients for kaempferol, quercetin, and rutin (Figs. 35E–G). Limits of detection (LOD) for kaempferol, quercetin, and rutin, respectively, were obtained as 202.72, 102.69, and 64.56 ng/µL. Limits of quantification (LOQ) for the same constituents found are 614.31, 311.17, and 195.62 ng/µL, respectively. These values show that the approach is precise, accurate, and sensitive enough. The spectra of the peak start, peak apex, as well as peak end regions of the spot were compared in order to determine the peak purity of each and every standard(Figs. 32-34).

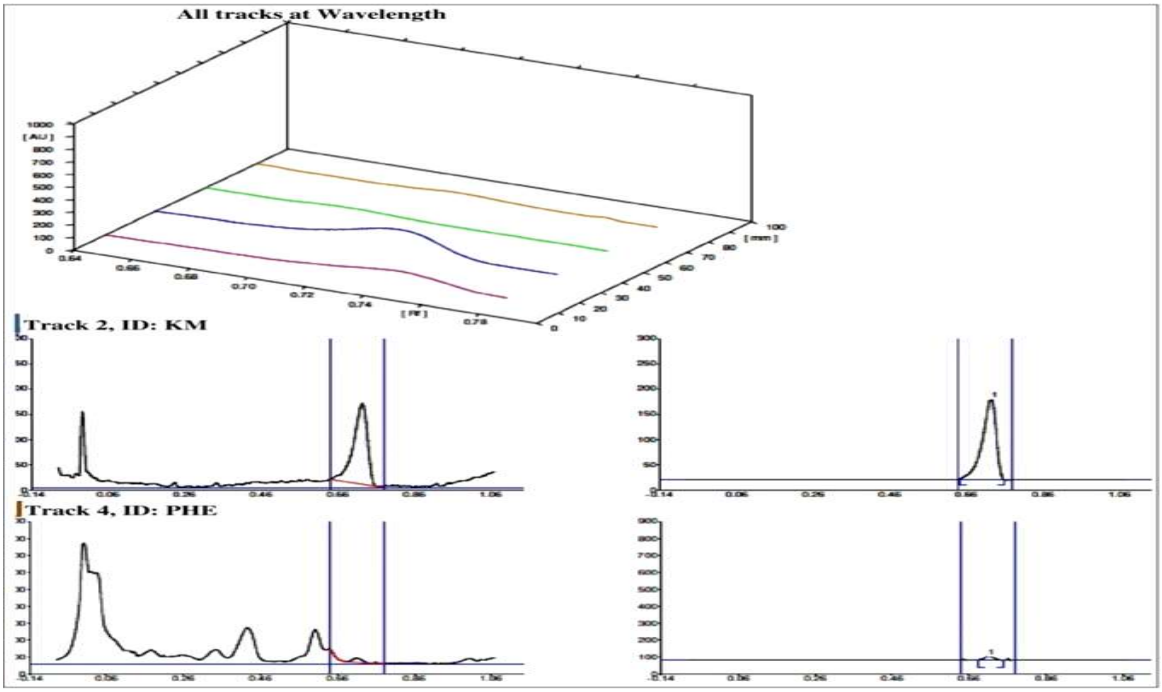

Figure 32 Overlay of HPTLC chromatogram of all tracks, at wavelength withstandard of kaempferol and PHE scanned at 254 nm

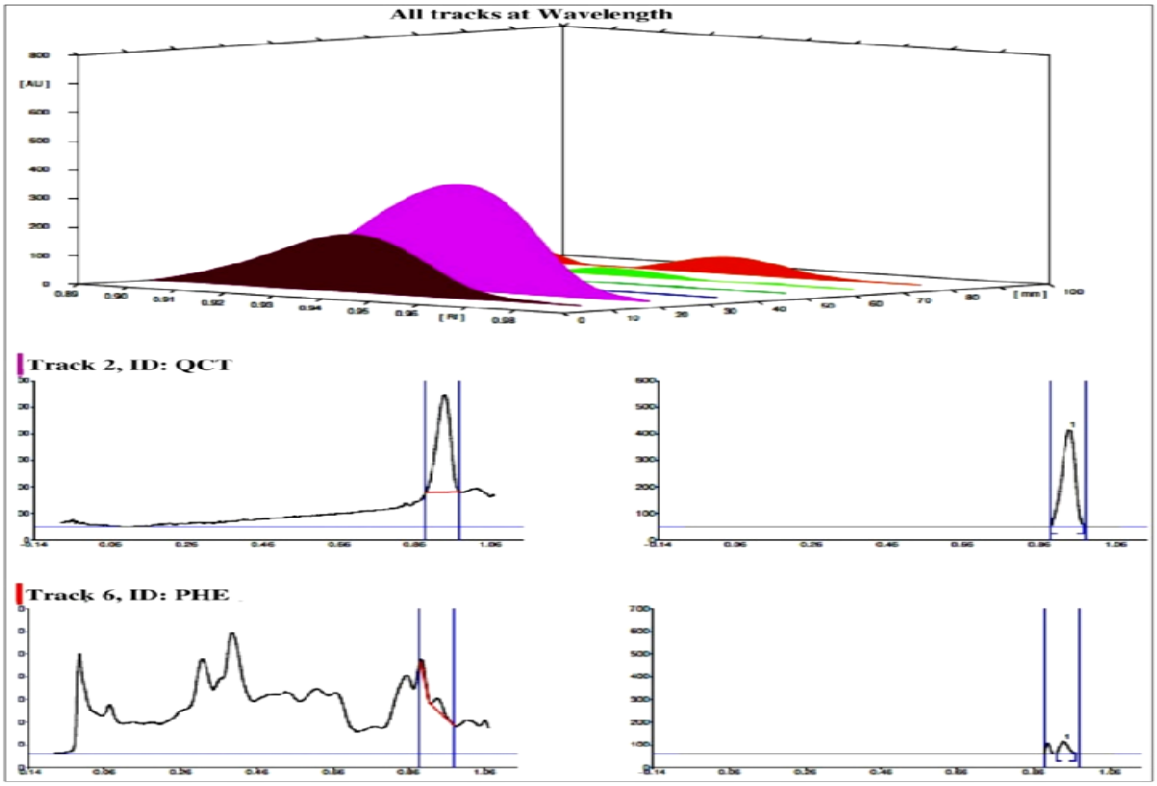

Figure 33 Overlay of HPTLC chromatogram of all tracks, at wavelength withstandard of quercetin and PHE scanned at 254 nm

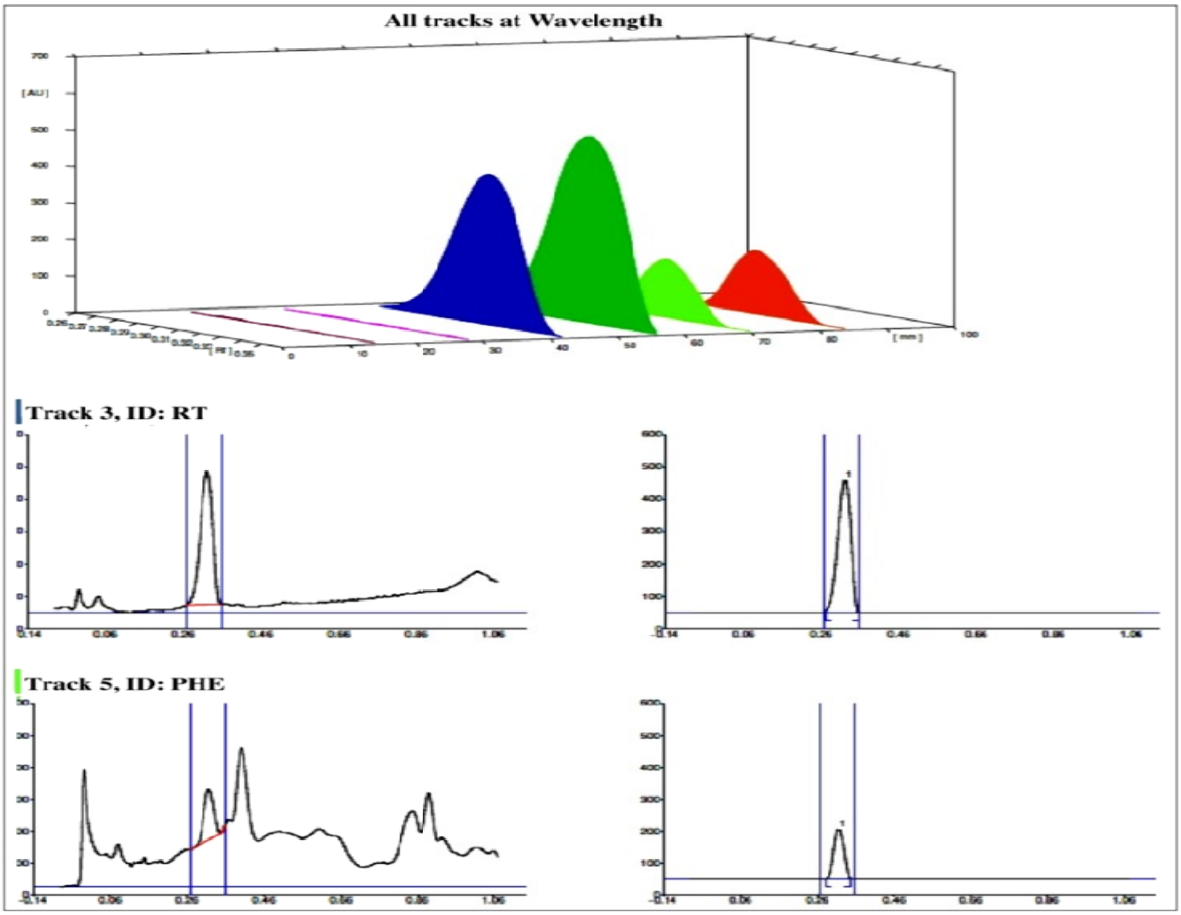

Figure 34 Overlay of HPTLC chromatogram of all tracks, at wavelength withstandard of rutin and PHE scanned at 254 nm

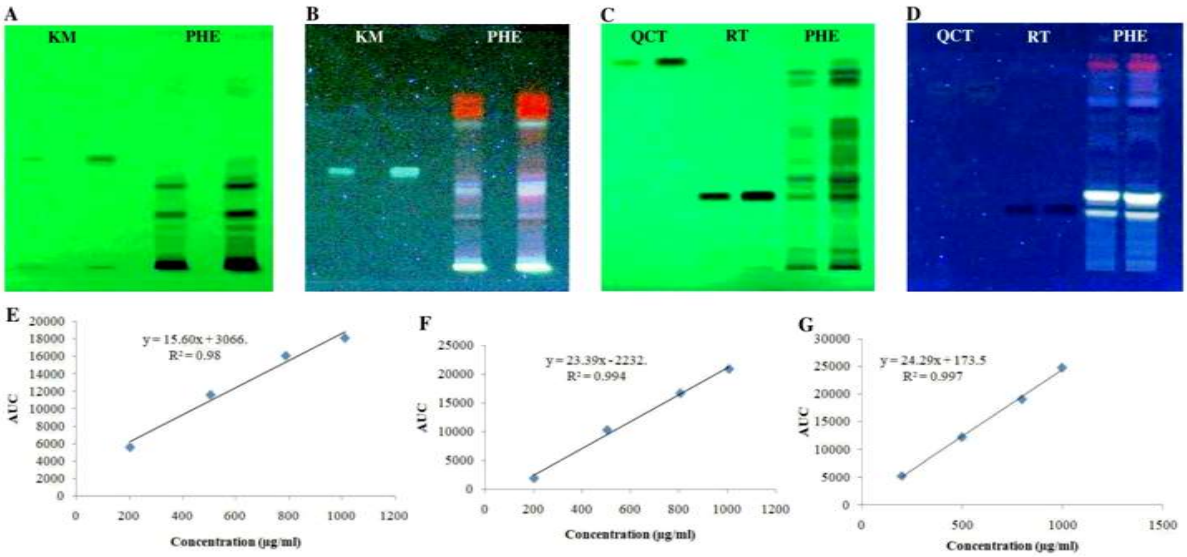

Figure 35HPTLC-images of kaempferol, quercetin, rutin and PHE scanned at 254 nm and 366 nm withstandards and standard calibration plots.

5.8Acute oral toxicity study

A dose of 2000 mg/kg of PHE orally administered to male and female rats did not result in any deaths or the development of any significant toxic symptoms in the animals. Throughout the experiment, all animals behaved normally and lived to see the completion of the 14-day period. The animals showed minimal clinical change throughout the duration of the study. Furthermore, an insignificant difference was observed between the weight gains (Table 25) and relative organ weight (Table 26) in these groups (male and female) in relation to the controls. Hematological analysis of both male and female groups showed that PHE did not cause changes in the parameters significantly listed in Table 27 and did not alter hepatic and renal functions, along with the insignificant parameters in Table 28, in relation to the control.

Table 25 Weight of rat treated with PHE

Day	PHE					
	MALE			FEMALE		
	Control	2000 mg/kg	*P	Control	2000 mg/kg	*P
1 day	151.12±4.95	150.48±3.55	0.52	150.70±3.22	150.49±3.79	0.62
7 days	175.25±5.93	179.74±6.02	0.37	169.83±6.56	175.94±4.37	0.06
14 days	204.56±3.01	208.46±4.96	0.18	186.94±3.83	197.58±8.69	0.12

The results obtained are mean ± SD (N=5) for rats/group. The differences between control and treated groups for male and female rats were evaluated byStudent's T-test and *p values were obtained.

Table 26 Relative organ weight (gm/150gm) of rat treated with PHE

PARAMETERS	PHE					
	MALE			FEMALE		
	Control	2000mg/kg	*P	Control	2000mg/kg	*P
Liver	2.64±0.04	2.59±0.06	0.09	2.07±0.03	2.04±0.05	0.58
Kidney	0.66±0.01	0.62±0.06	0.31	0.46±0.01	0.45±0.04	0.39
Heart	0.34±0.01	0.31±0.02	0.08	0.25±0.01	0.23±0.01	0.13
Spleen	0.32±0.01	0.30±0.02	0.24	0.22±0.02	0.21±0.01	0.63
Brain	0.53±0.01	0.52±0.04	0.61	0.47±0.01	0.45±0.03	0.26
Lung	0.77±0.01	0.70±0.06	0.16	0.56±0.02	0.55±0.03	0.53
Pancreas	0.38±0.06	0.37±0.03	0.66	0.24±0.02	0.23±0.01	0.26
Testis	0.49±0.02	0.45±0.07	0.34	0.03±0.00	0.03±0.00	0.16

The results obtained are mean ± SD (N=5) for rats/group. The differences between control and treated groups for male and female rats were evaluated byStudent's T-test and *p values were obtained

Table 27 Erythrogram, leukogram and platelet count of rats treated with PHE

PARAMETERS	PHE					
	MALE			FEMALE		
	Control	2000 mg/kg	*P	Control	2000 mg/kg	*P
RBC ($\times 10^6$ /µl)	5.82±0.16	5.99±0.38	0.42	5.12±0.22	5.38±0.48	0.37
WBC ($\times 10^3$ /µl)	8.02±0.11	8.12±0.08	0.37	7.07±0.40	7.67±0.70	0.07
Hgb(g /L)	120.73±2.28	121.40±2.52	0.53	124.41±3.57	129.08±1.00	0.12
HCT (%)	36.73±1.17	35.70±0.43	0.14	39.79±1.80	38.46±1.34	0.18
MCV (fL)	61.22±1.16	61.31±1.07	0.31	59.32±0.22	62.32±2.70	0.19
MCH (pg)	19.93±0.33	20.23±0.28	0.19	19.62±0.22	19.92±0.02	0.12
MCHC (g /L)	329.20±0.35	328.93±0.21	0.21	335.45±0.59	334.74±0.45	0.13
LYM ($\times 10^3$ /µl)	5.60±0.44	6.10±0.10	0.15	8.48±0.56	9.14±0.06	0.18
LYM (%)	75.14±0.14	76.17±0.96	0.19	72.31±0.32	75.80±1.19	0.05
PLT ($\times 10^3$ /µl)	872.56±87.57	992.30±32.08	0.07	994.74±8.45	997.62±12.73	0.58
MPV (fL)	6.42±0.35	6.11±0.02	0.24	5.98±0.25	6.05±0.13	0.42
GRA (%)	13.15±0.14	13.45±0.37	0.27	14.81±0.20	16.13±0.67	0.07
PLCR (%)	3.03±0.08	3.13±0.15	0.19	3.09±0.48	3.22±0.67	0.42
PDW (fL)	6.35±0.26	6.40±0.23	0.08	6.33±0.09	6.43±0.19	0.23
PCT (%)	0.48±0.02	0.52±0.04	0.28	0.35±0.00	0.34±0.01	0.25
MONO (%)	2.58±0.45	3.15±0.82	0.14	3.50±0.44	3.27±0.27	0.19
RDW (%)	14.31±1.06	15.90±0.21	0.15	14.51±0.55	14.84±0.30	0.42

The results obtained are mean ± SD (N=5) for rats/group. The differences between control and treated groups for male and female rats were evaluated byStudent's T-test and **p* values were obtained

Table 28 Biochemical parameters of rats treated with single dose of PHE

PARAMETERS	PHE					
	MALE			FEMALE		
	Control	2000 mg/kg	*P	Control	2000 mg/kg	*P
ALT (U/L)	60.63±6.28	68.61±2.69	0.06	57.41±4.97	61.36±2.71	0.12
AST (U/L)	106.82±11.40	127.82±15.66	0.06	113.79±8.80	138.17±18.65	0.05
TP (g /L)	62.13±5.24	66.29±8.40	0.17	57.63±1.71	56.72±0.62	0.29
ALP (U/L)	166.99±27.04	204.87±6.03	0.17	141.64±32.08	178.30±39.96	0.05
TBIL (µmol/L)	4.91±0.49	5.21±0.70	0.40	6.00±0.18	6.38±0.56	0.23
ALB (g/L)	20.65±2.74	24.04±1.54	0.12	26.57±2.60	28.74±1.75	0.07
UR (mg/dl)	22.61±0.86	24.63±2.44	0.32	24.69±1.25	29.41±5.17	0.17
CRE (mg /dl)	0.42±0.02	0.46±0.03	0.06	0.33±0.01	0.36±0.03	0.16
Ca (mg /dl)	10.19±0.17	11.57±1.33	0.18	10.07±0.05	10.73±0.36	0.07
P (mg /dl)	9.50±0.41	10.64±0.41	0.06	9.38±0.32	9.89±0.98	0.33
UA (mg /dl)	6.12±0.05	6.15±0.05	0.38	6.20±0.14	6.25±0.31	0.65
Na (mEq/L)	138.23±1.39	139.45±1.55	0.06	136.58±0.94	137.58±1.39	0.06
K (mEq/L)	4.68±0.27	4.91±0.95	0.65	5.48±0.47	6.29±0.91	0.09
Cl (mEq/L)	96.53±0.36	97.20±0.60	0.08	96.57±0.73	97.57±0.75	0.06
TC (mg /dl)	62.39±0.45	61.15±0.33	0.06	58.31±0.31	54.51±1.29	0.05
TG (mg /dl)	67.07±1.20	65.40±3.51	0.42	77.07±0.90	76.40±1.44	0.53
HDL (mg /dl)	22.71±0.70	22.04±0.84	0.18	23.47±0.42	23.00±0.81	0.25
LDL (mg /dl)	26.47±0.51	26.80±0.74	0.42	16.33±0.71	16.50±0.93	0.74
VLDL (mg /dl)	13.24±0.47	13.04±0.17	0.42	14.94±0.21	14.54±0.73	0.32

The results obtained are mean ± SD (N=5) for rats/group. The differences between control and treated groups for male and female rats were evaluated by Student's T-test and *p values were obtained

5.9 Sub-acute oral toxicity study

The sub-acute toxicity study showed that repeated administration of PHE to female and male rats for up to 28 days did not produce any major clinical signs of toxicity or death. The animals performed normally throughout the study and lived beyond the end of the experiment after 28 days. During the experimental study, changes in food, water intake, and body weight in the treated groups were found to be insignificant when compared to the control groups. There was an insignificant rise in the body weight (Tables 29) of rats treated with PHE at the 7th, 14th, 21st, and 28th days of treatment doses, as well as the relative organ weight of the kidney, heart, spleen, lung, and ovary (Tables 30) of rats treated with PHE doses. This suggests that there was no hazardous effect on the sub-acute administration of PHE doses.

5.9.1Hematological and serum biochemical analyses

In comparison to the control, no significant differences were observed in the hematological parameters of the rat, including hematocrit (HCT), white blood cells (WBC), platelets, hemoglobin (Hgb), mean red cell volume (MCV), monocytes, red blood cells (RBC), procalcitonin test (PCT), mean cell hemoglobin concentration (MCHC), as well as platelet distribution width (PDW) (Table 31). HDL, LDL, TG, and total cholesterol all show no significant changes when compared to the control group that was treated with PHE. As the levels of urea in the blood increase, this is an indication of renal impairment because urea is the primary byproduct of protein metabolism. There were no significant changes in renal parameters in this study. Further, p values for KFT parameters such as TBIL, P, ALP, BUN, and FBG are shown to be insignificant with regard to the control provided (Table 32). An important part of any toxicity study to evaluate liver damage caused by drugs or any other type of hepatotoxin is the evaluation of the levels of the enzymes alanine aminotransaminasterase (ALT) as well as aspartate aminotransaminasterase (AST). The transaminase markers AST and ALT, which are indicators of hepatocellular injury, did not show any significant differences in the PHE-treated groups compared to the control group in this study (Table 32).

Table 29 Body weight of rats treated with repeated doses of PHE

Day		PHE						
	Sex	Control	100 mg/kg	*P	200 mg/kg	*P	400 mg/kg	*P
1 day	F	150.37±4.03	150.42±3.53	0.94	150.74±3.18	0.64	150.41±5.11	0.96
	M	150.33±2.89	150.00±3.61	0.67	150.00±4.58	0.81	150.67±5.03	0.87
7 days	F	175.06±6.19	180.79±5.12	0.06	175.71±5.14	0.42	177.77±2.53	0.34
	M	175.33±5.51	159.67±3.22	0.01	174.67±2.52	0.77	177.00±4.58	0.55
14 days	F	186.75±3.05	192.36±6.51	0.11	183.43±4.46	0.06	193.42±6.05	0.07
	M	187.00±1.00	190.00±5.57	0.51	180.67±4.51	0.19	189.33±5.13	0.58
21 days	F	204.70±1.52	206.49±6.00	0.62	213.77±5.45	0.10	215.10±4.55	0.06
	M	205.67±2.08	202.00±7.55	0.58	201.00±5.57	0.35	212.67±2.08	0.09
28 days	F	213.47±2.56	219.53±5.40	0.07	219.05±5.98	0.19	223.40±7.69	0.08
	M	213.00±2.65	217.33±3.79	0.02	224.33±6.51	0.04	227.67±6.66	0.02

The results obtained are mean ± SD (N=5) for rats/group. The differences between control and treated groups for female rats were evaluated byStudent's T-test and **p* values were obtained. F = female and M = male

Table 30 Relative organ weight (gm/150gm) treated with repeated doses of PHE

PARAMETERS		PHE						
	Sex	Control	100 mg/kg	*P	200 mg/kg	*P	400 mg/kg	*P
Liver	F	2.16±0.12	2.06±0.04	0.39	2.13±0.08	0.36	2.18±0.08	0.88
	M	2.14±0.12	2.04±0.03	0.36	2.13±0.02	0.97	2.16±0.07	0.83
Kidney	F	0.46±0.01	0.43±0.03	0.05	0.45±0.03	0.03	0.50±0.03	0.08
	M	0.45±0.02	0.44±0.01	0.42	0.45±0.01	0.64	0.49±0.02	0.17
Heart	F	0.25±0.01	0.24±0.01	0.09	0.23±0.01	0.06	0.25±0.03	0.97
	M	0.25±0.02	0.25±0.01	0.84	0.24±0.01	0.46	0.25±0.03	0.74
Spleen	F	0.18±0.00	0.15±0.03	0.22	0.16±0.01	0.05	0.22±0.01	0.00
	M	0.17±0.01	0.14±0.03	0.20	0.15±0.01	0.01	0.22±0.02	0.02
Brain	F	0.47±0.01	0.45±0.00	0.07	0.46±0.01	0.06	0.47±0.01	0.85
	M	0.47±0.02	0.46±0.01	0.74	0.46±0.01	0.74	0.47±0.02	0.95
Lung	F	0.51±0.05	0.88±0.01	0.01	0.65±0.02	0.03	0.53±0.02	0.43
	M	0.50±0.05	0.90±0.06	0.02	0.66±0.02	0.02	0.53±0.03	0.48
Pancreas	F	0.18±0.01	0.19±0.00	0.72	0.18±0.02	0.56	0.19±0.01	0.37
	M	0.18±0.01	0.18±0.02	0.83	0.19±0.03	0.67	0.20±0.01	0.04
Ovary	F	0.04±0.00	0.03±0.00	0.01	0.02±0.00	0.01	0.04±0.00	0.12
	M	0.51±0.04	0.51±0.05	1.00	0.50±0.07	0.80	0.51±0.04	1.00

The results obtained are mean ± SD (N=5) for rats/group. The differences between control and treated groups for female rats were evaluated byStudent's T-test and **p* values were obtained.F = female and M = male

Table 31 Erythrogram, leukogram and platelet count treated with repeated doses of PHE

PARAMETERS		PHE						
	Sex	Control	100 mg/kg	*P	200 mg/kg	*P	400 mg/kg	*P
RBC ($\times10^6$ /µl)	F	6.21±0.19	7.03±0.82	0.15	7.50±1.31	0.18	7.99±0.93	0.05
	M	6.27±0.17	7.20±0.73	0.10	7.60±0.41	0.04	8.32±0.52	0.01
WBC ($\times10^3$ /µl)	F	8.41±1.57	6.28±1.94	0.05	14.49±4.33	0.06	12.48±3.31	0.06
	M	8.60±1.82	6.47±1.71	0.04	14.66±0.58	0.01	12.68±0.36	0.04
Hgb(g /L)	F	104.04±7.39	121.00±23.00	0.20	133.30±24.21	0.10	135.09±20.66	0.06
	M	104.71±8.89	123.37±13.96	0.02	133.30±10.12	0.00	137.06±2.49	0.03
HCT (%)	F	37.03±2.01	32.54±6.02	0.19	36.21±7.21	0.81	36.76±2.32	0.39
	M	36.68±0.75	31.49±1.71	0.01	37.51±2.97	0.62	36.69±0.74	0.99
MCV (fL)	F	45.82±1.88	46.26±2.05	0.10	47.24±1.09	0.09	46.51±0.92	0.34
	M	46.06±0.70	46.90±0.85	0.40	47.40±0.25	0.13	46.55±0.65	0.53
MCH (pg)	F	16.77±0.57	17.20±2.86	0.78	17.45±1.57	0.37	16.93±0.61	0.16
	M	16.70±0.29	17.74±1.46	0.26	17.60±0.48	0.18	16.66±0.36	0.94
MCHC (g /L)	F	366.03±7.28	372.48±19.17	0.45	382.94±15.41	0.07	367.02±3.40	0.70
	M	366.57±2.52	373.12±7.48	0.37	382.50±6.35	0.02	366.78±0.81	0.91
LYM ($\times10^3$ /µl)	F	6.71±0.25	5.40±1.31	0.17	7.40±1.16	0.32	6.90±0.20	0.08
	M	6.69±0.10	5.58±1.23	0.24	7.65±0.37	0.03	6.88±0.18	0.06
PLT ($\times10^3$ /µl)	F	986.15±4.89	1043.17±45.21	0.13	1037.14±37.22	0.11	1042.81±43.55	0.13
	M	991.13±4.97	1036.40±27.62	0.12	1037.97±13.91	0.04	1044.48±19.91	0.06
MPV (fL)	F	6.93±0.08	6.74±0.26	0.22	6.60±0.32	0.15	7.00±0.04	0.15
	M	7.02±0.09	6.93±0.28	0.53	6.63±0.19	0.02	7.20±0.19	0.37
GRA (%)	F	1.30±0.26	1.39±0.15	0.29	1.42±0.20	0.07	1.32±0.25	0.07
	M	1.31±0.16	1.40±0.05	0.34	1.47±0.08	0.27	1.38±0.04	0.60
PDW (fL)	F	5.60±0.35	6.96±0.92	0.05	6.78±0.92	0.08	5.90±0.12	0.16
	M	5.63±0.13	6.99±0.10	0.01	6.87±0.13	0.01	6.06±0.17	0.09
PCT (%)	F	0.32±0.01	0.79±0.19	0.05	0.49±0.08	0.05	0.31±0.02	0.14
	M	0.32±0.00	0.79±0.17	0.04	0.52±0.01	0.00	0.31±0.01	0.01
MONO (%)	F	0.44±0.03	0.50±0.07	0.12	0.42±0.08	0.56	0.38±0.06	0.07
	M	0.43±0.01	0.51±0.03	0.02	0.44±0.01	0.06	0.39±0.02	0.03
RDW (%)	F	14.00±0.17	16.60±2.21	0.16	14.33±0.69	0.40	14.17±0.26	0.10
	M	14.14±0.17	16.49±0.63	0.03	14.56±0.19	0.15	14.18±0.03	0.69

The results obtained are mean ± SD (N=5) for rats/group. The differences between control and treated groups for female rats were evaluated byStudent's T-test and **p* values were obtained.F = female and M = male

Table 32 Biochemical parameters treated orally with repeated doses of PHE

PARAMETERS		PHE						
	Sex	Control	100 mg/kg	*P	200 mg/kg	*P	400 mg/kg	*P
TBIL (mg/dl)	F	0.47±0.04	0.55±0.17	0.47	0.53±0.03	0.17	0.47±0.03	0.91
	M	0.49±0.08	0.63±0.09	0.02	0.55±0.01	0.31	0.50±0.04	0.82
AST (U/L)	F	172.97±12.48	178.30±5.73	0.45	170.20±17.82	0.77	165.13±14.73	0.44
	M	171.86±8.57	177.97±1.82	0.33	172.57±11.61	0.88	160.70±13.75	0.17
ALT (U/L)	F	43.78±6.25	48.11±6.10	0.21	43.61±8.79	0.99	42.14±6.08	0.57
	M	43.94±2.45	49.48±1.67	0.02	44.18±6.00	0.96	41.54±5.22	0.44
ALP (U/L)	F	212.07±34.58	319.64±42.44	0.02	183.30±15.87	0.38	161.63±13.29	0.16
	M	213.54±19.27	299.24±41.43	0.02	194.25±8.88	0.10	164.68±4.53	0.04
TP (mg/dl)	F	5.09±1.24	5.08±1.01	0.99	5.05±0.32	0.97	4.62±0.54	0.56
	M	5.31±0.81	5.43±0.06	0.82	5.40±0.47	0.90	5.35±0.11	0.94
ALB (mg/dl)	F	2.52±0.47	2.55±0.18	0.92	2.38±0.31	0.58	1.88±0.17	0.11
	M	2.61±0.08	2.65±0.06	0.57	2.63±0.10	0.23	2.61±0.14	0.98
GLB (mg/dl)	F	2.69±0.41	2.74±0.17	0.85	2.67±0.18	0.95	2.53±0.19	0.57
	M	2.56±0.19	2.93±0.05	0.10	2.68±0.20	0.57	2.56±0.23	0.99
FBG (mg/dl)	F	94.29±0.81	98.65±0.38	0.02	92.69±1.20	0.30	89.67±3.85	0.12
	M	95.08±0.06	99.25±1.20	0.03	92.26±0.42	0.01	89.27±3.91	0.12
BUN (mg/dl)	F	14.53±0.35	15.45±0.51	0.05	15.03±0.22	0.24	11.46±0.95	0.05
	M	14.51±0.10	15.60±0.17	0.01	15.02±0.16	0.07	12.00±0.86	0.04
CRE (mg /dl)	F	0.51±0.06	0.55±0.09	0.58	0.50±0.05	0.89	0.46±0.06	0.42
	M	0.52±0.04	0.55±0.03	0.52	0.51±0.05	0.78	0.46±0.03	0.25
Ca (mg /dl)	F	7.32±0.70	7.34±0.32	0.96	7.52±0.12	0.65	7.38±0.09	0.89
	M	7.53±0.07	7.64±0.14	0.28	7.51±0.03	0.51	7.36±0.08	0.01
P (mg /dl)	F	8.37±0.33	8.93±0.50	0.34	7.65±0.75	0.10	6.70±0.84	0.06
	M	8.41±0.10	9.02±0.29	0.03	8.65±0.13	0.15	8.43±0.28	0.87
UA (mg /dl)	F	2.69±0.23	2.81±0.16	0.40	2.58±0.07	0.46	2.37±0.11	0.10
	M	2.72±0.22	2.77±0.08	0.76	2.62±0.14	0.34	2.50±0.04	0.24
TC (mg /dl)	F	87.24±0.14	86.54±0.25	0.07	84.31±1.15	0.05	81.56±3.05	0.09
	M	88.21±0.15	88.23±0.28	0.93	86.74±0.52	0.02	82.30±2.96	0.08
HDL (mg /dl)	F	29.60±0.27	32.23±1.26	0.07	34.77±1.29	0.03	38.97±0.75	0.00
	M	29.68±0.26	32.22±1.40	0.08	34.92±1.64	0.02	37.77±3.42	0.05
LDL (mg /dl)	F	39.27±0.84	38.74±0.29	0.26	37.65±1.34	0.06	35.39±0.48	0.01
	M	39.24±0.86	39.03±0.36	0.63	38.32±0.98	0.01	36.06±0.88	0.00
VLDL(mg/dl)	F	13.80±0.98	13.74±0.26	0.92	12.92±0.15	0.29	12.24±0.24	0.10
	M	13.94±0.85	13.84±0.23	0.84	13.01±0.15	0.23	12.44±0.16	0.11
TG (mg /dl)	F	69.62±0.72	68.80±0.23	0.12	66.02±1.52	0.07	61.97±2.17	0.02
	M	69.78±0.73	68.98±0.49	0.17	66.48±1.67	0.11	63.54±1.57	0.01

The results obtained are mean ± SD (N=5) for rats/group. The differences between control and treated groups for female and male rats were evaluated byStudent's T-test and *p values were obtained. F = female and M = male

5.9.2Histopathological analyses of vital organs

The histopathological examinations show no significant weight changes and normal architectural changes in the vital organs such as the heart, brain, kidneys, liver, lungs, pancreas, ovary, and spleen, suggesting that PHE is free from the risk of serious organ

degenerative potential at all dose levels. The kidneys showed no histopathological degenerative symptoms in a rat treated with PHE. The lobular architecture of the kidneys was maintained, and the medullary pyramids were shielded by the cortical tissue that covered them. The Bowman capsules were finely distributed throughout the cortex. From a histological point of view, the Henle loop, collecting ducts, proximal and distal twisted tubules, and the collecting duct did not have any unique, noticeable features. Inflammation or fibrosis was not found in the interstices (Fig. 36).

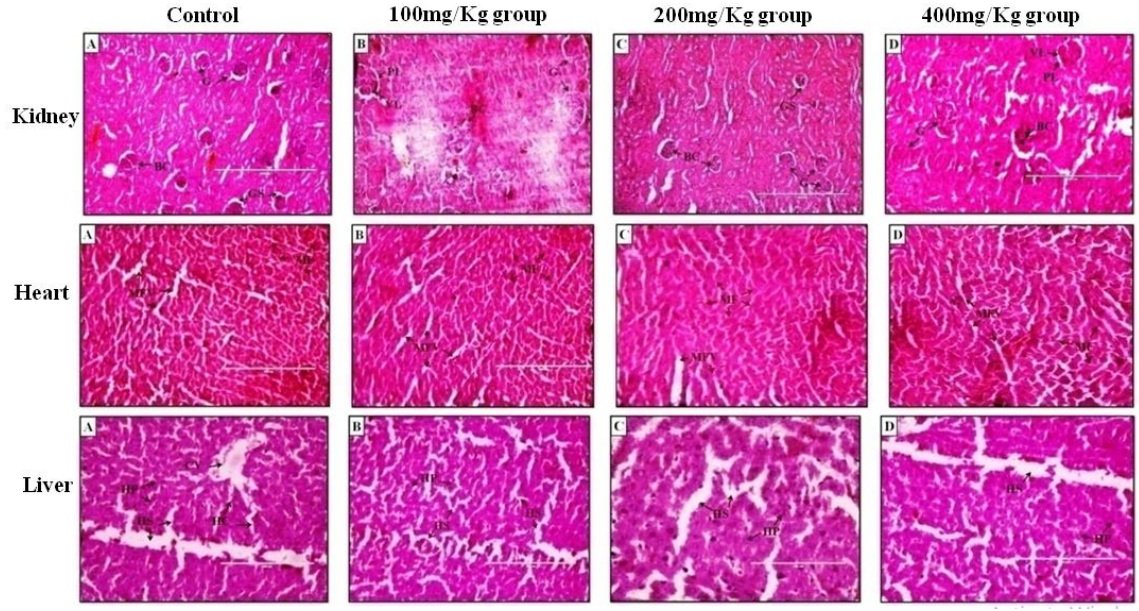

Figure 36 Images showing histology of the vital organs kidneys, heart and liver of rats treated with PHE doses. **A**) Control group;**B**) Treated dose 100mg/Kg group;**C**) Treated dose 200mg/Kg group;**D**) Treated dose 400mg/Kg group; (G: Glomerulus; BC: Bowman's capsule; GS: Glomerular space; PL: Parietal layer; VL: Visceral layer; MF: Cardiac muscle fibers; MFV: Cardiac muscle fiber vacuolation; CV: Central vein; HP: Hepatocytes; HS: Hepatic sinusoids and HC: Hepatic cord)

Heart muscle cells with transverse striations and single or double nuclei in the center were used to represent the myocardium. Vascular cavities and the heart valves are covered by a thin basal membrane of endothelium. The mesothelial pavement cells that coat the epicardium were completely preserved (Fig. 36). Regularly distributed hepatocyte cords as well as sinusoid capillaries in the liver parenchyma (the lobular center vein encircled by hepatic cell cords and capillaries) were observed. Despite its polygonal shape and spherical nucleus, the liver cell maintained its centralized, fully preserved nucleus and cytoplasm (Fig.

36). The morphological architecture of the lungs of rats in all experimental groups was found to be normal, with no treatment-related pathological changes, and to be similar to that of the rats in the normal control (Fig. 37). The histological analysis of the spleen was also the same as that of the control group (Fig.37). Histopathological examination of pancreatic histological sections from rats in all test groups showed that there were no pathological differences between the treatment and control groups (Fig. 37). When a piece of brain tissue was compared to a healthy control, there were no abnormalities, which showed that the histological assessment was correct (Fig. 37).

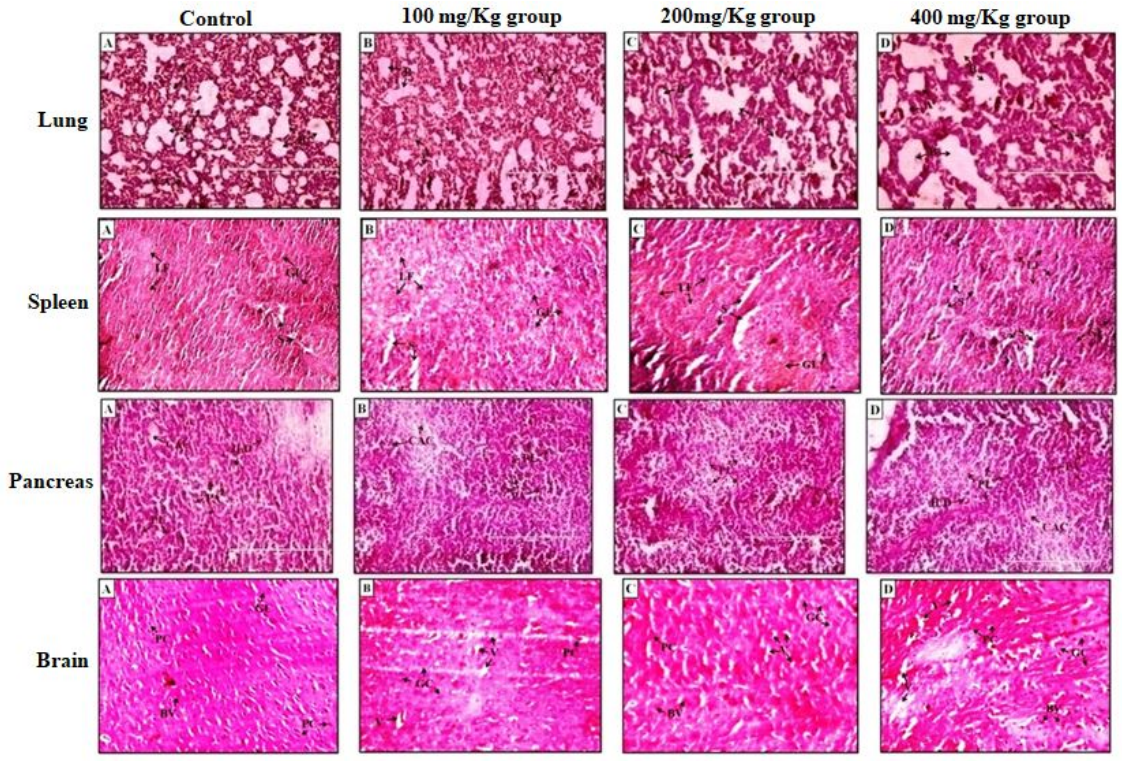

Figure37 Images showing histology of the lung, spleen, pancreas and brain of rats treated with PHE doses. **A**) Control group;**B**) Treated dose 100mg/Kg group;**C**) Treated dose 200mg/Kg group;**D**) Treated dose 400mg/Kg group; (A: Alveoli; B: Bronchiole;LF: Lymphoid follicles; GL: Granular leukocytes; S: Sinusoids;CAC: Centroacinar cells; ILD: Intralobular duct; PA: Pancreatic acini; PL: Pancreatic lobule;PC: Pyramidal cells; GC: Glial cells; BV: Blood vessels and V: Vacuolization)

5.10.1OGTT in STZ induced DM

Figure38displays the glucose tolerance as determined by the OGTT experiment. Blood glucose levels in control rats increased for 30 minutes before returning to normal levels under physiological hormonal regulation. Diabetic rats, on the other hand, had an altered glucose tolerance that did not return to normal. PHE, metformin, and DMR dosages administered to diabetic rats improved glucose tolerance significantly (Fig.38).

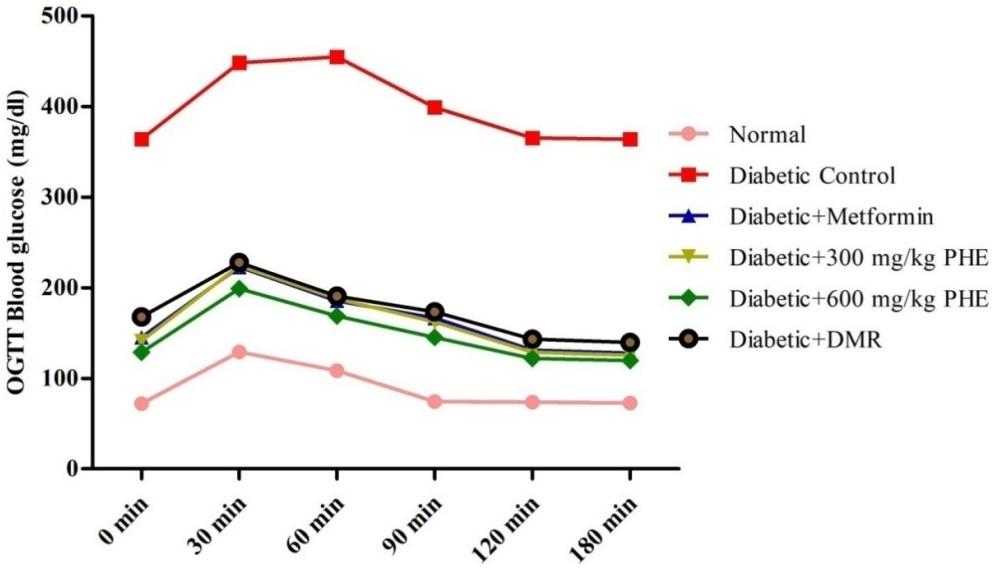

Figure38OGTT blood glucose levels of streptozotacin-induced diabetic rats after oral administration of PHE. Data are expressed as mean ± SEM (n = 6). *** Statistically significant ($p < 0.0001$) between diabetic to treatment group.PHE: Poly herbal extract; DMR: dabur madhu rakshak

5.10.2Body weight of diabetic rats administered PHE

The animals' body weights dropped significantly after streptozotocin treatment (Fig. 39), in contrast to the normal control group, which gained weight. Diabetic rats treated with PHE at doses of 300 mg/kg and 600 mg/kg gained weight significantly. The body weight of the PHE 300 mg/kg and PHE 600 mg/kg treatment rats groups increased more significantly than that of the metformin and DMRtreatment rats groups (Table 33). Diabetic rats exhibited a therapeutic change, as evidenced by a dose-dependent alteration in body weight across treatment groups.

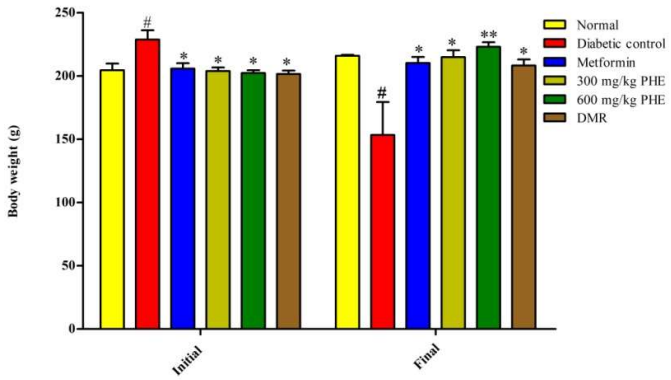

Figure 39 Effect of PHE on body weight.Data are expressed as mean ± SEM (n = 6). *Statistically significant(p < 0.05) to diabetic control; #statistically significant (p < 0.05) to normal; ** P < 0.01 is considered as very significant

Table 33 Body weight of streptozotacin-induced diabetic rats before and after oral administration of PHE

Treatment group	Initial weight (g)	Final weight (g)	Alteration in weight
Normal control	204.52±9.20	215.85±1.49	11.33 ↑
Diabetic control	228.69±12.69#	153.36±45.01#	-75.33 ↓
Diabetic + metformin (250 mg/kg)	205.84±7.31*	210.18±8.34*	4.33 ↑
Diabetic + PHE (300mg/kg)	203.87±4.99*	214.87±9.42*	11.00 ↑
Diabetic + PHE (600mg/kg)	202.34±3.70*	223.04±6.26**	20.70 ↑
Diabetic + DMR (1700mg/kg)	201.52±4.65*	208.18±8.42*	6.67 ↑

Data are expressed as mean ± SEM (n = 6). *Statistically significant(p < 0.05) to diabetic control; #statistically significant (p < 0.05) to normal; ** P < 0.01 is considered as very significant.PHE: Poly herbal extract; Weight loss (↓);Weight gain (↑).

5.10.3Fasting blood glucose level

Male rats in the untreated group had FBG levels above 250 mg/dl for the entirety of the experiment, even after 72 hours of streptozotocin induction (Fig. 40). PHE at 300 mg/kg, 600 mg/kg, metformin at 250 mg/kg, and DMR at 1700 mg/kg body weight all reduced FBG levels, as seen in Figure 40. FBG levels were reduced to levels similar to those in the non-diabetic group in the groups of rats given PHE at 300 mg/kg and 600 mg/kg, as well as metformin and DMR (Fig. 40). PHE was found to be more effective than metformin and DMR in lowering FBG levels in the present animal models. At 600 mg/kg of body weight, we saw the greatest change in FBG levels.

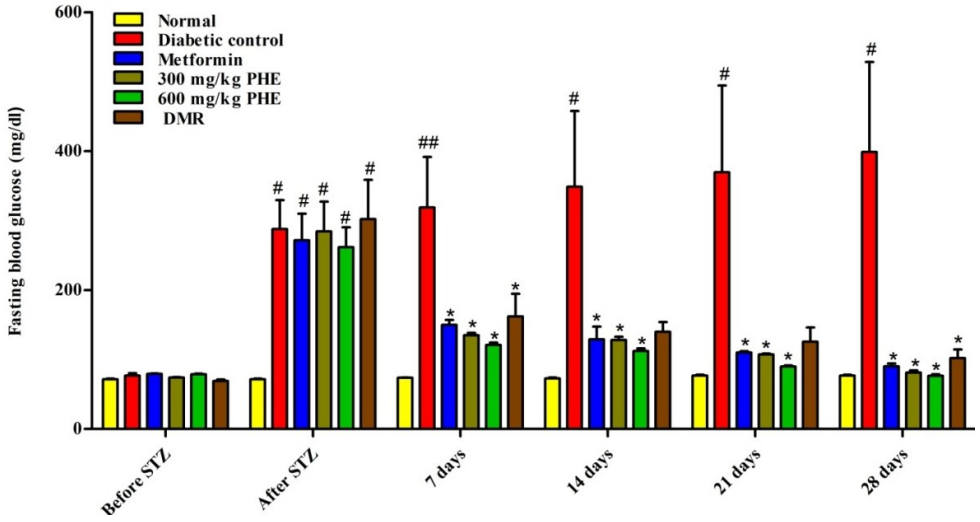

Figure 40 Effect of PHE on fasting blood glucose level.Data are expressed as mean ± SEM (n = 6). *Statistically significant ($p < 0.05$) to DC; # statistically significant ($p < 0.05$) to NC;## $P < 0.01$ is considered as very significant.PHE: Poly herbal extract; DMR: dabur madhu rakshak

5.10.4Serum HbA1c, insulin, HOMA‑IR, HOMA‑ β and biochemical levels of diabetic rats administered PHE

Glycated hemoglobin (HbA1c) is a measure of blood glucose's effect on hemoglobin and the blood oxygen transport protein. The normal range is between 6.0 and 6.5, whereas anything beyond 6.5 indicates diabetes. In this investigation, PHE, metformin, and DMR dosages all reduced the elevated HbA1c (above 6.5) seen in diabetic rats (Fig. 41A). This may be because the glycation process was stifled by the reduced blood glucose levels brought about by PHE, metformin, or DMR.The results showed that the blood insulin and HOMA-β levels of the untreated diabetics significantly decreased, but the HOMA-IR levels increased significantly. Blood insulin (Fig. 41B) and HOMA-β (Fig. 41C) levels became higher, whereas the HOMA-IR (Fig. 41D) levels dropped significantly in PHE (300 and 600 mg/kg), metformin (250 mg/kg), and DMR (1700 mg/kg)-treated rats.

In this study, diabetic control rats had muchhigher serum ALT levels (Fig. 41E), AST levels (Fig. 41F), ALP levels (Fig. 41G), TP concentrations (Fig. 41H), UA limits (Fig. 41I), CRE limits (Fig. 41J), and BUN levels (Fig. 41K) than normal rats. But diabetic rats given 300 mg/kg PHE, 600 mg/kg PHE, metformin, and DMR for 28 days had much lower serum levels.

5.10.5Serum lipid parameters in experimental rats

Streptozotocin administration resulted in an increase in LDL, VLDL, TC, and TG levels, while HDL levels decreased. Figures 41L, 41M, 42A, and 42B show that rats treated with 300 mg/kg of PHE, 600 mg/kg of PHE, 250 mg/kg of metformin, or 1700 mg/kg of DMR had lower levels of TC, TG, LDL, and VLDL, respectively. This was not the case in rats that had diabetes and were given any treatment. In comparison to diabetic control rats, the PHE treatment dosages increased serum levels of HDL more significantly than others (Fig.42C).

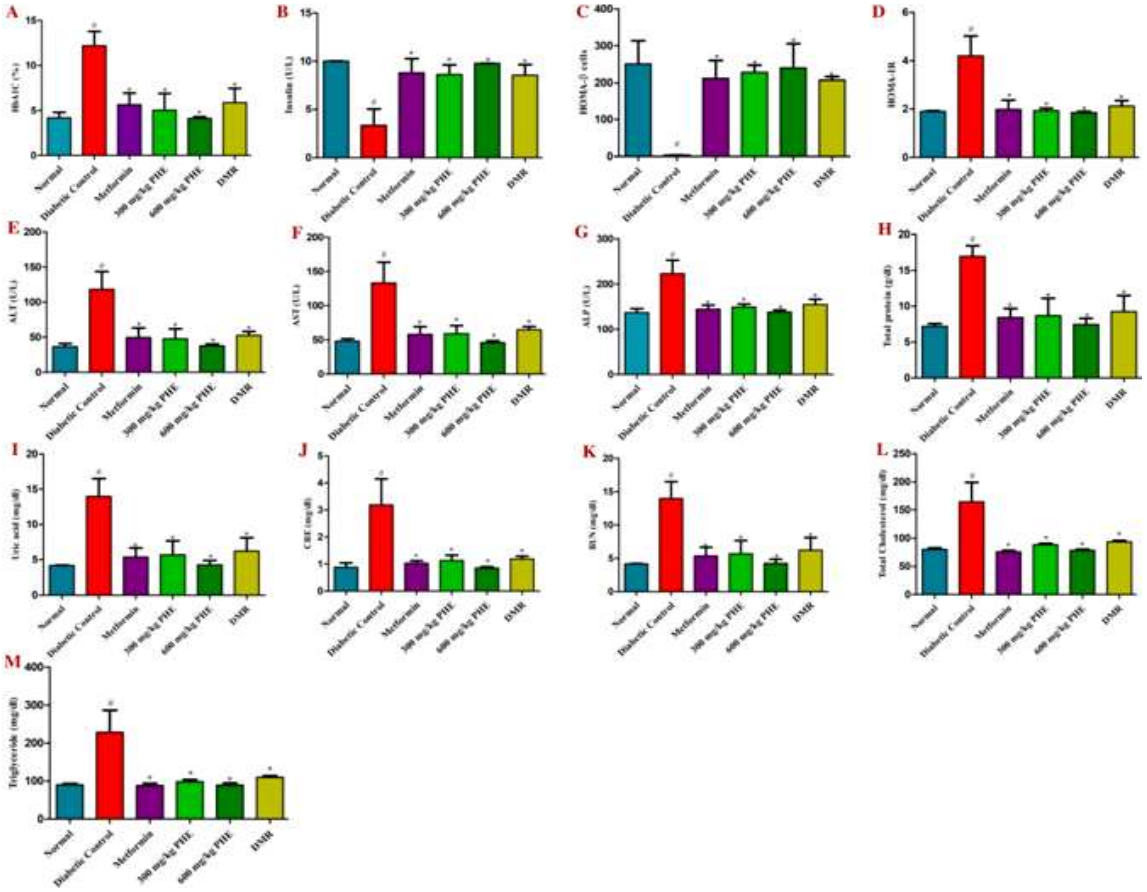

Figure41 Theeffects of PHE on *in-vivo* diabetic-parameters of streptozotacin-induced diabetic rats. **A**) HbA1C, **B**) Insulin, **C**) HOMA-β cells, **D**)HOMA-IR, **E**) ALT, **F**) AST, **G**) ALP, **H**) TP, **I**) UA, **J**) CRE, **K**) BUN levels, **L**) Total cholesterol, and **M**) Triglyceride. Data are expressed as mean ± SEM (n = 6). *Statistically significant ($p < 0.05$) to DC; # statistically significant ($p < 0.05$) to NC.PHE: Poly herbal extract; DMR: dabur madhu rakshak; HbA1c: hemoglobin A1c (glycated hemoglobin); HOMA-IR: homeostatic model assessment of insulin resistance; HOMA-β: homeostatic model assessment of β-cell function;ALT: alanine transaminase; AST: aspartate aminotransferase; ALP: alkaline phosphatase; TP: total protein; UA: uric acid; CRE: creatinine; BUN: blood urea nitrogen

5.10.6Antioxidant markers level

When diabetic rats were given PHE or metformin, the liver enzyme activities of catalase (CAT; Fig. 42D), superoxide dismutase (SOD; Fig. 42E), and reduced glutathione (GSH; Fig. 42F) were opposite to those of untreated diabetic rats. In contrast to the increased levels in the uncontrolled diabetic rats, lipid peroxidation (MDA; Fig. 42G) concentrations decreased after treatment with PHE or metformin, and the findings for PHE were dose-dependent. Antioxidant indicators in the pancreas, including CAT (Fig. 42H), SOD (Fig. 42I), and GSH (Fig. 42J), were significantly higher after PHE therapy. In addition, PHE and metformin treatment resulted in lower levels of malondialdehyde (MDA) in the pancreatic tissues compared to uncontrolled diabetic rats (Fig. 42K).

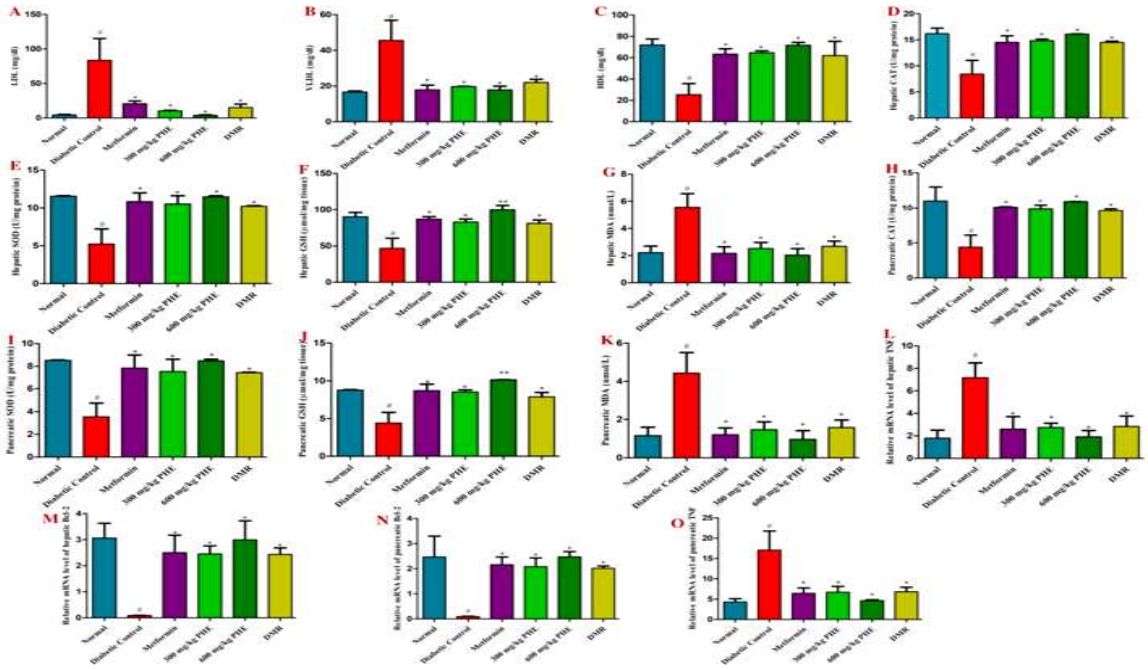

Figure 42 The effects of PHE on lipid metabolism parameters, antioxidant, anti-inflammatory, and apoptotic markers in the hepatic as well as pancreatic tissues of streptozotacin-induced diabetic rats. **A**) LDL, **B**) VLDL, **C**) HDL, **D**) Hepatic CAT, **E**) Hepatic GSH, **F**) Hepatic SOD, **G**) Hepatic MDA, **H**) Pancreatic CAT, **I**) Pancreatic GSH, **J**) Pancreatic SOD, **K**) Pancreatic MDA levels, **L**) Hepatic TNF, **M**) Hepatic Bcl-2, **N**) Pancreatic Bcl-2, and **O**)Pancreatic TNF. Data are expressed as mean ± SEM (n = 6). *Statistically significant ($p < 0.05$) to DC; # statistically significant ($p < 0.05$) to NC.PHE: Poly herbal extract; DMR: dabur madhu rakshak; TC: total cholesterol; TG: triglyceride; HDL: high density lipoprotein; VLDL: very low density lipoprotein; LDL: low density lipoprotein-cholesterol;CAT: catalase; SOD: superoxide dismutase; GSH: reduced glutathione; MDA: malondialdehyde

5.10.7Anti-inflammatory and antioxidant activities

The TNF, COX-2, IL-18, IL-4, SOX-9, and Bcl-2 mRNA expression levels in the liver and pancreas are presented by plotting them through GraphPad Prism5. The mRNA expression levels of TNF (Fig. 42L), COX-2 (Fig. 43A), IL-18 (Fig. 43B), and SOX-9 (Fig. 43C) were up-regulated while IL-4 (Fig. 43D) and Bcl-2 (Fig. 42M) were down-regulated in the liver, and the same order was followed by the pancreas of diabetic rats. Treatment with 300 and 600 mg/kg PHE, metformin, and DMR raised the mRNA expression levels of IL-4 (Fig. 43E) and Bcl-2 (Fig. 42N) in the pancreas, and the same order was observed in the liver as well, while PHE at all doses, metformin, and DMR treatment decreased the expression of TNF (Fig. 42O), COX-2 (Fig. 43F), IL-18 (Fig. 43G), and SOX-9 (Fig. 43H) in both tissues (pancreas and liver). The mRNA expression levels of inflammation markers like TNF, COX-2, IL-18, IL-4, SOX-9, and Bcl-2 treated with PHE were found to be dose-dependent.

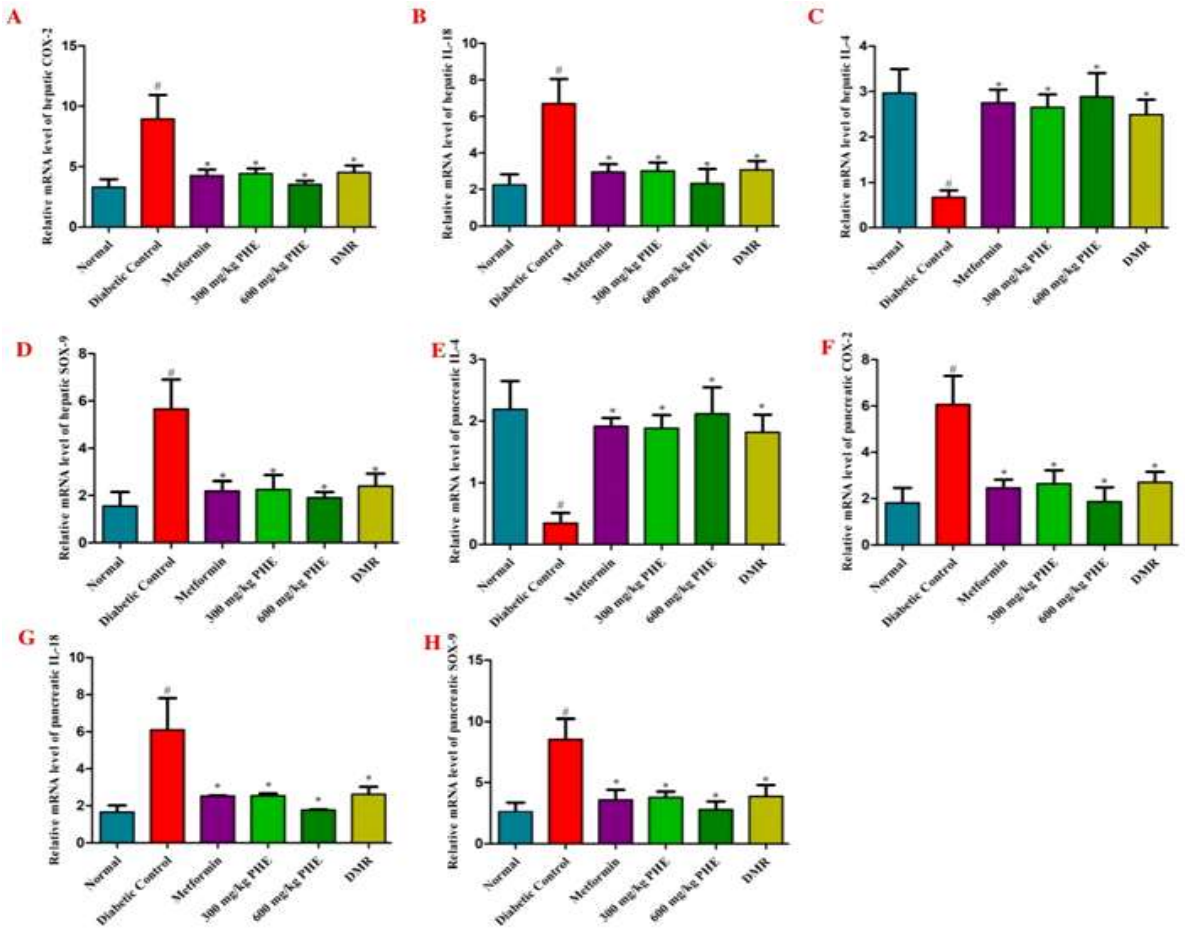

Figure 43 The effects of PHE on anti-inflammatory, and apoptotic markers in the hepatic as well as pancreatic tissues of streptozotacin-induced diabetic rats. **A**) Hepatic COX-2, **B**) Hepatic IL-18, **C**) Hepatic IL-4, **D**) Hepatic SOX-9, **E**) Pancreatic IL-4, **F**) Pancreatic COX-2, **G**)Pancreatic IL-18, **H**) Pancreatic SOX-9. Data are expressed as mean ± SEM (n = 6). *Statistically significant ($p < 0.05$) to DC; # statistically significant ($p < 0.05$) to NC

5.10.8Changes in the histopathology of the pancreas

There were no significant abnormalities observed in the pancreatic cellular structure of the normal control rats. Due to a drastic drop in β-cells within the islets of Langerhans, diabetic control rats had moderate to significant diffuse necrotic alterations in the pancreas. Metformin-treated rats served as a positive control because they displayed some beta-cell and islet Langerhans development. Enhancements in islets of Langerhans and specific growth in the β-cells were observed in 300mg/kg and 600mg/kg PHE-treated rats compared to diabetic control rats, while a regeneration of β-cells was also found in the DMR-treated rats.

5.10.8.1 Protection of beta cells against streptozotocin

All rat groups in the experiment had a simulated pancreatectomy performed at high magnification to assess the *in situ* distribution of β-cells throughout the organ. The size variation of the pancreatic pictures was analyzed using the Macros-plugins in Fiji/ImageJ. Surface area, total area, and circularity were all measured by segmenting the images containing β-cells. Visual examinations were performed, and the surfaces of each islet were measured by hand-tracing the way they appeared. TNF, COX-2, IL-18, and SOX-9-positive cells were observed to increase in the diabetic control group, while IL-4 and Bcl-2-positive cells were observed to decrease in this group. The treatment of diabetic rats with PHE at doses of 300 mg/kg and 600 mg/kg, metformin, and DMR at these doses decreased the expression of TNF (Fig. 44), COX-2 (Fig. 45), IL-18 (Fig. 46), and SOX-9 (Fig. 47) positive cells in the pancreatic islets, while an elevated number of IL-4 (Fig. 48) and Bcl-2 (Fig. 49) positive cells was found in the above treatment groups. A dose-dependent expression level of TNF, COX-2, IL-18, IL-4, SOX-9, and Bcl-2-positive cells was found in rats treated with PHE.

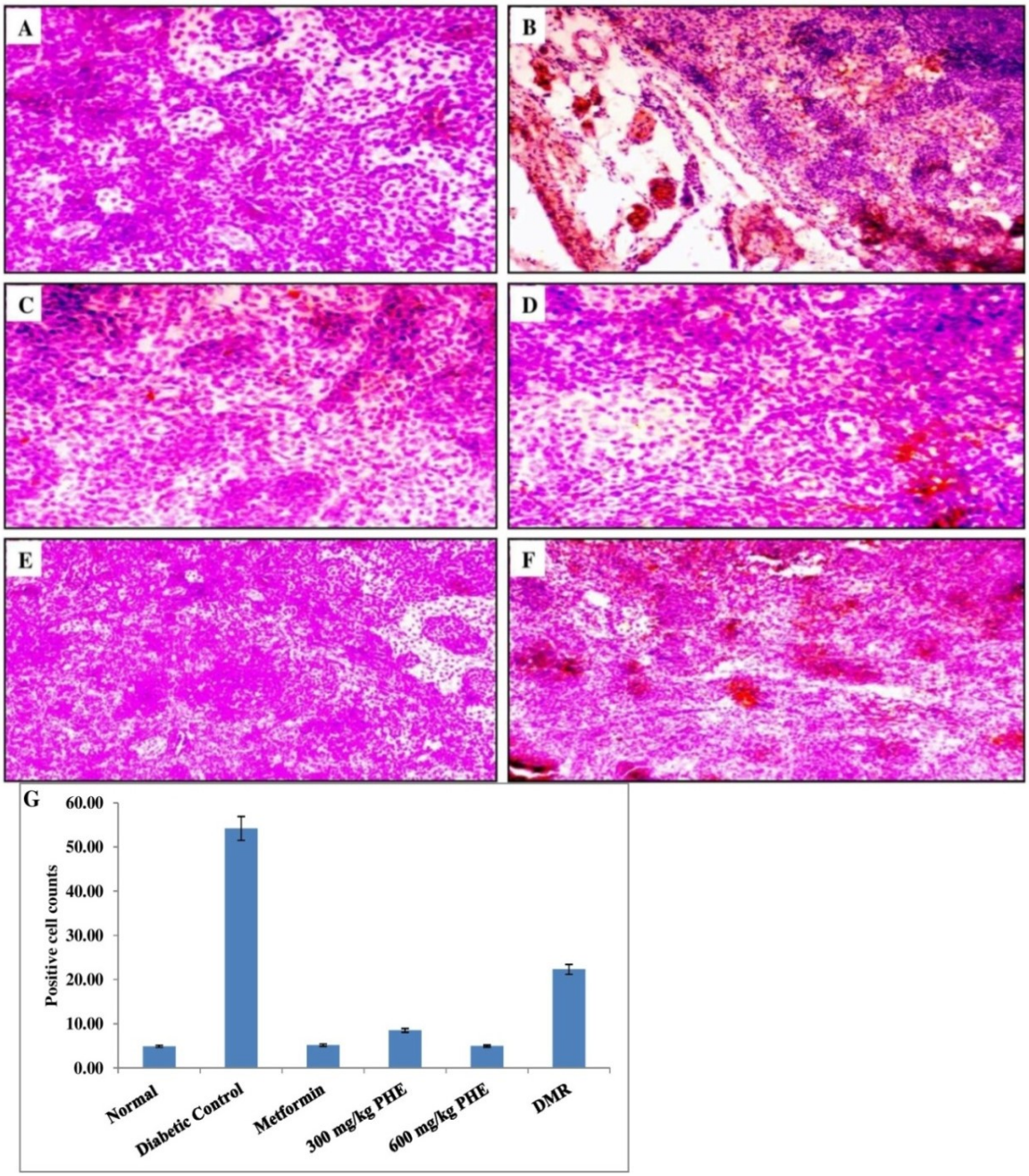

Figure 44 Light microscopic pictures of pancreas sections for TNF immunostaing (brown-red color; H&E x100). **A**) Normal control group showing normal structure of the Islets of Langerhans and acini; **B**) Diabetic control group showing degeneration of the islet; **C**) Diabetic + metformin treated group showing preservation of the architectural structure of Islet of Langerhans; **D**) Diabetic + PHE 300 mg/kg treated group showing restoration of the architectural structure of Islet of Langerhans; **E**) Diabetic + PHE 600 mg/kg treated group showing restoration of the architectural structure of Islet of Langerhans, acini; **F**) Diabetic + DMR treated group showing partial restoration of the architectural structure of Islet of Langerhans; **G**) TNF positive cells of streptozotacin-induced diabetic rats after oral administration of PHE. Data are expressed as mean ± SEM (n = 6)

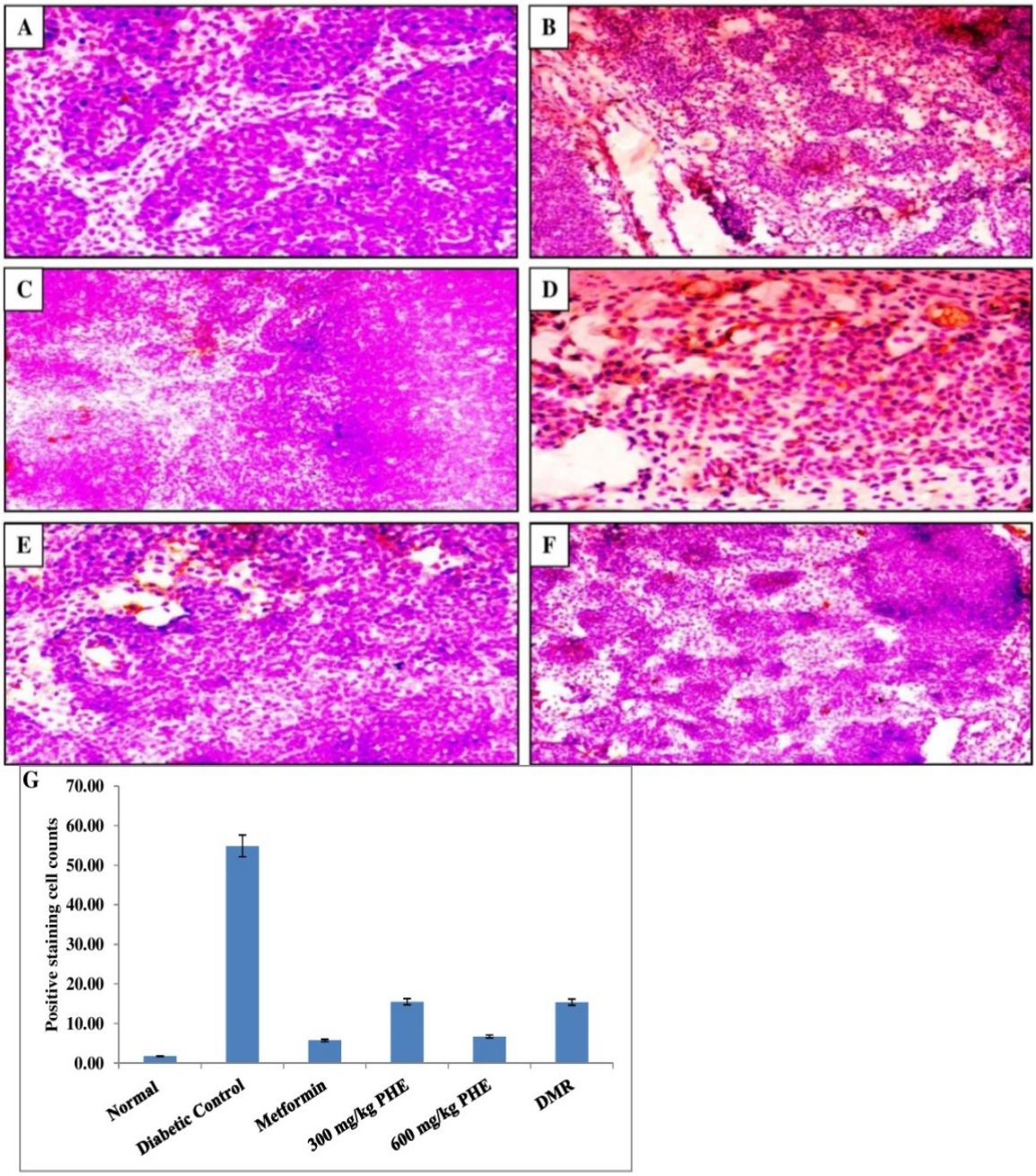

Figure 45 Light microscopic pictures of pancreas sections for COX-2 immunostaing (brown-red color; H&E x100). **A**) Normal control group showing normal structure of the Islets of Langerhans and acini; **B**) Diabetic control group showing degeneration of the islet; **C**) Diabetic + metformin treated group showing preservation of the architectural structure of Islet of Langerhans; **D**) Diabetic + PHE 300 mg/kg treated group showing restoration of the architectural structure of Islet of Langerhans; **E**) Diabetic + PHE 600 mg/kg treated group showing restoration of the architectural structure of Islet of Langerhans, acini; **F**) Diabetic + DMR treated group showing partial restoration of the architectural structure of Islet of Langerhans; **G**) COX-2 positive cells of streptozotacin-induced diabetic rats after oral administration of PHE. Data are expressed as mean ± SEM (n = 6)

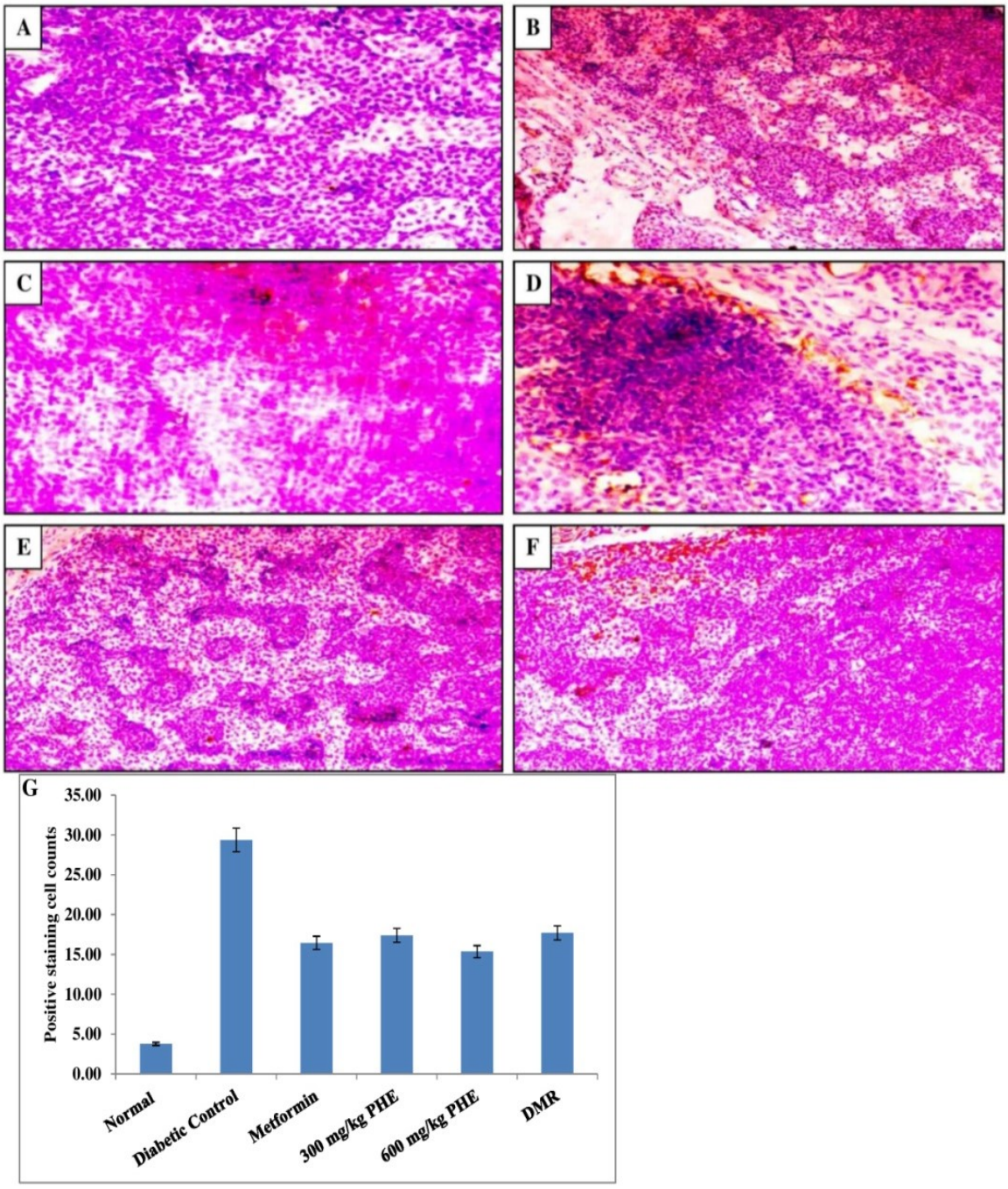

Figure 46 Light microscopic pictures of pancreas sections for IL-18 immunostaing (brown-red color; H&E x100). **A**) Normal control group showing normal structure of the Islets of Langerhans and acini; **B**) Diabetic control group showing degeneration of the islet; **C**) Diabetic + metformin treated group showing preservation of the architectural structure of Islet of Langerhans; **D**) Diabetic + PHE 300 mg/kg treated group showing restoration of the architectural structure of Islet of Langerhans; **E**) Diabetic + PHE 600 mg/kg treated group showing restoration of the architectural structure of Islet of Langerhans, acini; **F**) Diabetic + DMR treated group showing partial restoration of the architectural structure of Islet of Langerhans; **G**) IL-18 positive cells of streptozotacin-induced diabetic rats after oral administration of PHE. Data are expressed as mean ± SEM (n = 6)

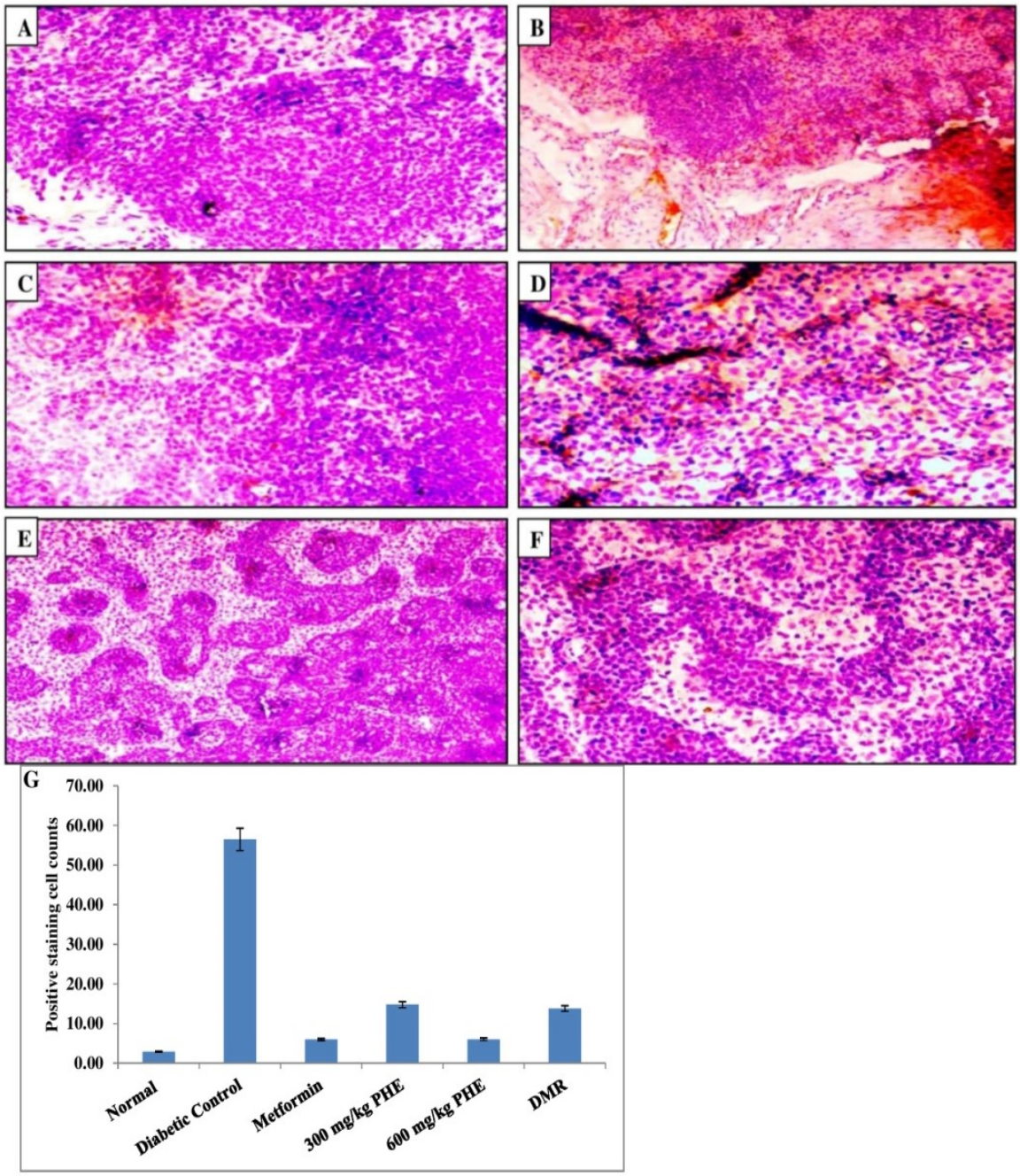

Figure 47 Light microscopic pictures of pancreas sections for SOX-9 immunostaing (brown-red color; H&E x100). **A**) Normal control group showing normal structure of the Islets of Langerhans and acini; **B**) Diabetic control group showing degeneration of the islet; **C**) Diabetic + metformin treated group showing preservation of the architectural structure of Islet of Langerhans; **D**) Diabetic + PHE 300 mg/kg treated group showing restoration of the architectural structure of Islet of Langerhans; **E**) Diabetic + PHE 600 mg/kg treated group showing restoration of the architectural structure of Islet of Langerhans, acini; **F**) Diabetic + DMR treated group showing partial restoration of the architectural structure of Islet of Langerhans; G) SOX-9 positive cells of streptozotacin-induced diabetic rats after oral administration of PHE. Data are expressed as mean ± SEM (n = 6)

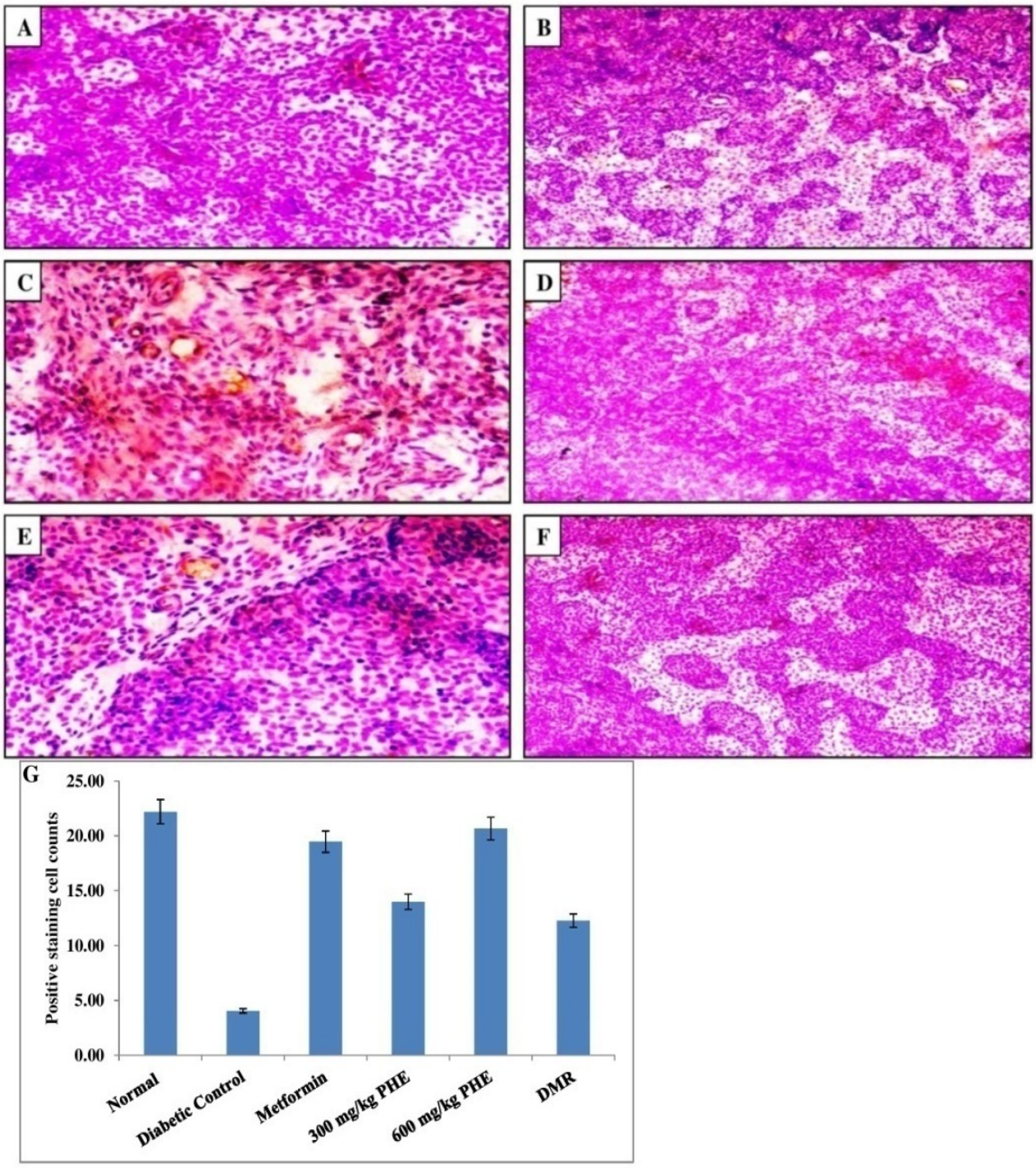

Figure 48 Light microscopic pictures of pancreas sections for IL-4 immunostaing (brown-red color; H&E x100). **A**) Normal control group showing normal structure of the Islets of Langerhans and acini; **B**) Diabetic control group showing degeneration of the islet; **C**) Diabetic + metformin treated group showing preservation of the architectural structure of Islet of Langerhans; **D**) Diabetic + PHE 300 mg/kg treated group showing restoration of the architectural structure of Islet of Langerhans; **E**) Diabetic + PHE 600 mg/kg treated group showing restoration of the architectural structure of Islet of Langerhans, acini; **F**) Diabetic + DMR treated group showing partial restoration of the architectural structure of Islet of Langerhans; **G**) IL-4 positive cells of streptozotacin-induced diabetic rats after oral administration of PHE. Data are expressed as mean ± SEM (n = 6)

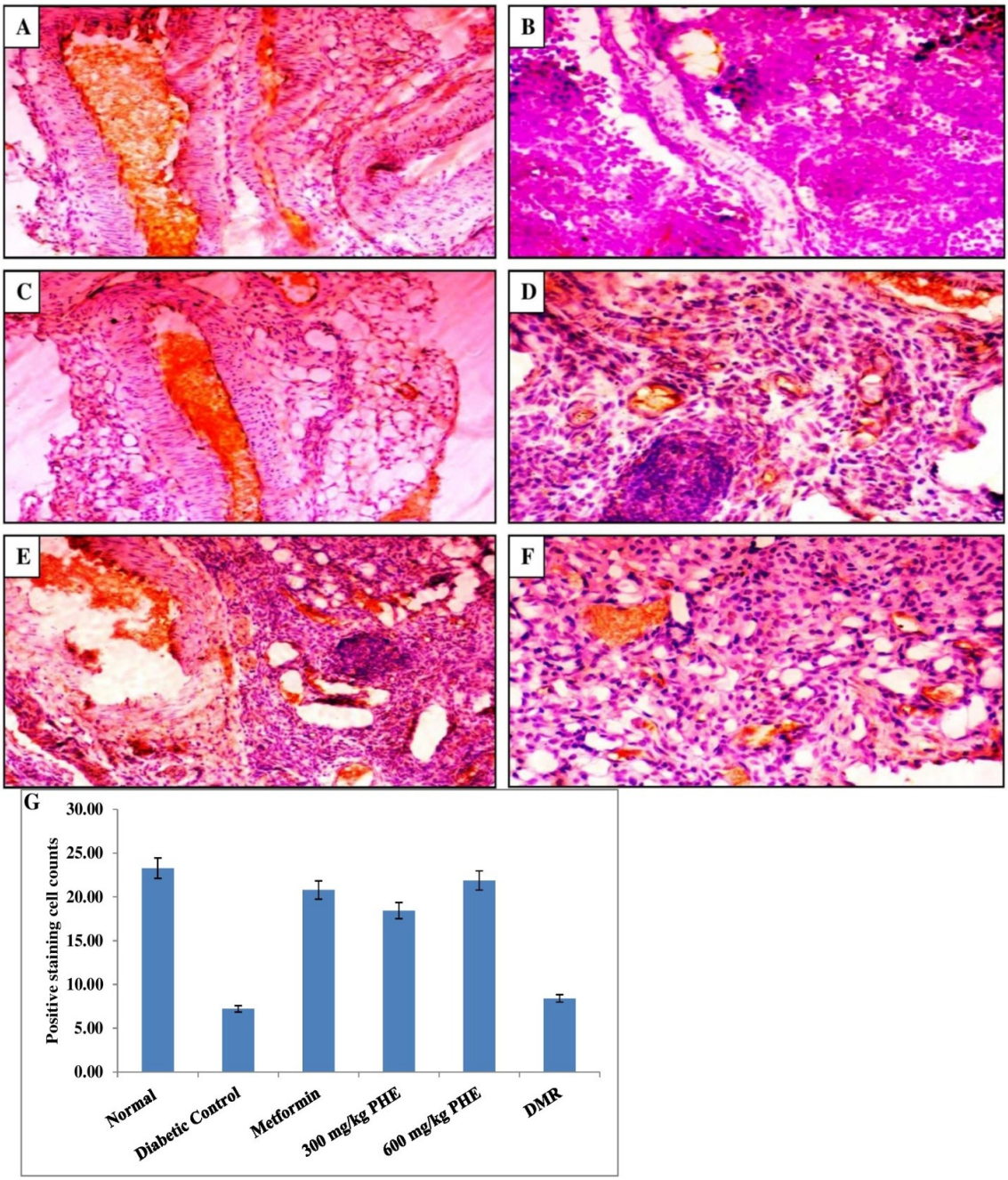

Figure 49 Light microscopic pictures of pancreas sections for Bcl-2 immunostaing (brown-red color; H&E x100). **A**) Normal control group showing normal structure of the Islets of Langerhans and acini; **B**) Diabetic control group showing degeneration of the islet; **C**) Diabetic + metformin treated group showing preservation of the architectural structure of Islet of Langerhans; **D**) Diabetic + PHE 300 mg/kg treated group showing restoration of the architectural structure of Islet of Langerhans; **E**) Diabetic + PHE 600 mg/kg treated group showing restoration of the architectural structure of Islet of Langerhans, acini; **F**) Diabetic + DMR treated group showing partial restoration of the architectural structure of Islet of Langerhans; **G**) Bcl-2 positive cells of streptozotacin-induced diabetic rats after oral administration of PHE. Data are expressed as mean ± SEM (n = 6)

5.10.9Effect of PHE on gut microbiota

Sequence score cards(Fig. 50A and 50B) were used to verify that an entire amplification at around 450 bp was present in each of the six samples (Table 34). High coverage was attained across all rat groups, as shown by the distribution plot of sequence (contig) length (Fig. 51A). The recorded gel picture (Fig. 51B) demonstrates the QC of samples from each group of experiments in our study and the trend for each of the rarefaction curves (Fig. 52). The diversity estimators and summary statistics showed that the gut microorganisms in the normal group (GP-1), diabetes group (GP-2), and treatment groups like metformin (GP-3), PHE (GP-4 and GP-5), and DMR (GP-6) were significantly different from one another. The diversity of the treated rats was significantly higher than that of the normal and diabetic rat groups. Based on the results of the microbial diversity analysis, we can observe that there are 10 main phyla covered in the present study of gut microbiota.

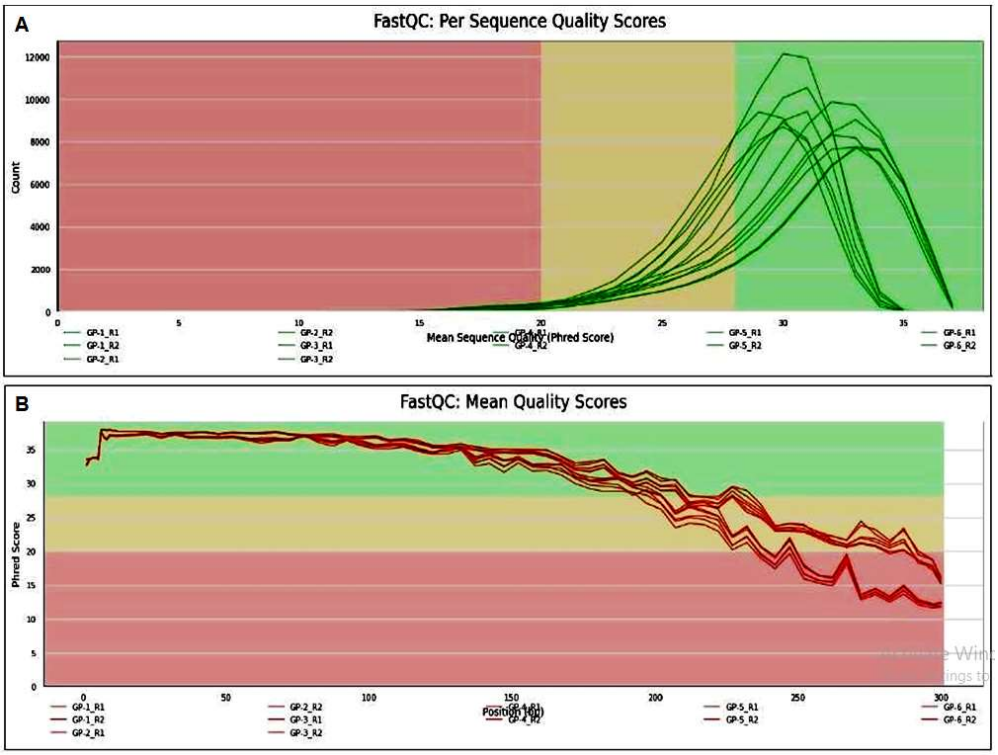

Figure 50 Histogram of Sequence reads. A) Per sequence quality score and B) Mean quality score

Table 34 Summary of raw sequence data and quality checks

Sample ID	No. of Reads	GC %	Read length	%Q20
Normal (GP-1)	105194	54	301	99.08
Diabetic Control (GP-2)	148638	53	301	99.08
Metformin (GP-3)	129190	54	301	99.09
PHE 300 mg/kg (GP-4)	123734	54	301	99.09
PHE 600 mg/kg (GP-5)	105590	53	301	99.29
DMR (GP-6)	115256	54	301	99.15

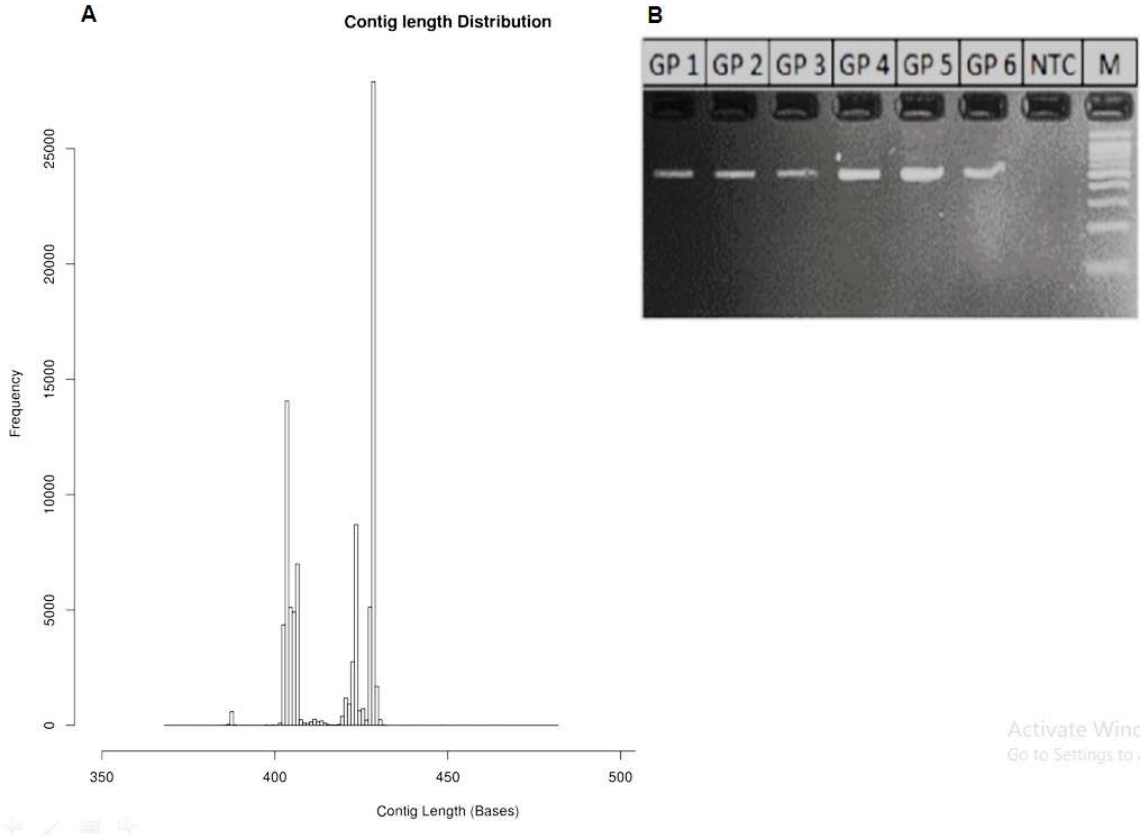

Figure 51 Histogram of sequence diversity;(**A**) Contig length distribution and (**B**) Gel Image showing the amplicon size along with 100bp ladder

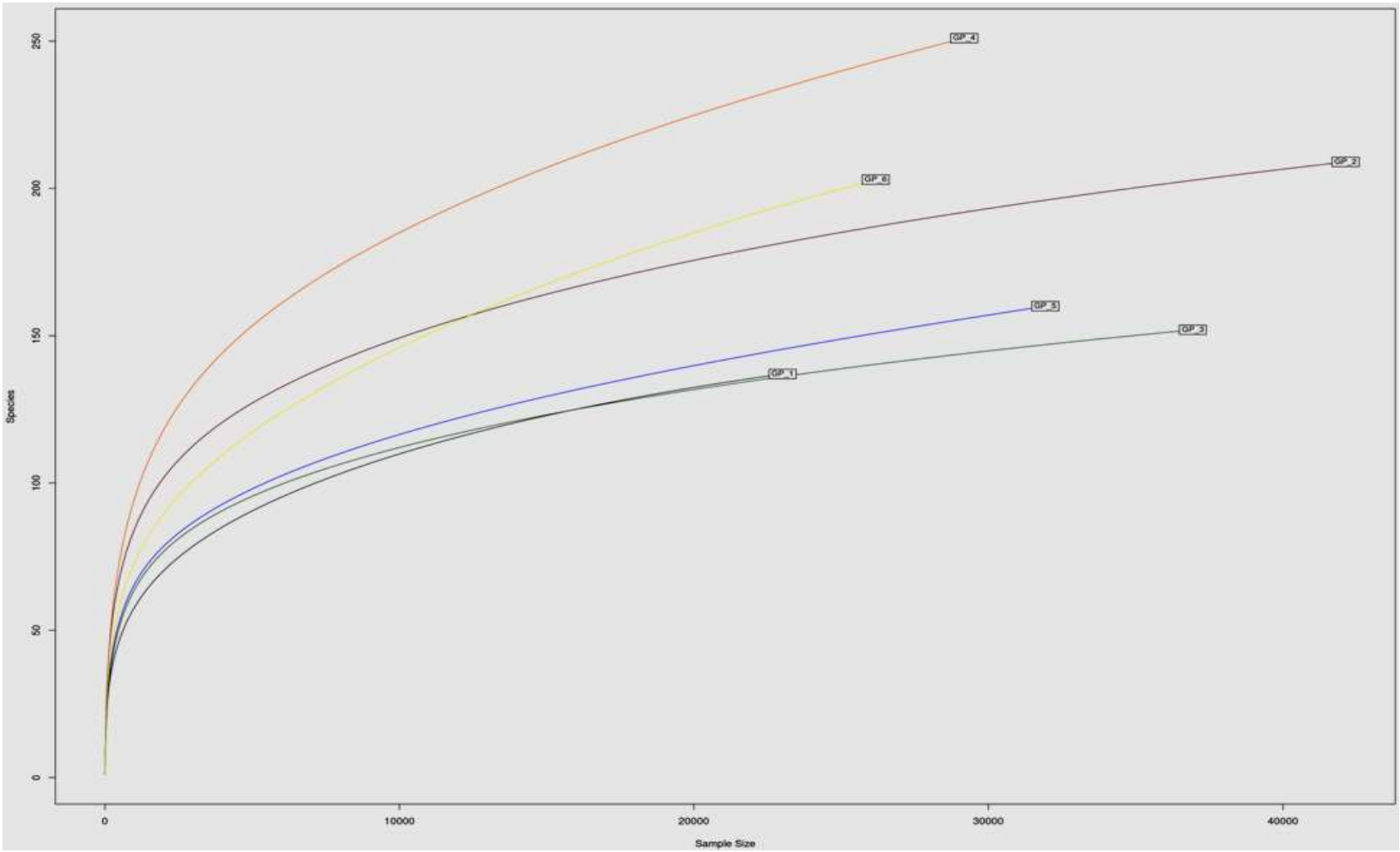

Figure 52 Rarefaction curve of sequence diversity GP1 (Normal), GP2 (Diabetic Control), GP3 (Metformin), GP4 (PHE 300 mg/kg), GP5 (PHE 600 mg/kg), and GP6 (DMR)

5.10.9.1Alpha diversity

Table35demonstrates the non-significant prevalent alpha diversity indices in the different groups of experiments (GP-1 to GP-6). GP-5 rats' feces demonstrated similar ACE and Chao1, as well as observed species indices towards GP-1 but not GP-2. GP-4 and GP-6 got similar outcomes as GP-2 in these tests (Fig. 53). Thus, GP-5, as well as other investigational treatment groups, had rich microbial communities. GP-2 diabetic rats had higher Fisher indices than GP-1 control rats. Fisher indices for the treatment animals (GP-5) were equivalent to those of metformin-treated rats (GP-3) and restored the diversity of bacteria to normal (GP-1). Table 35 shows that the treatment groups GP-4 and GP-6 have opposite Fisher indices. Thus, sequencing was sufficient to assess gut microbiota diversity. Table 35 showed that the Simpson, InvSimpson, and Shannon indices for both GP-5 and GP-1 did not differ significantly. Community richness and rarely-seen amplicon sequence variations (ASVs) affect the Shannon index more. A total of 28 days of high-dose PHE (GP-5) treatment may improve rat feces species diversity.

Table 35 Alpha diversity measurement of gut microbiota for different treatment groups

S. No.	Sample ID	Alpha diversity of gut microbiota						
		Observed	**Chao1**	**ACE**	**Shannon**	**Simpson**	**InvSimpson**	**Fisher**
1.	GP-1	137	160.62±11.00	171.27±6.73	3.17	0.93	15.34	19.34
2.	GP-2	209	262.71±20.74	263.06±7.97	3.70	0.96	25.56	28.65
3.	GP-3	152	189.19±16.76	194.43±7.16	2.91	0.87	7.45	20.24
4.	GP-4	251	354.88±33.08	362.74±10.36	3.70	0.96	24.28	37.73
5.	GP-5	160	290.67±56.91	234.66±7.78	3.35	0.95	18.44	21.97
6.	GP-6	203	283.90±26.15	315.43±10.18	3.41	0.95	18.67	29.97

Data are expressed as mean ± SE (n = 6).

5.10.9.2Beta diversity

This study has many microbial species. PCoA cluster analysis was used to investigate gut microbial populations in the feces of experimental rats. Based on taxonomical distribution, the principal coordinate analysis (PCoA) was employed to compare microbiota architectures. Gut microbial structure differed among rat groups. The two-axis principal component assessments explained 50.7% and 21.5% of the total variances (Fig. 54A). Axis 1 shows that GP-1 and GP-5 have a significant difference in PCoA1 compared to GP-2. GP-1 and GP-5 exhibit similar gut microbiota diversity at PCoA1, while GP-3, GP-4, followed by GP-6 remain close to GP-2. In addition, GP-3 and GP-4 were nearer to GP-2 on PCoA2, but GP-1, GP-5, followed by GP-6 were significantly different on Axis 2. Thus, the GP-3 and GP-4 in the present study had fewer microbial differences on PCoA2 and PCoA1 (Fig. 54A). The results of GP-1 and GP-5 were more similar, suggesting that rats' intestinal microbial communities might be altered by gavage with 600 mg/kg body weight of PHE for 28 days.

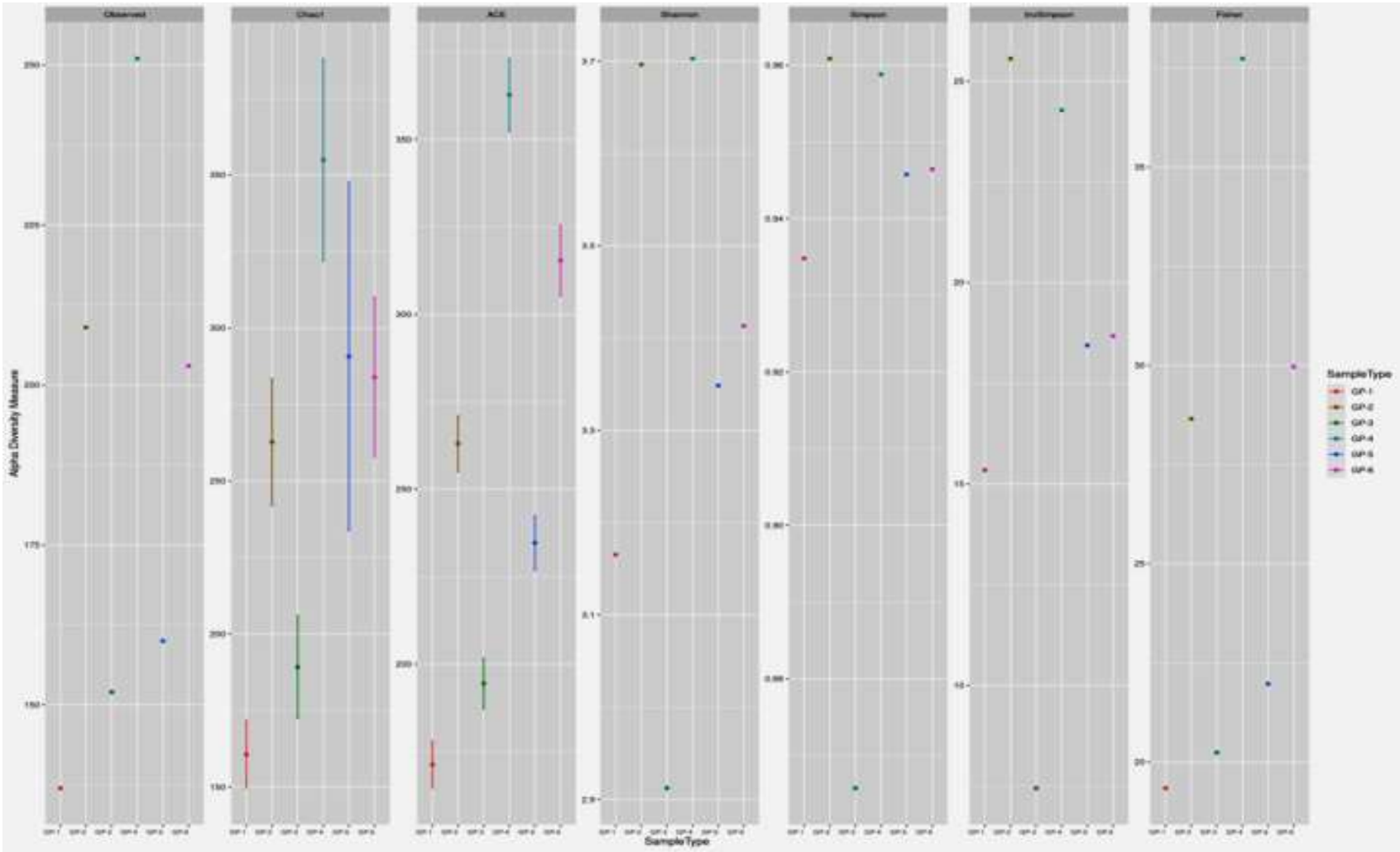

Figure53 Alpha diversity measurement of gut microbiomes for different treatment groups

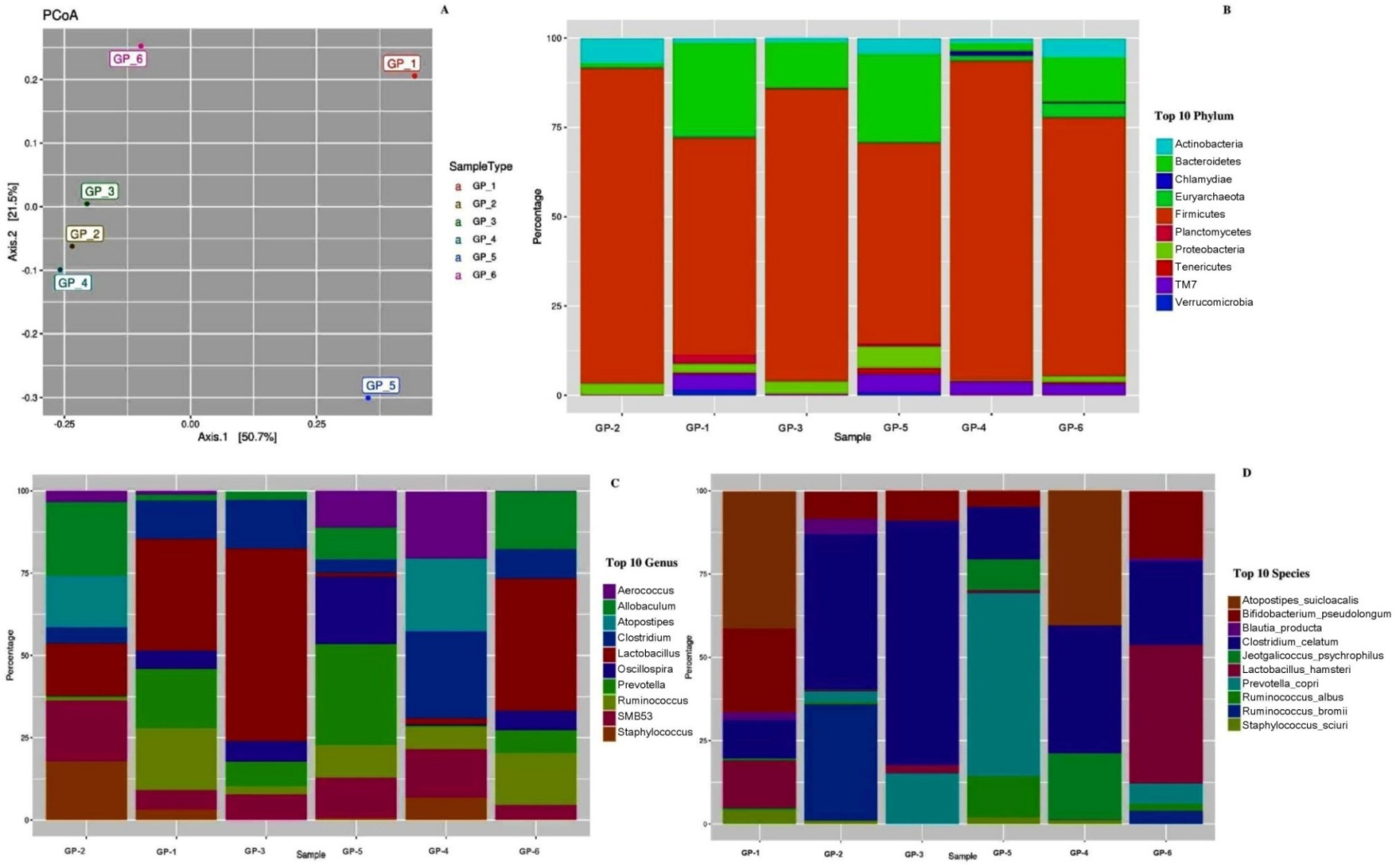

Figure 54 The taxonomic composition relative abundance of gut microbial in rat fecal sample of different experimental (GP-1 to GP-6) groups (n = 6). (**A**) PCoA plot, (**B**) Phylum level, (**C**) Genus level and (**D**) Species level

5.10.9.3Comparison of the gut microflora community composition

According to the results of the metagenomic study, the 10 phyla of the microbiome are the representatives of the present study, like*Actinobacteria*, *Bacteroidetes*, *Chlamydiae*, *Euryarchaeota*, *Firmicutes*, *Planctomycetes*, *Proteobacteria*, *Tenericutes*, and TM7, as well as *Verrucomicrobia* (Fig. 54B). The phylum *Firmicutes* was present in the highest percentage among samples. The results showed that a bloom of *Actinobacteria* was associated with normal (GP-1), diabetic control (GP-2), metformin (GP-3), PHE (GP-4 to GP-5), and DMR (GP-6)-treated group samples. An increase in*Firmicutes* and a reduction in*Bacteroidetes* along with *Euryarchaeota*, *Planctomycetes*, *Proteobacteria*, *Tenericutes*, *TM7*, and *Verrucomicrobia* in GP-2 rats were detected compared with GP-1 rats. In contrast, overall treatment groups reduced the prevalence of *Firmicutes* relative to *Bacteroidetes* as compared to diabetic rats with GP-2. However, treatment groups GP-3, GP-4, and GP-6, as compared to GP-5, remarkably enriched the amount of *Firmicutes*. The treatment GP-5 showed a reduction of *Firmicutes*, *Chlamydiae, andEuryarchaeota* associated with an elevation of the amount of *Bacteroidetes*, *Planctomycetes*, *Proteobacteria*, *Tenericutes*, and *TM7* in comparison to GP-2. The microbial diversity in GP-3, GP-4, and GP-6 was endorsed by microbiota phyla lateral to GP-5 and restored the microbial phyla abundance compared to GP-1, as seen in Figure 54B.

In our investigation, we found that there were substantial differences between the groups of rats in terms of 10 different genera of bacterial microbiome. Figure 54C showed the gut microbiota: *Aerococcus*, *Allobaculum*, *Atopostipes*, SMB53, and *Staphylococcus* genera, which obviously increased, while *Clostridium*, *Lactobacillus*, *Oscillospira*, *Prevotella,* and *Ruminococcus* groups decreased in GP-2 rat samples in comparison to GP-1 rat samples. The gut microbiota: *Allobaculum*, *Atopostipes*, *Lactobacillus*, SMB53, and *Staphylococcus* declined, while *Oscillospira*, *Prevotella,* and *Ruminococcus* increased in the GP-5 rats in

comparison to the GP-2 and restored microbiota abundance as in the GP-1. The microbial diversity at the genus level in GP-3, GP-4, and GP-6 was also regulated, as seen in Figure 54C. The gut microbiota diversity of [*Prevotella*], *Bacteroides*, *Desulfovibrio*, *Adlercreutzia*, and *Bifidobacterium* was also regulated for treatment groups including PHE to rehabilitate good health.

Furthermore, as shown in Figure 54D, there were notable differences in the abundance of species-level gut microbiota among the various rat groups. Expression in various conditions is controlled by the species composition and abundance of gut bacteria. The result revealed that the abundance of *Atopostipes suicloacalis*, *Bifidobacterium pseudolongum*, *Lactobacillus hamsteri*, *Jeotgalicoccus psychrophilus*, *Staphylococcus sciuri*, and *Blautia producta* was increased,while the abundance of *Clostridium celatum*, *Prevotella copri*, and *Ruminococcus bromii* was decreased in GP-1 as compared to GP-2. *Clostridium celatum*, *Atopostipes suicloacalis*, *Jeotgalicoccus psychrophilus*, *Staphylococcus sciuri*, and *Ruminococcus albus* showed regulated abundance in different treatment groups as compared to a group of diabetic rats. The relative abundance of *Bifidobacterium pseudolongum* was found to decline in PHE treatment groups as compared to diabetic, metformin, and DMR groups. The relative abundance of *Lactobacillus hamsteri* was elevated in PHE treatment groups as compared to diabetic groups,while it was lower in metformin and DMR groups. *Prevotella copri* abundance was also found to increase in PHE treatment groups as well as metformin and DMR groups as compared to the diabetic group. *Ruminococcus bromii* and *Blautia producta* showed almost similar declines in abundance in different treatment groups as compared to the diabetic group. At the species level, 10 species shown in Figure 54D had markedly changed abundance levels with the treatment doses. The taxonomic composition with relative abundance Aheat map of gut microbial activity in rat fecal samplesfrom different experimental groups also showed significant diversity between groups (Figs. 53 and 55). The

results indicated that the administration of 600 mg/kg body weight of PHE (GP-5) for 28 days was sufficient to alter the gut microbiota composition of the rat. Therefore, the PHE groups were selected for the subsequent study of SCFAs in this study.

5.10.9.4 Correlation of gut microflora with metabolic parameters

DM-related indices (body weight and FBG) are shown in Figure 56, along with their correlations with the microbiota of the gut (markedly modified ten genera of microorganisms by PHE) using canonical correspondence analysis (CCA) on multiple samples. The resultant ordination plots showed that the first axis for both body weight and FBG against gut microbiota explained the majority of the variance (73.82 and 52.42 percent, respectively), while the corresponding second axis accounted for only 26.18 and 29.03 percent, respectively. Based on CCA, we found that *Lactobacillus*, *Oscillospira*, *Prevotella*, *Clostridium*, *Ruminococcus*, *Desulfovibrio*, [*Prevotell*], *Bacteroides*, and *Aerococcus* were positively correlated with body weight (final weight) on the first axis. In contrast, the other bacteria (*Adlercreutzia*, *Bifidobacterium*, *Allobaculum*, *Atopostipes*, *Staphylococcus*, and SMB53 group) were negatively correlated with the body weight on the same axis (Fig. 56A). Furthermore, the gut microbiota *Lactobacillus*, *Oscillospira*, *Prevotella*, *Ruminococcus*, *Desulfovibrio*, [*Prevotell*], and *Bacteroides* were associated with a negative correlation with the level of fasting blood glucose (FBG) on the first axis, while the other bacteria (*Adlercreutzia*, *Bifidobacterium*, *Allobaculum*, *Clostridium*, *Atopostipes*, *Aerococcus*, *Staphylococcus*, and SMB53 group) were positively correlated with FBG on the same axis (Fig. 56 B). Both T2DM-related indicators were found to be more significantly correlated with the gut microbiota species *Lactobacillus*, *Oscillospira*, *Prevotella*, *Ruminococcus*, *Desulfovibrio*, [*Prevotell*], and *Bacteroides*.

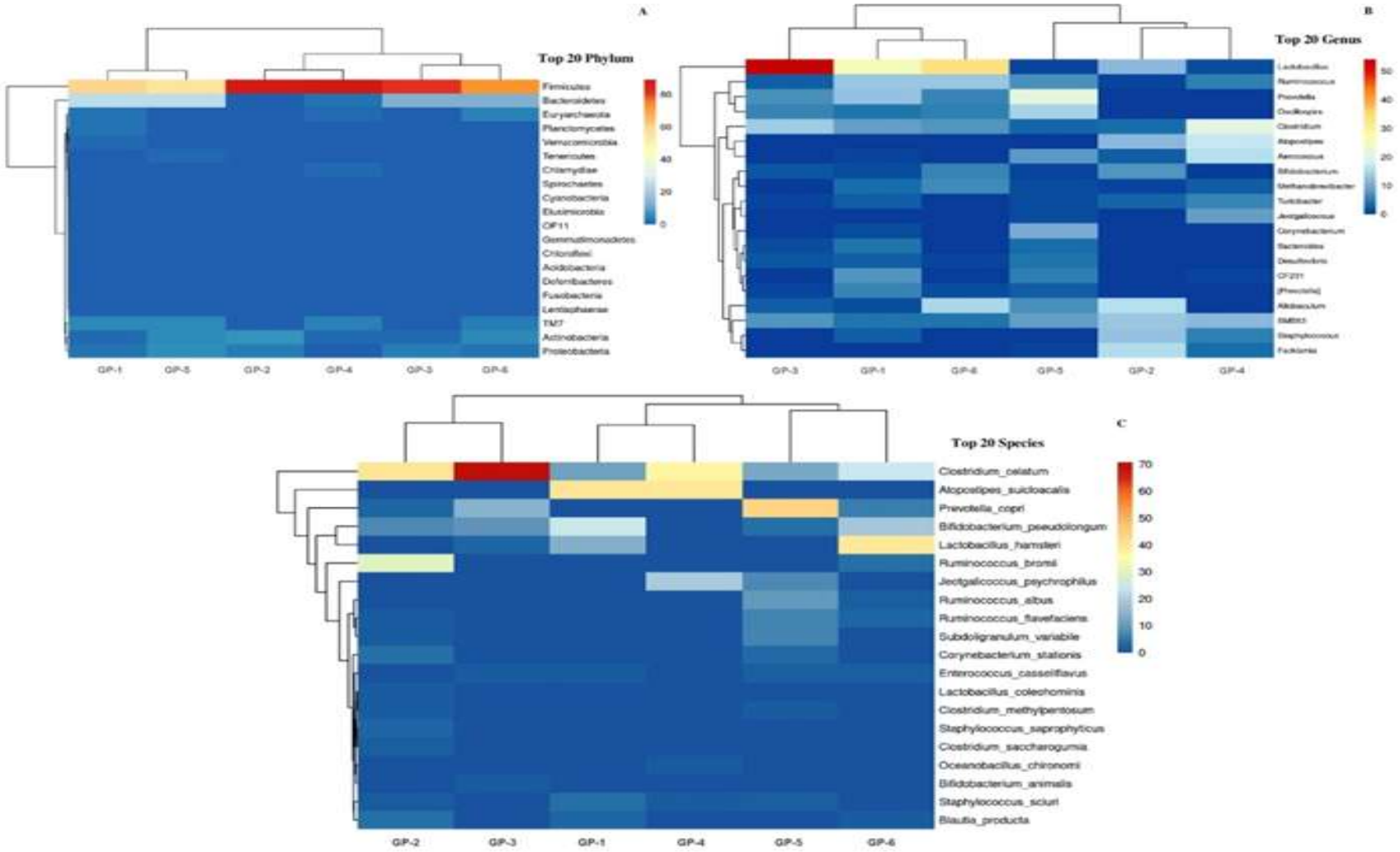

Figure 55 The taxonomic composition with relative abundance heat map of gut microbial in rat fecal sample of different experimental (GP-1 to GP-6) groups (n = 6). (**A**) Phylum level, (**B**) Genus level and (**C**) Species level

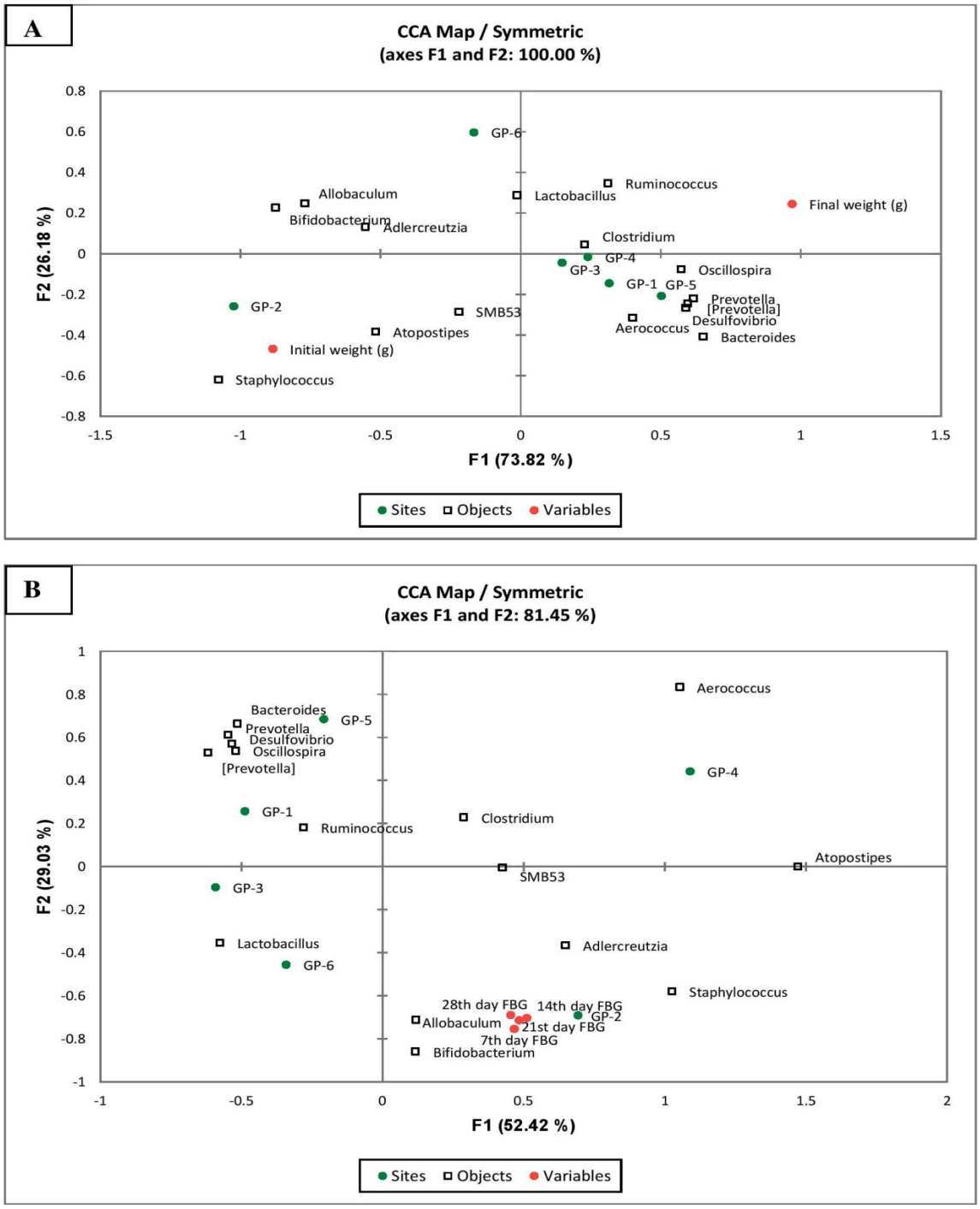

Figure 56 Correlation analysis between DM-related parameters (body weight and FBG) and gut microbiota at genus level. Canonical correspondence analysis (**A**) Body weight Vs gut microbiota and (**B**) FBG Vs gut microbiota

5.10.9.5SCFAs content of fecal sample

Standard graphs from 5 dilutions (50–5000 nM) were plotted for peak area versus concentration. A linear relationship was established, with regression coefficients of 0.998 and 0.996 for acetate and propionate, respectively. Details of molecular weight (g/mol), density (g/ml), standard equation, retention time, molecular formula, and R^2 values of standards run on HPLC are shown in Table 36, with the standard graph in Figure 57A-B. Subsequent calculations of SCFAs concentration in the sample groups were done using the standard linear equation derived and summarized in Table 36. Fecal SCFAs can indirectly reflect colon SCFAs, which are linked to intestinal health. The content of the two dominant main SCFAs in rat feces was affected through PHE, as shown in Figure 57C-D. After 28 days of treatment with different doses of GP-3, GP-4, GP-5, and GP-6, all groups had higher SCFAs concentrations than GP-1 at the end of the experiment. GP-2 had lower SCFAs concentrations among other groups. GP-4 and GP-5 had significantly higher acetate content than GP-1 ($p < 0.05$ and 0.01, respectively). GP-4 and GP-5 increase feces acetate levels (Fig. 57C). GP-3 and GP-6 doses also increased acetic acid concentrations in feces ($p < 0.05$), but GP-2 decreased acetate (Fig. 57C). Both PHE dosages increased fecal acetic acid concentrations after 28 days of continuous administration in rats from various groups. A consistent finding for propionate concentration for both doses of PHE within GP-4 as well as GP-5 was also seen, with large and highly significant increases in propionic acid concentration in feces compared to other groups (Fig. 57D). This indicated that both dosages of PHE administered to rats for 28 days could also influence the intestinal environment. These studies demonstrated that PHE's effect on the gut is dose-dependent; particularly that 600 mg/kg body weight of PHE-treated rats for 28 days increased the primary SCFA content of their feces.

Table 36HPLC-based estimation of standard SCFAs

Standards	Molecular weight (g/mol)	Molecular Formula	Density (g/ml)	Retention time (minute)	Standard Equation	R^2 value
Acetic acid	60.052	CH_3COOH	1.053	17	Y= 11.27x+39565	0.998
Propionic acid	74.08	CH_3CH_2COOH	0.992	22	Y= 47.13x+38316	0.996

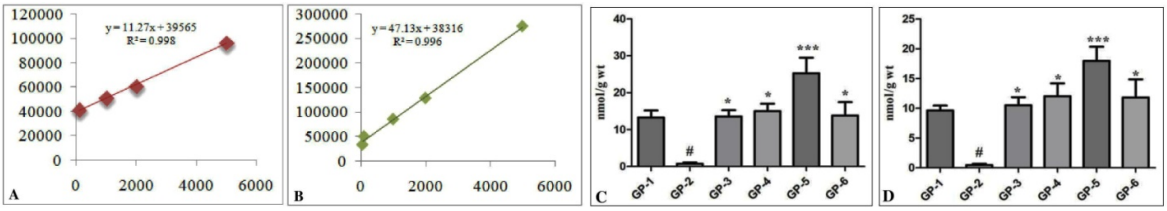

Figure 57SCFAs analysis in the fecal sample of different rat groups. **A**)Standard graph of acetic acid (with R^2 = 0.998) and **B**) propionic acid (with R^2 =0.996). C) The concentration of acetic acid, **D**) The concentration of propionic acid

5.10.9.6Polyphenols in the enrichment of symbiotics

The diversity estimators and summary statistics show that the gut microorganisms in the normal group, diabetes control group, and treatment groups like metformin, PHE, and DMR were significantly different from one another in terms of 10 different families of intestinal bacteria (Fig. 58). Figure 58A-B showed the Krona-pie charts of gut microbiota of the families Clostridiaceae, Aerococcaceae, Staphylococcaceae, and Turicibacteraceae, which obviously increased, while Lactobacillaceae, Prevotellaceae, Bacteroidaceae, and Ruminococcaceae gut microbiota groups decreased in diabetic control rat fecal samples in comparison to normal rat fecal samples (Table 37). The gut microbiota of families like Prevotellaceae (7%), Desulfovibrionaceae (1%), Bacteroidaceae (1%), and Ruminococcaceae (13%) increased in the 600 mg/kg PHE-treated rats (Fig. 58E) in comparison to the diabetic control rats and restored microbiota abundance as in the normal rats. The microbial diversity at the family level in metformin-group rats (Fig. 58C), 300 mg/kg PHE-treated rats (Fig.

58D), and DMR-treated rats (Fig. 58F) was also regulated. The gut microbiota diversity was regulated for treatment groups, including PHE, to restore good health.

5.10.9.7Correlations between gut microbiota and lipid metabolism indexes

In order to gain a deeper understanding of the specific intestinal strains that contribute to lipid metabolism, we conducted an analysis to examine the associations between the relative abundances of various prominent gut microbiota (Table 38), such as cellulolytic bacteria, and markers of lipid levels. This analysis yielded a maximum value of 44.74% for the F1 axes of the canonical correlation analysis (CCA) plot. According to the data shown in Figure 59, there is a notable association between the elevated abundance of *Prevotella*, *Ruminococcus*, *Oscillospira*, *Bacteroides*, *Lactobacillus*, and *Desulfovibrio* in the PHE 600 groups and a negative correlation with serum TC, TG, and LDL levels. Conversely, there is a positive correlation between the aforementioned microbial abundance and HDL levels.

Table 37 Gut microbiota (%) diversity at family level

Family	Normal	Diabetic	Metformin	PHE 300	PHE 600	DMR
Lactobacillaceae	12	9	37	1	0.4	21
Prevotellaceae	6	0.2	4	0.2	7	4
Bifidobacteriaceae	0.6	5	1	0.07	0.3	4
Desulfovibrionaceae	1	0.1	1	0.1	1	0.6
Bacteroidaceae	2	0.08	0.9	0.2	1	0.4
Ruminococcaceae	16	0.8	8	4	13	15
Clostridiaceae	6	13	13	20	4	7
Aerococcaceae	0.4	23	0.01	25	3	0.05
Staphylococcaceae	1	10	0.008	10	0.7	0.09
Turicibacteraceae	1	2	0.5	4	0.4	0.2
Coriobacteriaceae	0.1	1	0.3	1	0.3	1

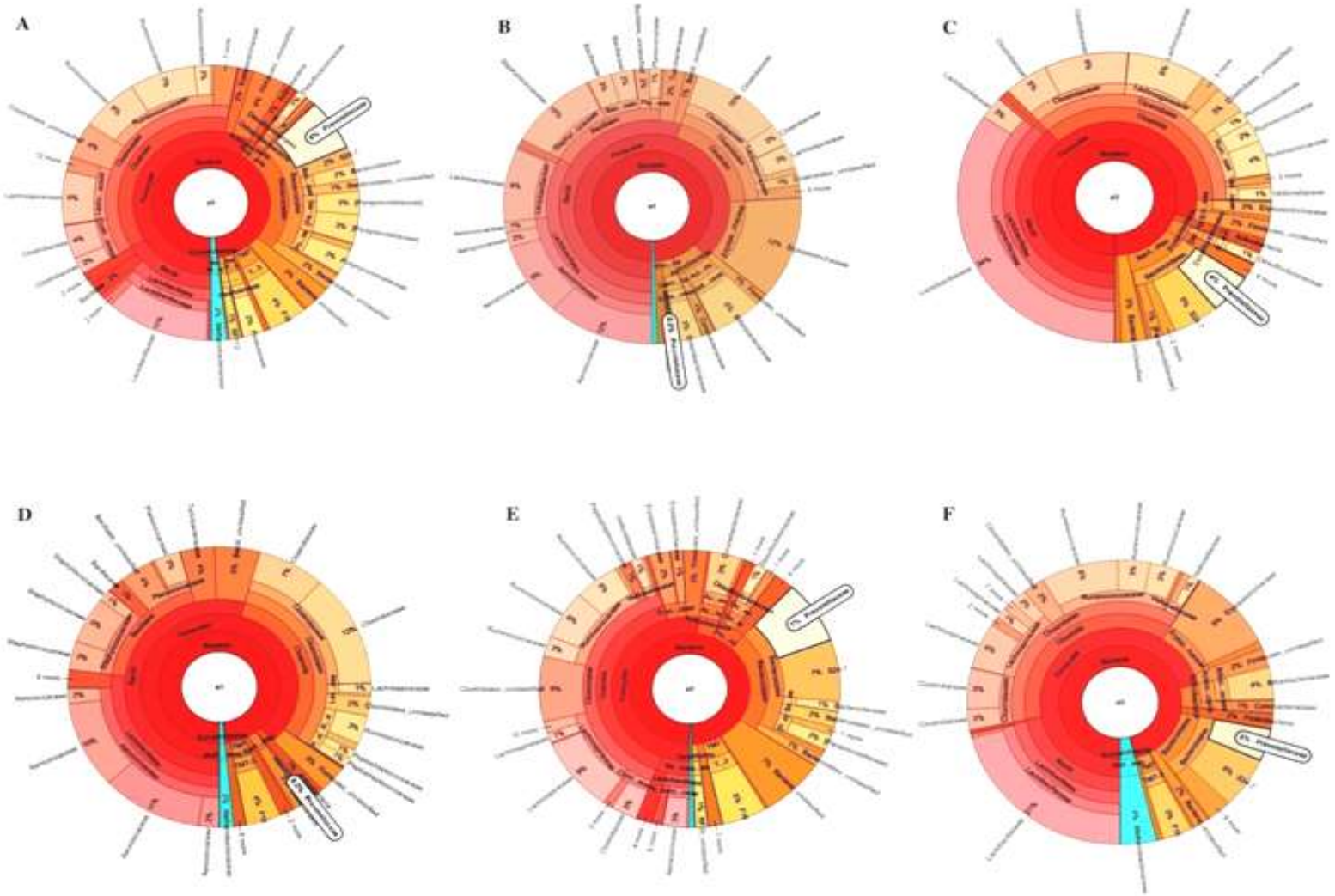

Figure 58 Krona-pie-charts of gut microbiota structures at family level. **A**) Normal rats with 6% Prevotellaceae, **B**) Diabetic control rats with 0.2% Prevotellaceae, **C**) Metformin group rats with 4% Prevotellaceae, **D**) 300 mg/kg PHE-treated rats with 0.2% Prevotellaceae, **E**) 600 mg/kg PHE-treated rats with 7% Prevotellaceae, and **F**) DMR-treated rats with 4% Prevotellaceae

Table 38 Gut microbiota (%) abundance at genus level

Genus	Normal	Diabetic	Metformin	PHE 300	PHE 600	DMR
Lactobacillus	21.38	10.32	49.15	1.32	0.68	29.36
Clostridium	7.38	3.1	12.46	18.99	2.21	6.51
SMB53	3.77	11.92	6.57	10.61	6.79	3.31
Prevotella	11.38	0.25	6.25	0.31	17.02	5.02
Ruminococcus	11.86	0.58	2.07	4.78	5.58	11.51
Allobaculum	1.14	14.38	2.22	0.07	5.3	12.86
Atopostipes	0	10.17	0	15.89	0.03	0.01
Aerococcus	0.67	2.17	0.01	14.66	6.17	0.05
Oscillospira	3.46	0.04	5.34	0.38	11.39	4.33
Staphylococcus	1.95	11.48	0.01	4.83	0.34	0.09
Adlercreutzia	0.06	1.09	0.14	0.93	0.22	0.81
Bifidobacterium	1.22	6.44	1.66	0.1	0.64	5.12
Turicibacter	2.05	2.84	0.69	5.42	0.87	0.21
Bacteroides	3.52	0.08	1.29	0.36	2.7	0.31
Desulfovibrio	1.96	0.11	1.74	0.15	3.07	0.73

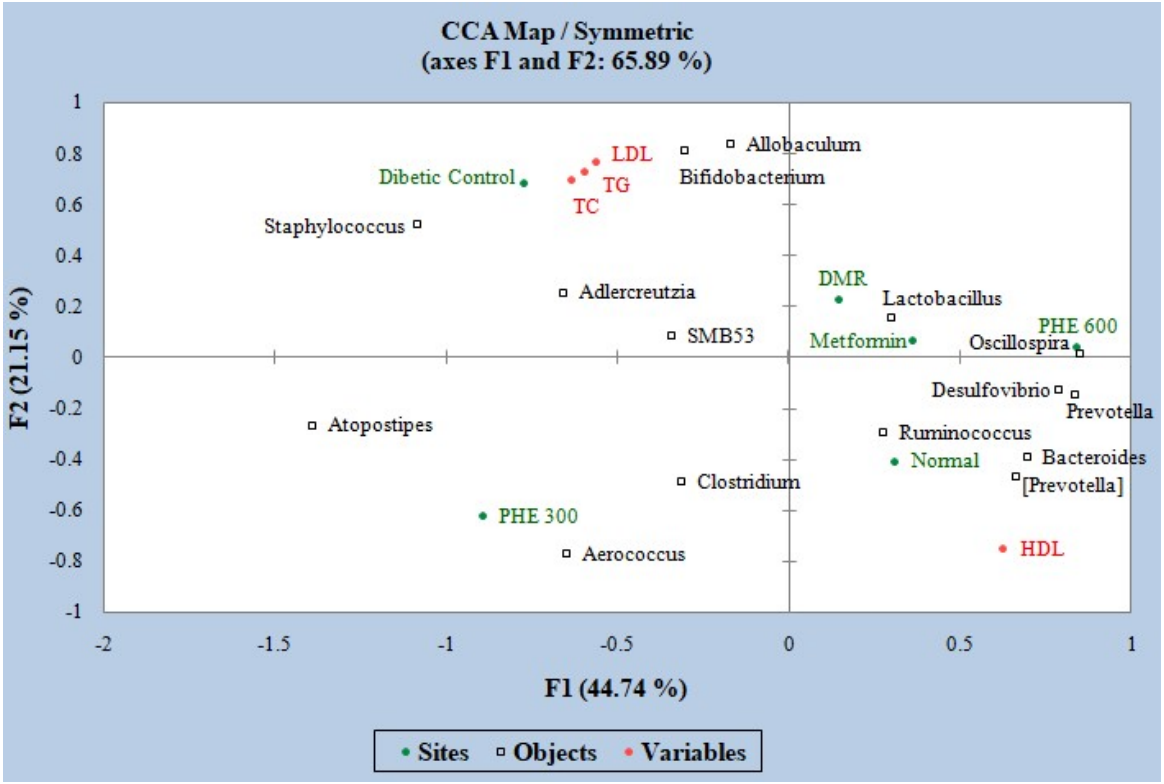

Figure 59 Canonical correlation analysis (CCA) between gut microbiota and lipid metabolism indexes performed through XLSTAT 2023.1.2.1406

5.11Bioinformatics study of bioactive compounds identified in GC-MS

5.11.1 ADMET and drug-likeness score

The Swiss ADMET database predicted results in the form of Lipinski's rule for all these compounds, confirming that these compounds possess drug-like properties. A deficit in the targets and interactions with all the screened compounds of PHE was found with the online servers SEA and Targetnet. Thus, the STP databases were used to select targets from all the screened compounds that interacted with the genes, and these interacted compounds were considered to be the therapeutic components among them. Consequently, among all the compounds of PHE, only compound ATA resulted as the most suitable for further network pharmacology study because it had a comparatively higher (0.22) drug like score (DLS) from the MolSoft server, no side effects predicted from the ADVERPred database, valuable predicted ADMET properties (Fig. 60A), and also cleared all crucial parameters from the Admet SAR 2.0 (Table 39). Therefore, ATA is found to be a novel drug that is being utilized for the first time in a network pharmacology study against DM.

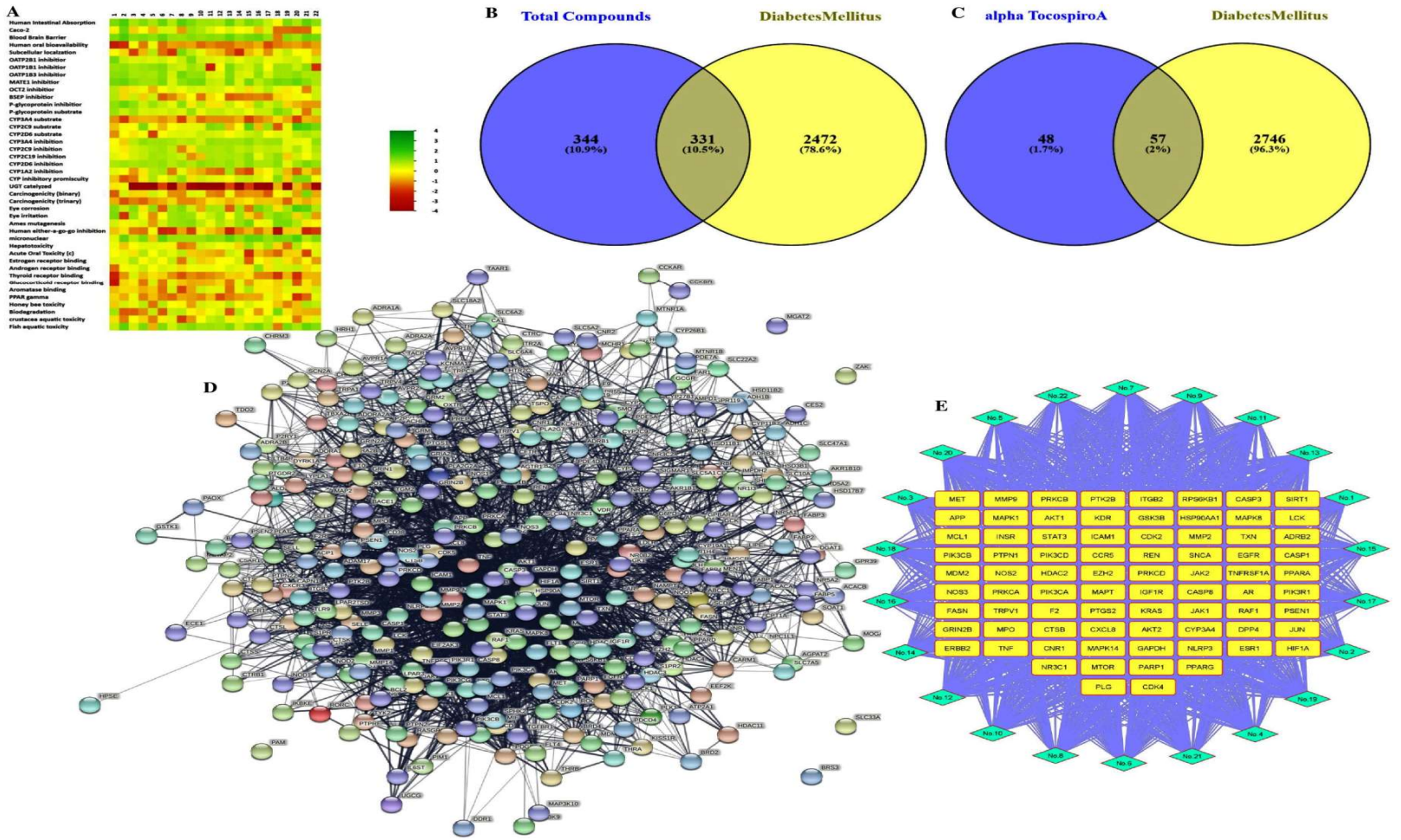

Figure60 Potential active ingredients of PHE, core targets identification and network construction for the treatment of DM. **A)** ADMET score of all the compounds to have drug like property, **B)** Potential 331 core targets identification between 675 STP genes related to all compounds and 2803 DisGenet genes related to DM, **C)** Potential 57 core targets identification between 105 STP genes related to ATA compound and 2803 DisGenet genes related to DM, **D)** PPI network of PHE, and **E)** Compound target network of PHE with top selected genes, light blue diamond shapes represent core compounds and yellow squares represent important potential targets

Table 39 ADMET score of all compounds of PHE

S.N.	Name of Compound	CID	MF	MW	NHBA	NHBD	MolLogP	BBB	DLS
1.	Phenol, 2,4-bis(1,1-dimethylethyl)-	7311	$C_{14}H_{22}O$	206.32	1	1	5.22	4.86	-1.24
2.	2-Buten-1-ol, 2-ethyl-4-(2,2,3-trimethyl-3-cyclopenten-1-yl	119898	$C_{14}H_{24}O$	208.34	1	1	4.37	4.36	-0.40
3.	1,2,5,6-Tetrahydrobenzonitrile	66013	C_7H_9N	107.15	1	0	2.05	3.62	-1.73
4.	Neophytadiene	10446	$C_{20}H_{38}$	278.52	0	0	8.48	1.34	-1.22
5.	4-Piperidinamine, 2,2,6,6-tetramethyl-	37524	$C_9H_{20}N_2$	156.27	2	2	0.53	3.75	-1.10
6.	3,7,11,15-Tetramethyl-2-hexadecen-1-ol	5366244	$C_{20}H_{40}O$	296.53	1	1	7.72	4.31	-0.87
7.	Hexadecanoic acid, methyl ester	8181	$C_{17}H_{34}O_2$	270.5	2	0	7.36	4.53	-1.31
8.	Benzenepropanoic acid, 3,5-bis(1,1-dimethylethyl)-4-hydroxy-, methyl ester	62603	$C_{18}H_{28}O_3$	292.4	3	1	4.77	4.60	-1.21
9.	1,2-Benzenedicarboxylic acid, dibutyl ester	3026	$C_{16}H_{22}O_4$	278.34	4	0	4.39	4.18	-0.38
10.	13-Hexyloxacyclotridec-10-en-2-one	566650	$C_{18}H_{32}O_2$	280.4	2	0	6.52	4.52	-0.95
11.	9,12-Octadecadienoic acid, methyl ester	5284421	$C_{19}H_{34}O_2$	294.5	2	0	7.32	4.51	-1.04
12.	6-Octadecenoic acid, methyl ester, (Z)-	5362717	$C_{19}H_{36}O_2$	296.5	2	0	7.82	4.51	-1.04
13.	Phytol	5280435	$C_{20}H_{40}O$	296.5	1	1	7.72	4.31	-0.87
14.	Methyl stearate	8201	$C_{19}H_{38}O_2$	298.5	2	0	8.37	4.51	-1.31
15.	9-Octadecenoic acid, 12-hydroxy-, methyl ester, [R-(Z)]-	5354133	$C_{19}H_{36}O_3$	312.5	3	1	6.39	4.13	-0.68
16.	Undecanoic acid, 5-chloro-, chloromethyl ester	543301	$C_{12}H_{22}Cl_2O_2$	269.20	2	0	4.83	4.47	-0.93
17.	cis-9-Hexadecenal	5364643	$C_{16}H_{30}O$	238.41	1	0	6.54	4.41	-1.25
18.	15-Hydroxypentadecanoic acid	78360	$C_{15}H_{30}O_3$	258.40	2	2	4.40	3.56	-0.13
19.	Dioctyl phthalate	8346	$C_{24}H_{38}O_4$	390.6	4	0	8.47	4.29	-0.43
20.	1-Glyceryl ricinoleate	5319880	$C_{21}H_{40}O_5$	372.5	5	3	5.18	2.23	-0.07
21.	Alpha Tocospiro A	21674156	$C_{29}H_{50}O_4$	462.7	4	1	7.96	3.40	0.22
22.	Isopropyl linoleate	5352860	$C_{21}H_{38}O_2$	322.5	2	0	7.99	4.47	-0.32

5.11.2 Target genes associated with the compounds and DM

It was observed that a total of 675 genes were associated with all the bioactive compounds in the PHE screen, and 105 genes were associated with the bioactive ingredient ATA by STP databases. Additionally, a maximum of 2,803 DM-related genes were observed by searching DisGeNet databases. By analyzing the Venn diagram (Fig. 60B), 331 intersecting genes were identified in the correlation between genes of all compounds of PHE and DM-related genes. Further, it was also identified that 57 intersecting genes (Fig. 60C) were observed between ATA and DM-related genes.

5.11.3 Hub genes and essential active ingredients of PHE against DM

The above intersecting genes were studied for network construction by the String database with 0.4 confidence as an analysis parameter and visualized. All selected compounds of PHE manifested 331 nodes and 4272 edges in the network pharmacology analysis. This data revealed the presence of 25.8 average node degrees, a 0.45 average local clustering coefficient, a 1658 expected number of edges, and a p-value of 1.0e-16 for PPI enrichment in the network. It was noticed that some valuable genes, such as PAM, BRS3, SLC33A1, ZAK, and MGAT2, have an unconstructed role in the network directly, and such genes were excluded from further study. Based on network pharmacology analysis in reference to the nodes, the edges, and the degree centralities (DC) values of genes from CytoNCA plugged into Cytoscape, a total of 331 genes for all identified PHE compounds may be found to be effective against diabetes with synergistic effects.

Consequently, it was determined that the genes AKT1, TNF, GAPDH, EGFR, STAT3, JUN, CASP3, PPARG, HSP90AA1, ESR1, HIF1A, CXCL8, and MMP9 manifested a higher degree value than others in the network (Table 40). These genes served as the hub genes for protection from diabetes. The network generated by string recommended that the clinical manifestations of PHE in diabetes be closely intertwined with the 331 genes observed in the

PPI network of PHE (Fig. 60D) as well as all compounds collectively observed in thecompound target network (Fig. 60E). Table 41 shows the preferable DC value of ATA from the network pharmacology study for the treatment of DM, along with all the screened compounds of PHE by cytoscape in this study. The ingredients compounds in PHE like 1-Glyceryl ricinoleate, 15-Hydroxypentadecanoic acid, and Methyl stearate also have equal or higher degree values (32, 32, and 37, respectively) comparedto ATA (32) as shown in Table 41. Due to the lack of some crucial parameters of drug likeness, these compounds (Table 39) were excluded from further study.

Table 40 Degree value of top genes related to PHE in network

S.N.	Name of Gene	Value	S.N.	Name of Gene	Value	S.N.	Name of Gene	Value
1.	AKT1	167	5.	STAT3	112	9.	HSP90AA1	99
2.	TNF	162	6.	JUN	108	10.	ESR1	95
3.	GAPDH	147	7.	CASP3	105	11.	HIF1A	92
4.	EGFR	120	8.	PPARG	104	12.	CXCL8	89
13.	MMP9	87						

Table 41 Degree value of compounds of PHE in network

S.N.	Name of Compound	Value	S.N.	Name of Compound	Value
1.	Phenol, 2,4-bis(1,1-dimethylethyl)-	26	12.	6-Octadecenoic acid, methyl ester, (Z)-	27
2.	2-Buten-1-ol, 2-ethyl-4-(2,2,3-trimethyl-3-cyclopenten-1-yl	11	13.	Phytol	9
3.	1,2,5,6-Tetrahydrobenzonitrile	8	14.	Methyl stearate	37
4.	Neophytadiene	15	15.	9-Octadecenoic acid, 12-hydroxy-, methyl ester, [R-(Z)]-	26
5.	4-Piperidinamine, 2,2,6,6-tetramethyl-	12	16.	Undecanoic acid, 5-chloro-, chloromethyl ester	28
6.	3,7,11,15-Tetramethyl-2-hexadecen-1-ol	9	17.	cis-9-Hexadecenal	26
7.	Hexadecanoic acid, methyl ester	22	18.	15-Hydroxypentadecanoic acid	32
8.	Benzenepropanoic acid, 3,5-bis(1,1-dimethylethyl)-4-hydroxy-, methyl ester	17	19.	Dioctyl phthalate	20
9.	1,2-Benzenedicarboxylic acid, dibutyl ester	14	20.	1-Glyceryl ricinoleate	32
10.	13-Hexyloxacyclotridec-10-en-2-one	17	21.	Alpha Tocospiro A	32
11.	9,12-Octadecadienoic acid, methyl ester	23	22.	Isopropyl linoleate	31

5.11.4 Network construction, hub gene analysis and functional annotation of ATA against DM

With the help of the Venny 2.1 tool online, the genes encoding for ATA and the genes of DM were picked, recognized, and visualized. 57 intersected genes were found for PPI network construction (Fig. 61A). The compound target disease network was visualized using data from the STRING database (Fig. 61B). It was a net gain of 57 nodes and 175 edges, with 6.14 an average node degree, 0.489 an average local clustering coefficient, 55 an expected number of edges, and a p-value of <1.0e-16 PPI enrichment from the network pharmacology analysis of ATA and DM intersected genes. In this network pharmacology analysis, some intersecting genes, such as MAP3K9, SMO, CHRM3, P2RX3, BRS3, ATP2A1, and SLC33A1, were

excluded from the study due to a lack of direct network construction.Based on the higher DC values of genes than others in the network and network pharmacology analysis data, genes such as TNF, CASP3, SIRT1, HSP90AA1, MAPK1, CASP8, MDM2, MAPK14, MCL1, MAPK8, CASP1, IGF1R, and CDK2 were considered hub genes for ATA against DM (Fig. 61C). With the selection of hub genes, the further activities of these genes were analyzed by utilizing the Gene Ontology (GO) study and the gene enrichment analysis with KEGG pathways by using the ShinyGO v0.741 database. Molecular function (MF; Fig. 61D), biological process (BP; Fig. 61E), as well as cellular component (CC; Fig. 61F), the three valuable classes with detectable properties for target hub genes, were collected from the GO study. The GO detected properties for target hub genes such as apoptotic signaling pathways, catalytic activity, protein domain-specific binding, cellular response to environmental stimulus as well as chemical stress, regulation of the apoptotic process, death-inducing signaling complex, mitochondrion, nucleoplasm, and nuclear lumen from all three valuable classes show higher values than other important predicted values in reference to FDR and number of genes. It was determined that the selected hub gene TNF, which manifested with the highest degree value, i.e., 32, served as the top hub gene of ATA for protection from DM, and it was also the hub gene of PHE with the 2nd higher DC value (162) as observed in the above study. Thus, the top two genes, AKT1 (167) and TNF (162), were selected for further studies.

5.11.5. Potential molecular pathways of ATA against DM

Following the KEGG pathway enrichment analysis, the top intertwining genes of ATA with network topologies genes of DM were significantly enriched in 100 pathways with P values, i.e., $p<0.05$, with 29 signaling pathways being the most abundant; the top pathways are shown in Figure 61G. Table 42 provides extensive information on pathways that contribute to the development and progression of diabetes. Aside from that, in this study, the hub gene

"TNF" was found to be precisely strengthened in 49 pathways, along with 14 signaling pathways. TNF plays a major role in all 49 pathways studied by metabolic pathways, inferring that the TNF signaling pathway (Fig. 62A) might be the hub signaling pathway, along with the JNK/MAPK/ERK and IRS/PI3K/AKT-GLUT4 signaling pathways, for PHE against diabetes, highlighted in Table 42. Furthermore, a crucial and noticeable scenario was also observed here: the hub genes of ATA were also involved in the present COVID-19 pandemic management, with enrichment of 5 genes (MAPK14, MAPK1, MAPK8, TNF, and CASP1) through the Corona virus disease pathway (hsa05171) in this study.

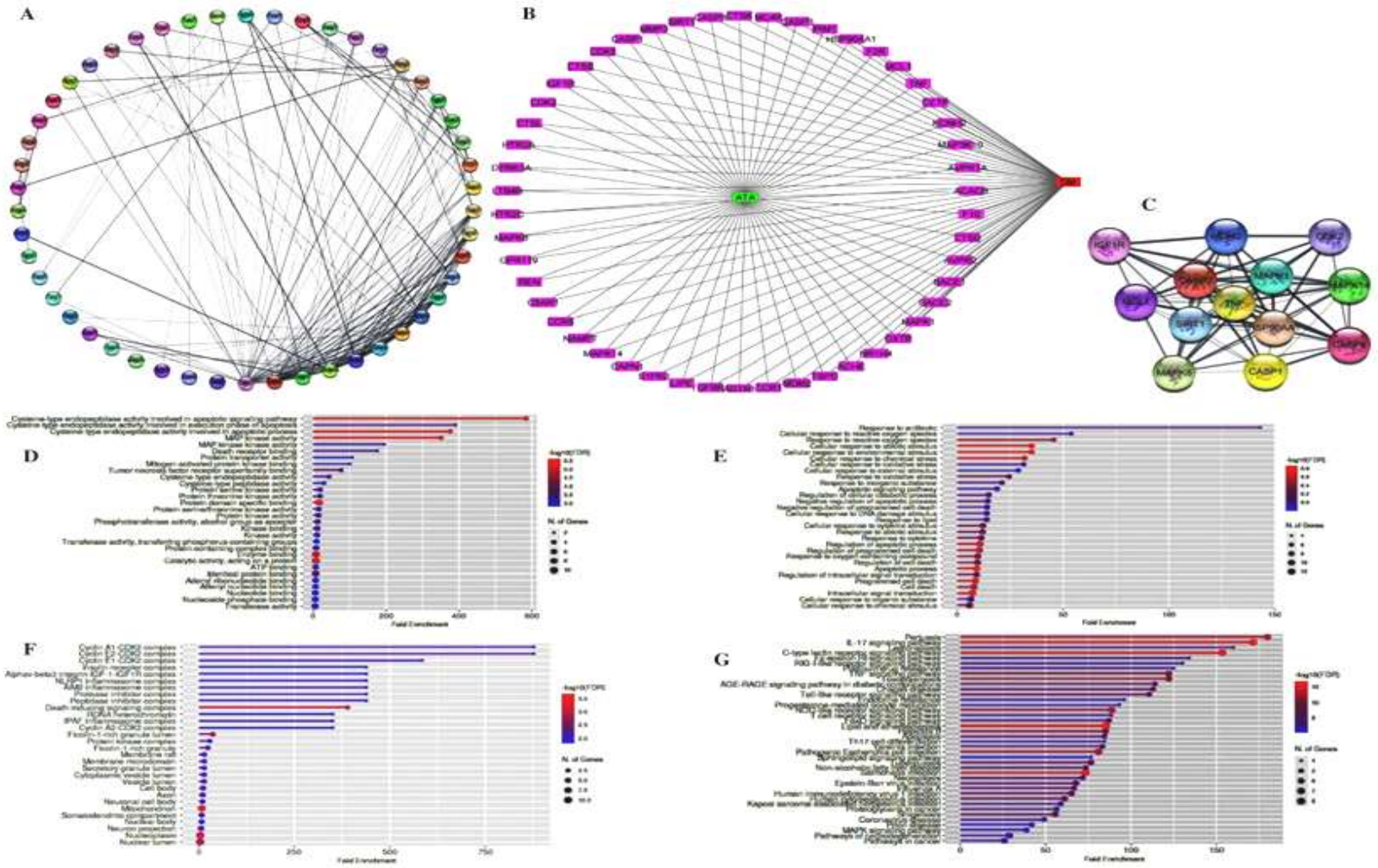

Figure 61 Network construction, hub gene analysis, functional annotation and potential molecular pathways of ATA for the treatment of DM. **A)**PPI network of ATA, **B)** Compound target disease network of ATA, green square represents important potential core compound-ATA, pink rectangles represent important potential targets and red square represents DM. **C)** Top 13 selected hub genes network of ATA, **D)** Molecular functions, **E)** Biological processes, **F)** Cellular components, **G)** Top most KEGG pathway enrichment in study of ATA

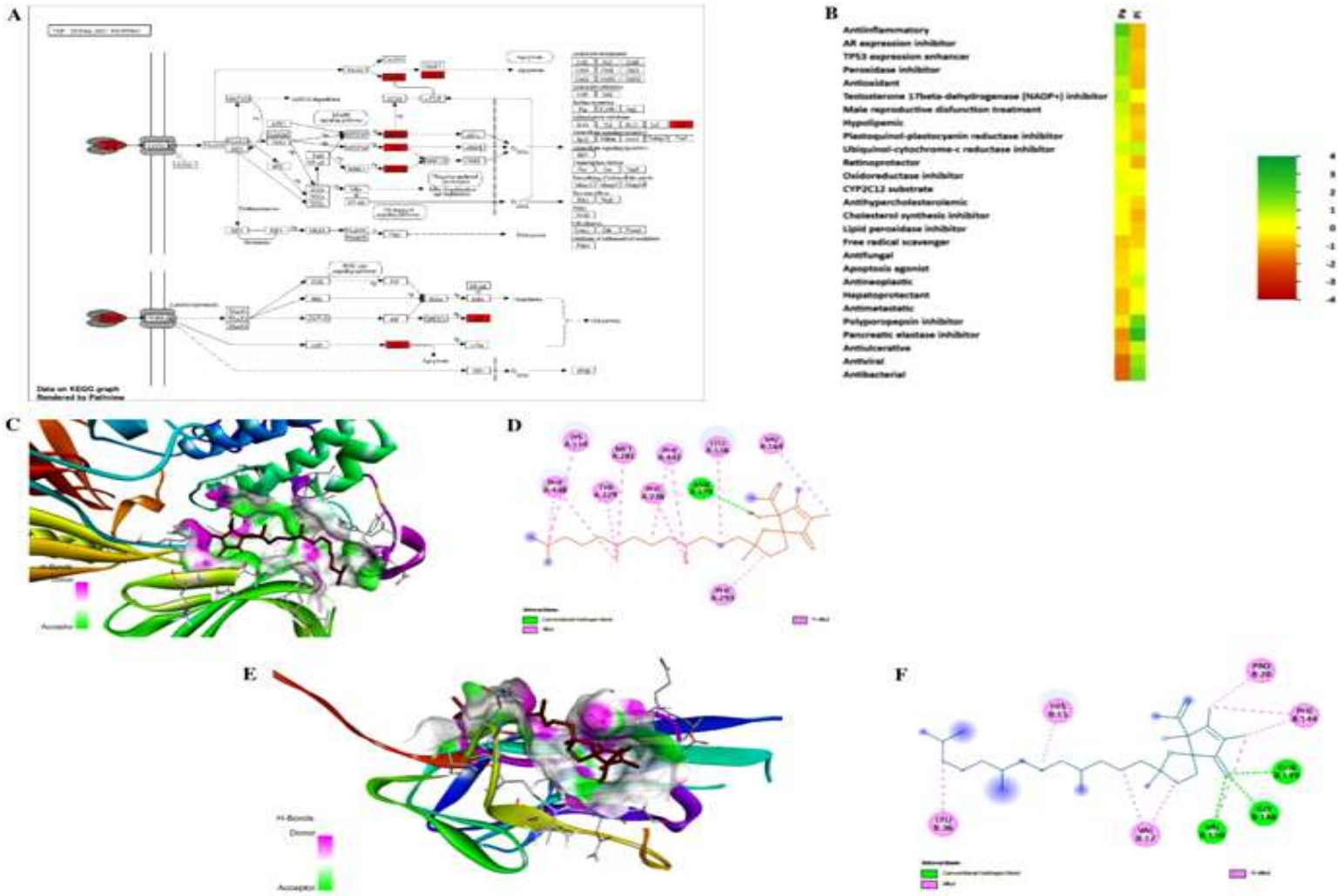

Figure62 KEGG pathway enrichment, heat map of PASS activity and molecular docking diagram of the ATA with key targets. **A)** TNF as hub signaling pathway from KEGG pathway enrichment, **B)** Heat map of top probable bioactivities in the PASS study, **C)** 3D interaction diagram with AKT1, **D)** 2D interaction diagram with AKT1, **E)** 3D interaction diagram with TNF, **F)** 2D interaction diagram with TNF

Table 42 Target genes of KEGG pathways enrichment analysis of ATA related to DM

S.N.	Enrichment FDR	No. Genes	Pathway	KEGG ID	Genes
1.	**1.04E-11**	**7**	**FoxO signaling pathway**	**hsa04068**	**CDK2 MAPK14 SIRT1 IGF1R MDM2 MAPK1 MAPK8**
2.	**2.79E-10**	**6**	**TNF signaling pathway**	**hsa04668**	**MAPK14 MAPK1 MAPK8 TNF CASP3 CASP8**
3.	8.09E-10	6	Apoptosis	hsa04210	MCL1 MAPK1 MAPK8 TNF CASP3 CASP8
4.	1.25E-08	5	Endocrine resistance	hsa01522	MAPK14 IGF1R MDM2 MAPK1 MAPK8
5.	**1.48E-08**	**5**	**AGE-RAGE signaling pathway in diabetic complications**	**hsa04933**	**MAPK14 MAPK1 MAPK8 TNF CASP3**
6.	1.57E-08	5	Toll-like receptor signaling pathway	hsa04620	MAPK14 MAPK1 MAPK8 TNF CASP8
7.	**4.74E-08**	**6**	**MAPK signaling pathway**	**hsa04010**	**MAPK14 IGF1R MAPK1 MAPK8 TNF CASP3**
8.	**1.02E-07**	**5**	**Non-alcoholic fatty liver disease**	**hsa04932**	**MAPK14 MAPK8 TNF CASP3 CASP8**
9.	**1.10E-07**	**6**	**PI3K-Akt signaling pathway**	**hsa04151**	**CDK2 HSP90AA1 IGF1R MCL1 MDM2 MAPK1**
10.	5.07E-07	6	Pathways of neurodegeneration	hsa05022	MAPK14 MAPK1 MAPK8 TNF CASP3 CASP8
11.	**5.18E-07**	**5**	**Coronavirus disease**	**hsa05171**	**MAPK14 MAPK1 MAPK8 TNF CASP1**
12.	5.02E-06	5	Alzheimer disease	hsa05010	MAPK1 MAPK8 TNF CASP3 CASP8
13.	**7.11E-06**	**3**	**Type II diabetes mellitus**	**hsa04930**	**MAPK1 MAPK8 TNF**
14.	2.41E-05	3	Prolactin signaling pathway	hsa04917	MAPK14 MAPK1 MAPK8
15.	2.64E-05	3	P53 signaling pathway	hsa04115	MDM2 CASP3 CASP8
16.	**0.000199503**	**3**	**MTOR signaling pathway**	**hsa04150**	**IGF1R MAPK1 TNF**
17.	**0.001680442**	**2**	**Pancreatic cancer**	**hsa05212**	**MAPK1 MAPK8**
18.	0.001774563	2	EGFR tyrosine kinase inhibitor resistance	hsa01521	IGF1R MAPK1
19.	**0.002997332**	**2**	**Insulin resistance**	**hsa04931**	**MAPK8 TNF**
20.	0.003021852	2	HIF-1 signaling pathway	hsa04066	IGF1R MAPK1

5.11.6 Activity spectra for substances (PASS)

The PASS online prediction revealed different crucial data in Table 43, which showed the anticipated activities for the bioactive constituent ATA. Bioactivities like anti-inflammatory, antioxidant, hypolipemic, retinol protector, antihypercholesterolemic, cholesterol synthesis inhibitor, antineoplastic, hepatoprotectant, antiviral, etc. are primarily detected for ATA in this study (Fig. 62B). Anti-inflammatory activity had the greatest predicted effectiveness. As demonstrated by the findings, the probable activity (Pa) values were quite close to 1 and the probable inactivity (Pi) values were extremely close to 0, indicating that the selected bioactive constituent ATA is highly likely to be engaging in these activities.

5.11.7. Molecular docking analysis

5.11.7.1. Validation of top selected hub genes protein

Receptor proteins were validated using a Ramachandran plot evaluation. When the plot for AKT1, the top hub gene, was generated, it showed that 92.8 percent of amino acids remained present in the preferred zone. The plot for TNF-α was generated, and it showed that 91.9 percent of amino acids persisted in the preferred zone. The ProSA web was also utilized to evaluate the quality of the conformations of the selected proteins (AKT1 and TNF-α). The Z-score map of PDB proteins is scientifically verified by NMR spectroscopy (deep blue) as well as X-ray diffraction (pale blue). The Z-score of the chosen proteins AKT1 (-7.28) and TNF-α (-4.3) is shown, respectively.

5.11.7.2. Affinity binding score of a key bioactive ingredient Alpha Tocospiro A on hub genes protein

AutoDock 4.0 was utilized to estimate affinity-binding energy for hub genes. The most significant compound, ATA, was docked with hub genes (AKT1; PDB ID 6hhg; and TNF-α; PDB ID 6op0). With the grid point spacing of 0.575 Angstroms, 126-X, 126-Y, 126-Z, and 13.601, -11.818, and -15.800 as Central Grid Point coordinates, the binding energy score for

chain A of 6hhg against ATA was -6.99 kcal/mol, and through 0.486 Angstroms grid point spacing, 126-X, 126-Y, 126-Z, and -0.559, -0.686, and 27.615 as Central Grid Point coordinates, the binding energy score for chain B of 6op0 against ATA was -6.05 kcal/mol. As shown in Table 44, the binding energy scores of chain A of 6op0 against ATA (-4.80 kcal/mol) and chain C of 6op0 against ATA (-5.59 kcal/mol), as well as the binding site residues on hub genes, were calculated. Discovery Studio was utilized for structure visualization in 3D and 2D. The most important residues on the AKT1 and ATA complex with hydrophobic interaction are LYS154, VAL164, MET281, TYR229, PHE236, PHE293, PHE438, LEU156, PHE442, and also ASN279 with hydrogen bond interaction. The relevant amino acids for chain B of the TNF-α and ATA complex are shown in Table 44. The most important amino acid residues for chain B of the TNF-α and ATA complex with hydrophobic interactions are VAL17, PRO20, VAL150, LEU36, HIS15, and PHE144, along with hydrogen bond interactions GLY148, GLN149, and VAL150. 3D and 2D structures for the AKT1 complex with ATA were illustrated in Fig. 62C-D, and the structures for the TNF-α complex with ATA were illustrated in Fig. 62E-F, along with Figs. 63 and 64.

Table 43 Pass predicted bioactivity of Alpha Tocospiro A

Pa	Pi	Bioactivity	Pa	Pi	Bioactivity
0.896	0.004	Antiinflammatory	0.496	0.127	CDP-glycerol glycerophosphotransferase inhibitor
0.753	0.004	AR expression inhibitor	0.383	0.025	Glycogen synthase stimulant
0.751	0.017	TP53 expression enhancer	0.410	0.053	Prostaglandin-E2 9-reductase inhibitor
0.734	0.009	Peroxidase inhibitor	0.360	0.004	Retinyl-palmitate esterase inhibitor
0.640	0.004	Antioxidant	0.488	0.132	CYP2H substrate
0.685	0.060	Testosterone 17beta-dehydrogenase (NADP+) inhibitor	0.377	0.023	Prion diseases treatment
0.624	0.005	Male reproductive disfunction treatment	0.423	0.068	Antiviral (Rhinovirus)
0.597	0.023	Hypolipemic	0.361	0.015	Anticataract
0.558	0.014	Plastoquinol-plastocyanin reductase inhibitor	0.418	0.074	Antipruritic, allergic
0.614	0.102	Ubiquinol-cytochrome-c reductase inhibitor	0.349	0.011	Aldose reductase substrate
0.507	0.003	Retinoprotector	0.359	0.021	Free radical scavenger
0.554	0.053	Oxidoreductase inhibitor	0.368	0.032	Proliferative diseases treatment
0.576	0.077	CYP2C12 substrate	0.359	0.023	Antiinflammatory, ophthalmic
0.500	0.022	Antihypercholesterolemic	0.362	0.027	Chemopreventive
0.479	0.004	Cholesterol synthesis inhibitor	0.387	0.053	Antifungal
0.491	0.018	Lipid peroxidase inhibitor	0.442	0.108	Platelet aggregation stimulant
0.473	0.019	Myc inhibitor	0.403	0.072	Apoptosis agonist
0.465	0.041	Nucleotide metabolism regulator	0.413	0.082	CYP3A substrate
0.445	0.036	CYP3A inducer	0.327	0.005	Vitamin
0.412	0.008	Lipocortins synthesis antagonist	0.416	0.098	Antineoplastic
0.439	0.038	CYP3A4 inducer	0.221	0.014	Radical formation agonist
0.392	0.003	HMG CoA synthase inhibitor	0.266	0.062	Antiprotozoal
0.424	0.050	Antisecretoric	0.249	0.045	Metabolic disease treatment
0.455	0.147	CYP2J substrate	0.219	0.015	Antineoplastic antibiotic
0.357	0.051	Cell adhesion molecule inhibitor	0.379	0.177	CYP2J2 substrate
0.415	0.109	Macrophage colony stimulating factor agonist	0.297	0.100	Antiulcerative
0.371	0.068	Menopausal disorders treatment	0.224	0.029	Nitric oxide antagonist
0.339	0.043	DELTA14-sterol reductase inhibitor	0.375	0.181	Saccharopepsin inhibitor
0.337	0.048	Hepatoprotectant	0.375	0.181	Chymosin inhibitor
0.355	0.072	P-glycoprotein substrate	0.375	0.181	Acrocylindropepsin inhibitor

Table 44 The docking results (binding energy) of ligand (Alpha Tocospiro A) and the hub genes (AKT1 and TNF-α) along their respective number of hydrogen bonds as well as interacting amino acids related to DM

S.N.	Name	AKT1				TNF			
		BE	HBT	HBD	BR	BE	HBT	HBD	BR
1.	Alpha-Tocospiro A (ATA)	-6.99 Chain A	ATA:H14-ASN279:OD1	2.67171	ATA:C15 - VAL164 ATA - LEU156 ATA:C25 - MET281, ATA:C27 - A:LYS154 TYR229 - ATA:C25 PHE236 - ATA:C20 PHE293 - ATA PHE438 - ATA:C25 PHE438 - ATA:C27, PHE442 - ATA:C20 PHE442 - ATA	-6.05 Chain B	GLY148:HN - ATA:O3 GLN149:HN - ATA:O3 VAL150:HN - ATA:O3	2.11665 2.00624 2.49152	VAL17 - ATA VAL17 - ATA ATA:C14 - PRO20 ATA:C15 - VAL150 ATA:C27 - LEU36 HIS15 - ATA PHE144 - ATA:C14 PHE144 - ATA:C15
						-5.59 Chain C	ALA18:HN - ATA:O2 GLY148:HN2 - ATA:O4 GLY148:HN3 - ATA:O4 GLN149:HN - ATA:O4 VAL150:HN - ATA:O4 ATA:H14 - VAL150:O	2.39248 1.86834 2.03964 2.51555 2.13886 1.82938	ALA18 - ATA:C27 ATA:C10 - VAL150 ATA:C14 - VAL17 ATA:C15 - VAL17 ATA:C25 - LEU142 ATA:C27 - LEU142
						-4.80 Chain A	ATA:H14-ASP143:OD1, PHE144:HN - :ATA:O3, LYS65:HZ2 - :ATA:O4, LYS65:HZ2 - :ATA:O2	2.12181, 2.59333, 1.91317, 1.945	LYS65 – ATA, ALA145 - ATA:C14, ATA:C10 -LYS65

BE: Binding energy (kcal/mol); HBT: Hydrogen bonding type; HBD: Hydrogen bond distance; BR: Bonding residue

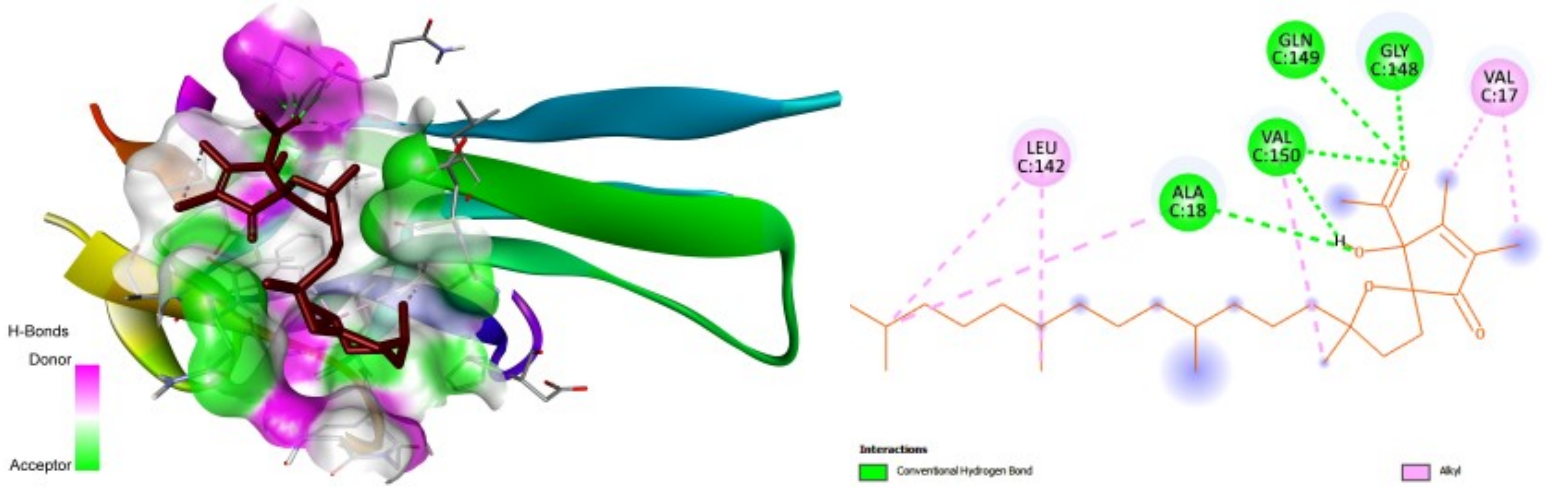

Fig. 63 Interaction of Alpha Tocospiro A with TNF-α chain-C, A) 3D and B) 2D

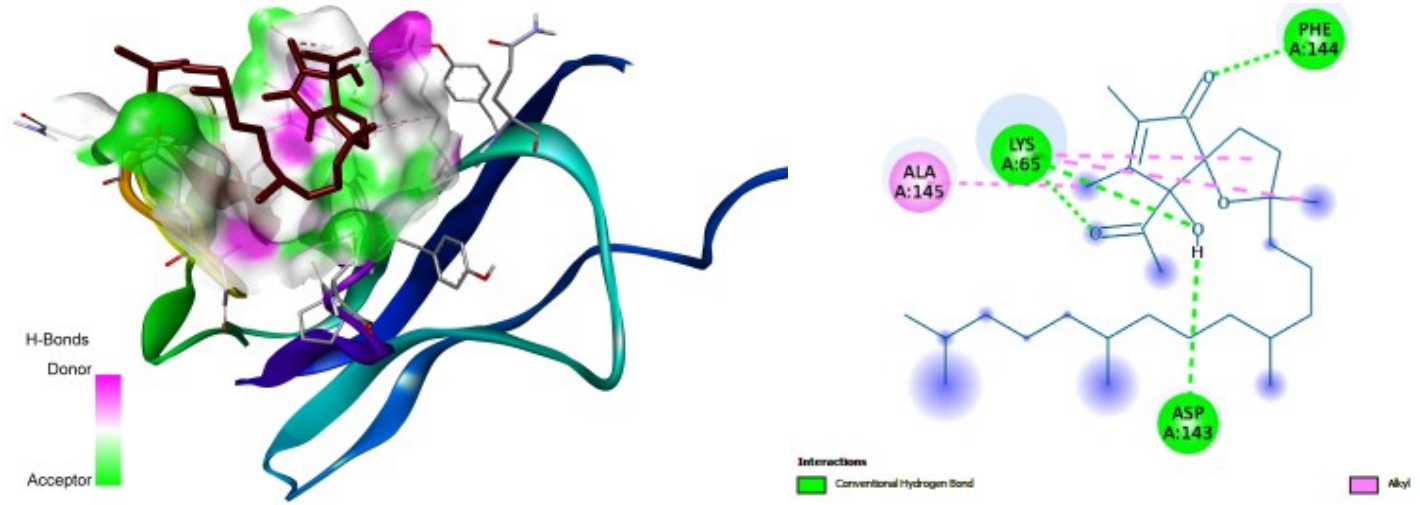

Fig. 64 Interaction of Alpha Tocospiro A with TNF-α chain-A, A) 3D and B) 2D

5.12 ADMET and drug-likeness score of biomarker compounds of PHE identified in LC-MS and HR-MS

The Swiss ADMET database predicted results in the form of Lipinski's rule for all biomarker compounds for PHE, confirming that these compounds possess drug-like properties (Table 45). All six biomarker compounds interacted with the genes, and were considered to be therapeutic components. Consequently, all six biomarker compounds of PHE, were the most suitable for further network pharmacology studies because they had a higher drug-like score (DLS) from the TCMSP and valuable predicted ADMET properties (Table 45).

Table 45ADMET and drug-like properties of biomarker compounds of PHE

Biomarker compounds	MW	AlogP	Hdon	Hacc	OB (%)	Caco-2	BBB	DL	FASA-	TPSA	RBN	HL	Lipinski
Berberine	336.39	3.45	0	4	36.86	1.24	0.57	0.78	0.19	40.8	2	6.57	0
Chebulic acid	356.26	-0.26	6	11	72	-1.4	-1.75	0.32	0.4	198.89	5	3.44	2
Gallic acid	170.13	0.63	4	5	31.69	-0.09	-0.54	0.04	0.41	97.99	1	11.78	0
Andrographolide	350.5	2.06	3	5	46.96	-0.25	-0.88	0.36	0.27	86.99	3	1.72	0
apigenin	270.25	2.33	3	5	23.06	0.43	-0.61	0.21	0.41	90.9	1	-	0
quercetin	302.25	1.5	5	7	46.43	0.05	-0.77	0.28	0.38	131.36	1	14.4	0
Kaempferol	286.25	1.77	4	6	41.88	0.26	-0.55	0.24	0.00	111.13	1	14.74	0

5.12.1 Network pharmacology analysis of the common targets and possible pathways regulated by biomarker compounds in DM

To identify the possible targets and pathways involved in the anti-DM activities of biomarker compounds, we performed network pharmacology analysis. According to the database we searched, 569 biomarker compounds-associated targets and 16949 DM-related targets were identified, and 422 common potential targets were obtained (Fig. 65). Then, the common targets were uploaded to the STRING database, and a PPI network among 249 targets was constructed (Fig. 66). And the 249 core targets in the PPI network are shown in Figure67, along with the top10 hub targets (Fig. 68).

Furthermore, GO and KEGG analyses were performed to identify the potential involved pathways. The top 20 obviously enriched items in GO analysis and the top 20 significantly enriched pathways in KEGG analysis are indicated in Figures 69 and 70, respectively. Of

note, the pathways in pancreatic cancer ranked first on the basis of fold enrichment, and the PI3K-AKT signaling pathway in DM was prominently observed in the KEGG analysis, which supports the anti-DM activities of biomarker compounds in PHE. Moreover, protein serine kinase activity was identified in molecular function items of GO analysis, and FoxO signaling, lipid, and atherosclerosis-related pathways ranked highly in KEGG analysis. Because the protein serine kinase and FoxO signaling, lipid and atherosclerosis-related pathways play essential roles in DM and pancreatic cancer, our results of network pharmacology analysis suggest that biomarker compounds of PHE may exert anti-DM activities.

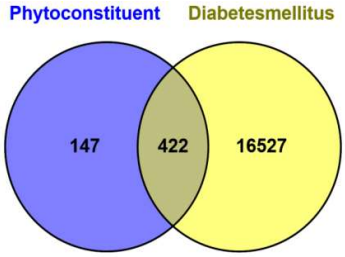

Figure 65 Common potential targets of biomarker compounds of PHE against DM

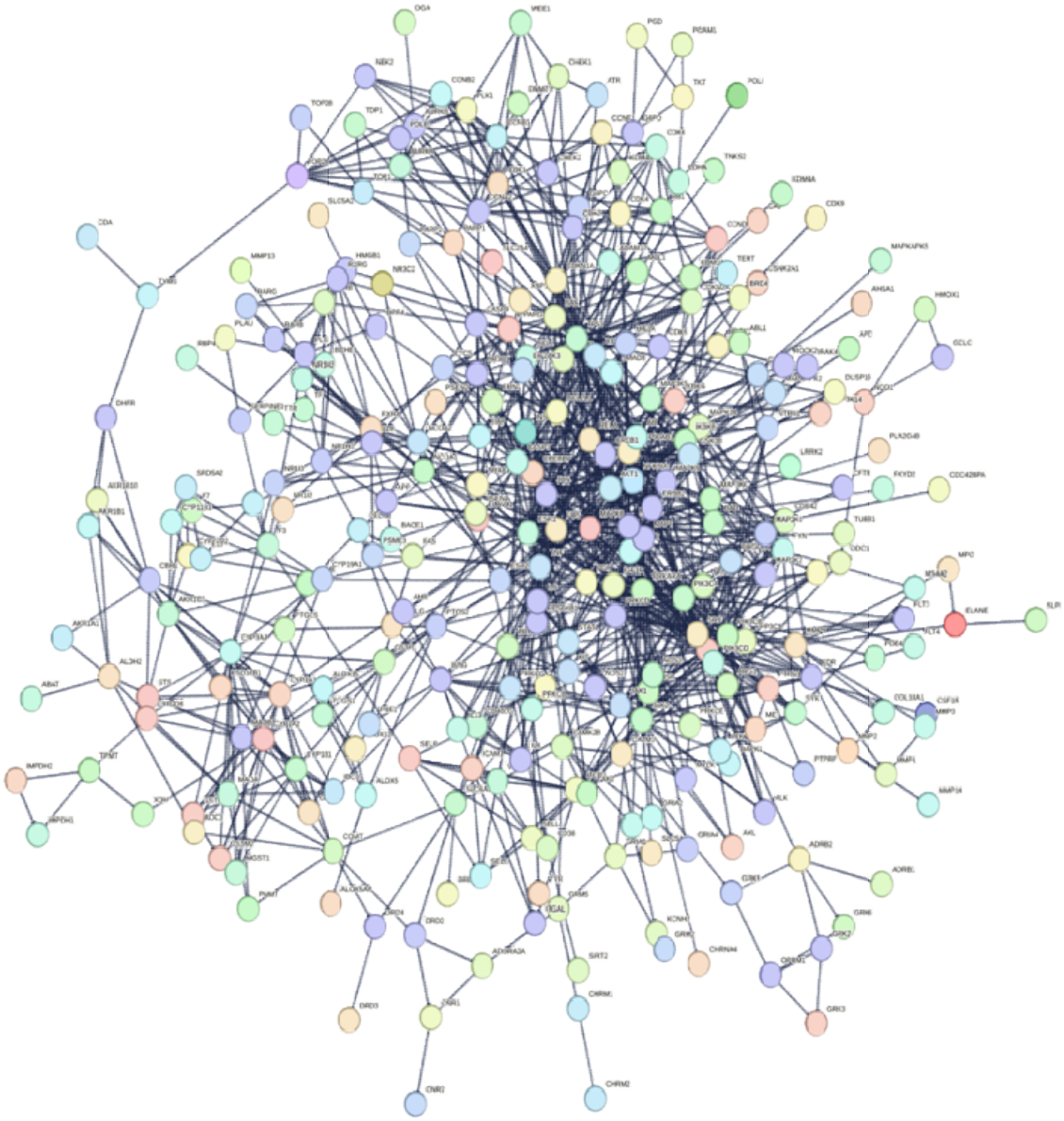

Figure 66 The PPI network for common targets of biomarker compounds and DM

Figure 67 The 249 core targets of biomarker compounds of PHE against DM

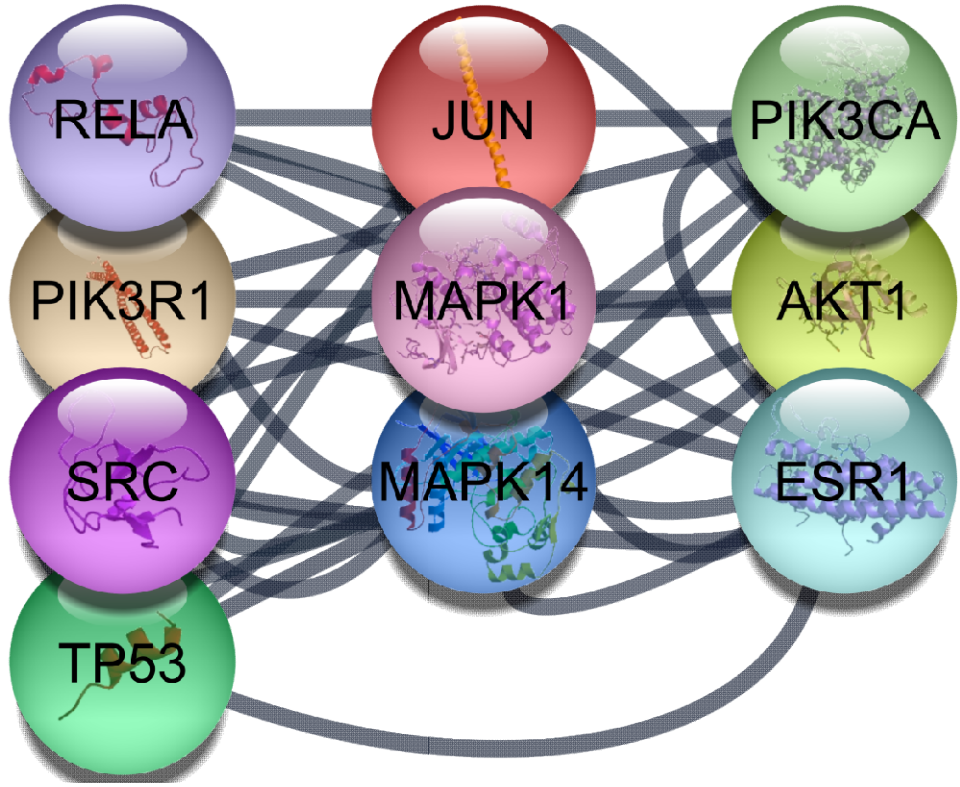

Figure 68 The top 10 hub targets of biomarker compounds of PHE against DM

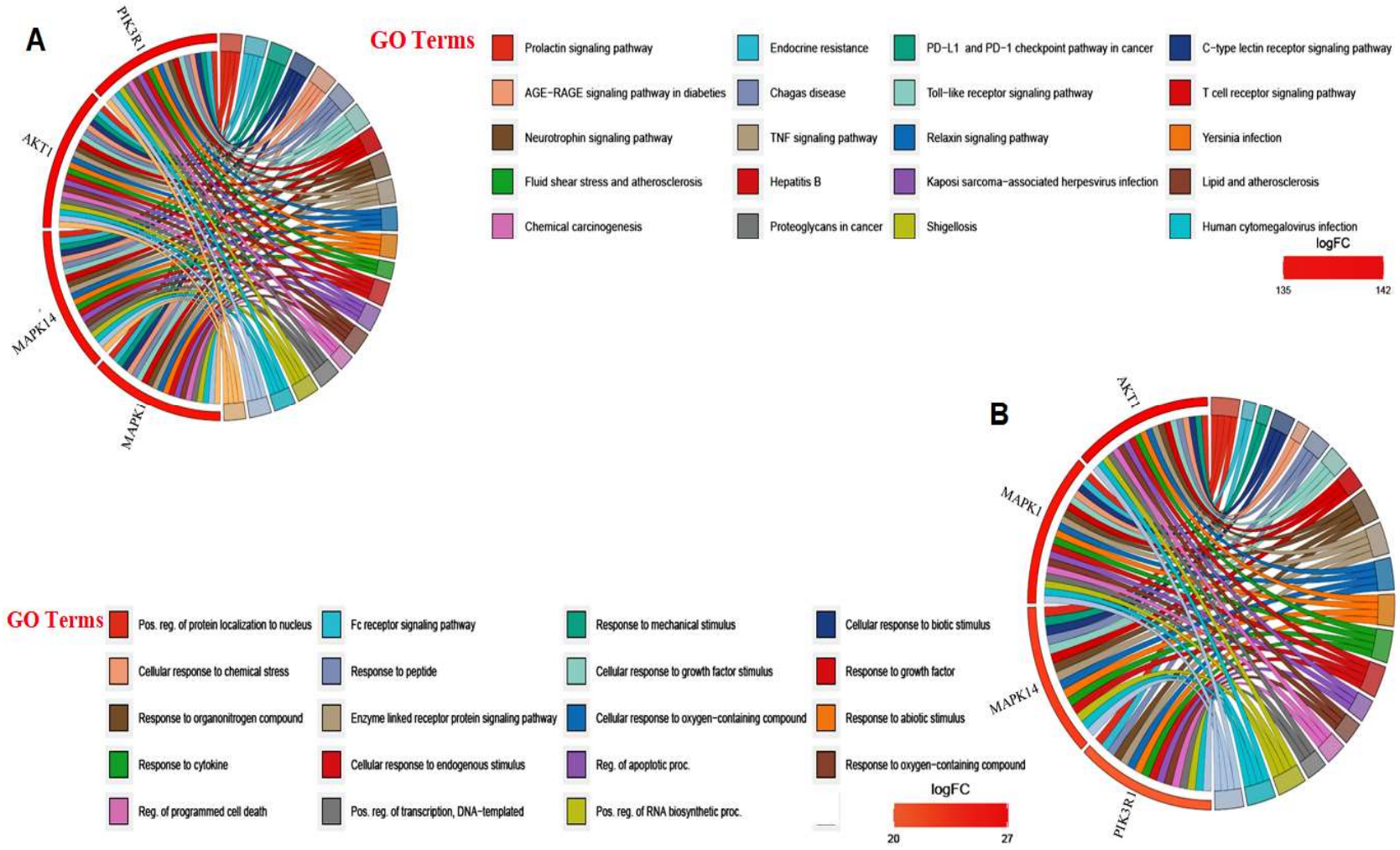

Figure 69 A) Prominent signaling pathway involve in KEGG analysis and **B)**biological processes of GO analysisfor biomarker compounds of PHE against DM

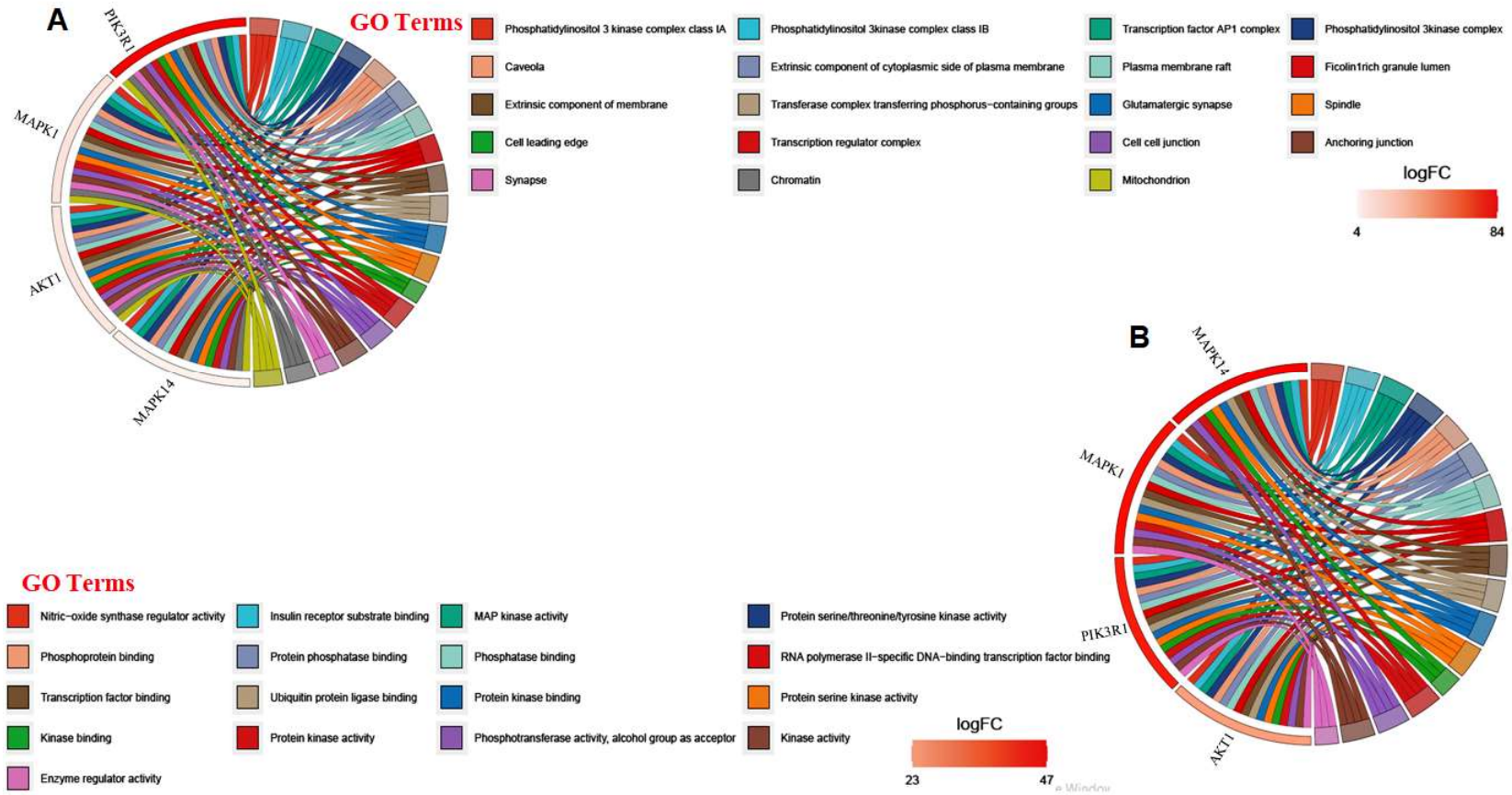

Figure 70A) Cellular component and**B)**molecular function of GO analysis for biomarker compounds of PHE against DM

5.12.2 Molecular docking assessment

Then, we performed molecular docking to predict the interaction between the six biomarker compounds of PHE and the 10 DM-related targets. The results revealed that all six biomarker compounds of PHE had a high binding affinity with TP53, MAPK1, AKT1, PIK3R1, PIK3CA, RELA, IL4, TNF, PPARG, and BCL2 as indicated by binding energies less than -5.0 (Table46-47). And the detailed information about the binding energies and the hydrogen bonds formed between the biomarker compounds of PHE and the targets is demonstrated in Table 47. These results indicate that TP53, MAPK1, AKT1, PIK3R1, PIK3CA, RELA, IL4, TNF, PPARG, and BCL2 might serve as potential targets of biomarker compounds of PHE against DM. Figures71-73 showed the 3D and 2D interaction images of apigenin and berberine against TP53, IL4, and TNF, the DM-related targets.

Table 46 Molecular docking test results of biomarker compounds of PHE and high scoring DM-related targets

S.No.	Core genes (Human)	PDB ID	Binding energy of biomarker compound (kJ/mol)					
			ANDR	AP	BBR	CA	GA	KM
1.	TP53	1tup	-6.83	-7.86	-6.62	-5.80	-5.56	-7.59
2.	MAPK1	6g9n	-6.38	-6.52	-7.30	-4.58	-4.76	-6.72
3.	AKT1	7apj	-6.10	-6.38	-6.30	-4.65	-5.22	-6.06
4.	PIK3R1	4ovv	-5.66	-5.83	-7.12	-3.02	-3.33	-5.80
5.	PIK3CA	8gub	-6.81	-6.10	-6.94	-4.45	-5.62	-6.19
6.	RELA	6yp8	-7.51	-6.74	-6.79	-3.73	-4.96	-5.82
7.	IL4	8ch7	-7.32	-7.23	-7.69	-7.07	-5.67	-6.23
8.	TNF	7kp8	-6.15	-7.03	-7.61	-3.77	-4.11	-6.71
9.	PPARG	8dsz	-7.44	-6.02	-6.99	-6.16	-5.61	-5.96
10.	BCL2	8hlm	-7.31	-7.38	-6.79	-6.07	-4.93	-6.86

ANDR=Andrographolide, AP=Apigenin, BBR=Berberine, CA=Chebulic acid,GA=Gallic acid, and KM=Kaempferol

Table 47 Molecular docking test information of biomarker compounds of PHE and high scoring DM-related targets

S.No.	Marker compound	Core genes (Human)	Binding energy (kcal/mol)	Bond number	Binding site	Bond category types	Bond length (Å)
1.	AP	TP53	-7.86	7	SER116	Conventional HB	2.10
					TYR126	Conventional HB	1.89
					ARG282	Conventional HB	2.74
					LEU111	Conventional HB	1.98
					THR125	Conventional HB	1.91
					HIS115	Pi-Donor HB	2.01
					HIS115	Pi-Donor HB	2.96
		BCL2	-7.38	4	ARG202	Conventional HB	1.94
					GLU224	Conventional HB	2.10
					CYS229	Conventional HB	2.04
					PRO219	Conventional HB	1.83
		AKT1	-6.38	3	LEU268	Conventional HB	2.17
					GLY327	Carbon HB	3.26
					THR305	Pi-Donor HB	2.98
2.	BBR	IL4	-7.69	1	HIS59	Carbon HB	3.11
		TNF	-7.61	1	HIS15	Conventional HB	1.93
		MAPK1	-7.30	5	LYS151	Conventional HB	1.96
					LYS151	Conventional HB	2.02
					ASN154	Carbon HB	3.25
					ASN154	Carbon HB	3.36
					ASP167	Carbon HB	2.93
		PIK3R1	-7.12	3	ARG662	Conventional HB	2.13
					GLU263	Carbon HB	3.11
					SER161	Carbon HB	3.13
		PIK3CA	-6.94	-	-	-	-
3.	ANDR	RELA	-7.51	5	TYR48	Conventional HB	1.94
					GLU20	Conventional HB	2.37
					GLU20	Conventional HB	1.89
					GLU20	Conventional HB	2.08
					GLU20	Conventional HB	2.09
		PPARG	-7.44	2	GLN458	Conventional HB	2.22
					PRO454	Conventional HB	2.24

ANDR=Andrographolide, AP=Apigenin, BBR=Berberine, CA=Chebulic acid,GA=Gallic acid, KM=Kaempferol, and HB=Hydrogen bond.

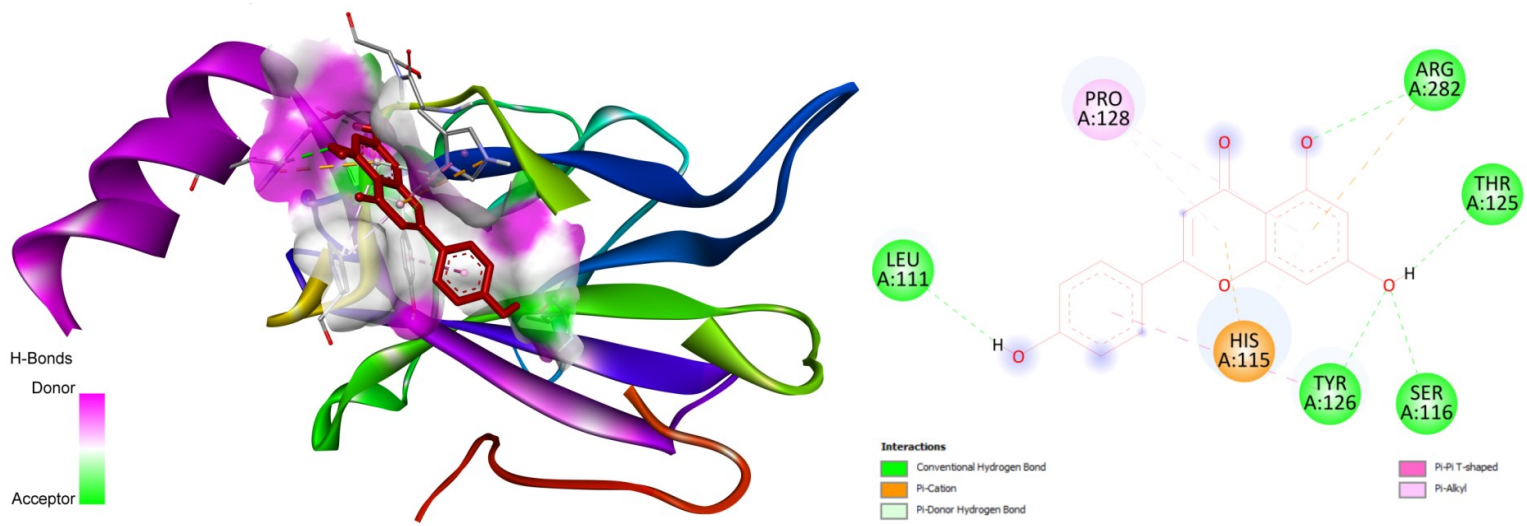

Figure 71 3D and 2D interaction images of apigenin against the DM-related target TP53

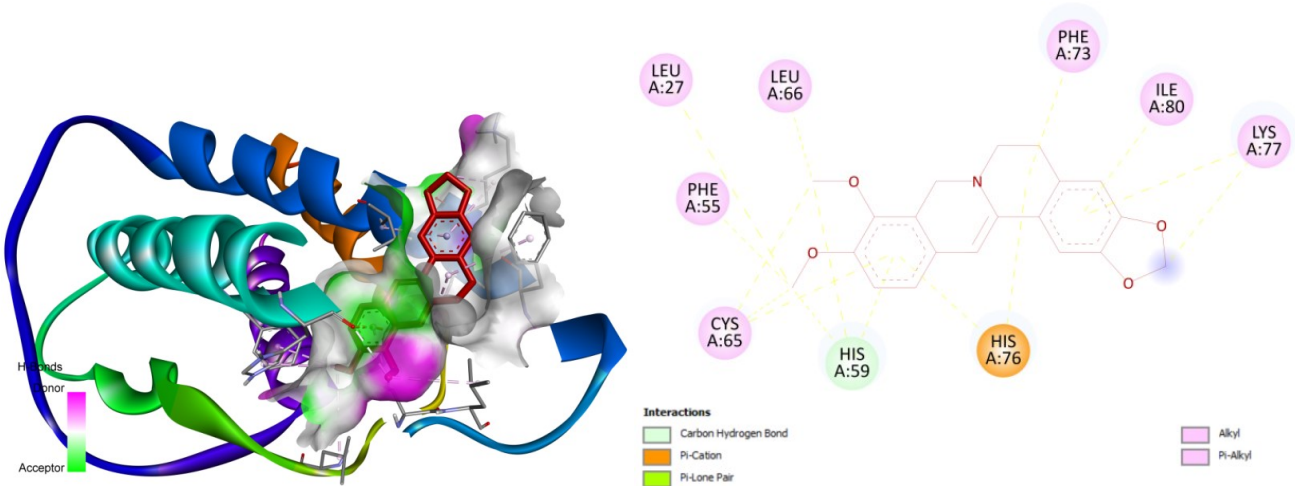

Figure 72 3D and 2D interaction images of berberine against the DM-related target IL4

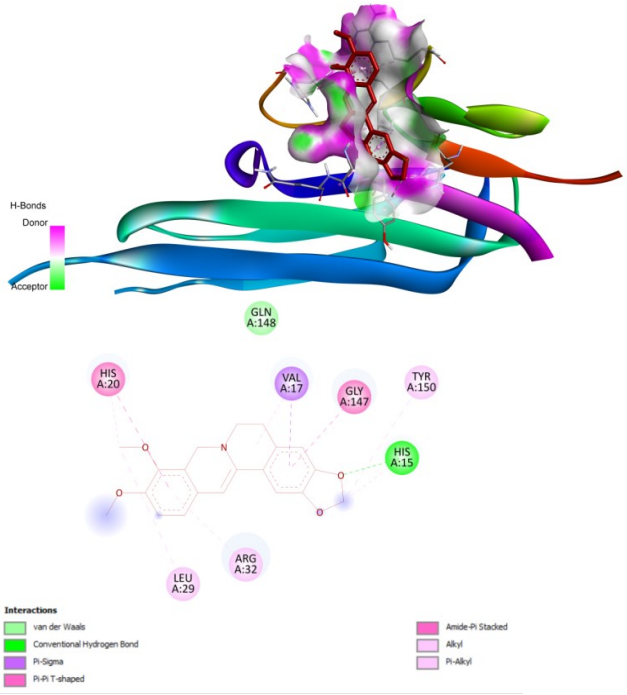

Figure 733D and 2D interaction images of berberine against the DM-related target TNF

5.13Acquisition of gut metabolites and their potential targets

Metabolites (27) were obtained from the 6 genus out of 15 genus (*Lactobacillus*, *Prevotella*, *Bacteroides*, *Clostridium*, *Bifidobacterium*, and *Ruminococcus*) of gut microbiota from the 10 family through the gutMgene microbiome database, choosing the mouse as an organism. Figure 74A-B shows the gut microbiota diversity in the heat map from all group rats, suggesting beneficial effects in PHE treatment groups. A total of 23 gene targets from all the above metabolites of mouse gut were obtained through the gutMgene database (Table 48), and Figure 74C–G showed a gut microbiota-metabolite-target network. These targets were scored through the string web server using confidence 0.7, selecting *Musmusculus* as an organism (Table 49), and 4 target genes were selected for molecular docking studies on the basis of the string web server (score above 0.995). The obtained targets and metabolites were considered significant components for analyzing the therapeutic effects of PHE through the gut microbiota in the rat model of the present study.

Table 48 Gut metabolites and their potential target genes through gutMgene database

Mouse	Gut Microbiota (ID)	Metabolite (ID)	Gene (ID)	Alteration
mouse	*Lactobacillus*	Butyrate	Tjp1	Elevated
mouse	*Lactobacillus*	13-hydroxy-9(Z),15(Z)-octadecadienoic acid	Arg1	Elevated
mouse	*Lactobacillus*	13-oxo-9(Z),15(Z)-octadecadienoic acid	Arg1	Elevated
mouse	*Lactobacillus*	Acetate		
mouse	*Lactobacillus*	Propionate		
mouse	*Clostridium*	3-Phenylpropionic acid		
mouse	*Clostridium*	Benzoic acid		
mouse	*Clostridium*	Hypoxanthine		
mouse	*Clostridium*	Butyrate	Prkaa2	Elevated
mouse	*Clostridium*	Butyrate	Prkaa1	Elevated
mouse	*Clostridium*	Indole	Gcg	Reduced
mouse	*Clostridium*	Deoxycholic acid	Il6	Elevated
mouse	*Clostridium*	Deoxycholic acid	Tnf	Elevated
mouse	*Clostridium*	Deoxycholic acid	Il1b	Elevated
mouse	*Clostridium*	Deoxycholic acid	Nos2	Elevated
mouse	*Clostridium*	Deoxycholic acid	Chrm2	Elevated
mouse	*Clostridium*	Deoxycholic acid	Tlr2	Elevated
mouse	*Clostridium*	3-Indolepropionic acid	Srebf1	Reduced
mouse	*Clostridium*	3-Indolepropionic acid	Fas	Reduced
mouse	*Clostridium*	3-Indolepropionic acid	Srebf2	Reduced
mouse	*Clostridium*	3-Indolepropionic acid	Hmgcr	Reduced
mouse	*Prevotella*	Myristic acid		
mouse	*Prevotella*	l-Isoleucine		
mouse	*Prevotella*	Benzoic acid		
mouse	*Prevotella*	Indole-3-acetic acid		
mouse	*Bifidobacterium*		Ido1	Elevated
mouse	*Bifidobacterium*	Acetate		
mouse	*Bifidobacterium*	Propionate		
mouse	*Bacteroides*	Indole	Gcg	Reduced
mouse	*Bacteroides*	Deoxycholic acid	Nr1h4	Elevated
mouse	*Bacteroides*	Deoxycholic acid	Fgf15	Elevated
mouse	*Bacteroides*	Deoxycholic acid	Fgfr4	Elevated
mouse	*Bacteroides*	Deoxycholic acid	Cyp7a1	Reduced
mouse	*Bacteroides*	Deoxycholic acid	Sirpa	Reduced
mouse	*Bacteroides*	Deoxycholic acid	Cpt1b	Reduced
mouse	*Bacteroides*	Deoxycholic acid	Fas	Elevated
mouse	*Ruminococcus*	Creatine		
mouse	*Ruminococcus*	5-Hydroxyindole-3-acetic acid		
mouse	*Ruminococcus*	Tyramine		
mouse	*Ruminococcus*	Valine		
mouse	*Ruminococcus*	l-Isoleucine		
mouse	*Ruminococcus*	Chenodeoxycholic acid		

mouse	*Ruminococcus*	Ursodeoxycholic acid
mouse	*Ruminococcus*	2-Hydroxy-2-methylbutanenitrile
mouse	*Ruminococcus*	N-Acetylputrescine
mouse	*Ruminococcus*	Proline
mouse	*Ruminococcus*	Betonicine
mouse	*Ruminococcus*	Cholic acid
mouse	*Ruminococcus*	Deoxycholic acid
mouse	*Ruminococcus*	N-Acetyl-D-Mannosamine
mouse	*Ruminococcus*	2-Formaminobenzoylacetate
mouse	*Ruminococcus*	12-Ketolithocholic acid
mouse	*Ruminococcus*	Hyocholate

Table 49 Target genes network-score through STRING sever

S. No.	Target	Score	S. No.	Target	Score
1.	FGF15	0.999	11.	IL18	0.957
2.	FGFR4	0.999	12.	TLR2	0.952
3.	TNF	0.996	13.	HMGCR	0.947
4.	FAS	0.996	14.	NR1H4	0.945
5.	IL1b	0.989	15.	CYP7A1	0.945
6.	NOS2	0.984	16.	SREBF2	0.928
7.	ARG1	0.984	17.	SREBF1	0.924
8.	IL6	0.983	18.	IDO1	0.803
9.	PRKAA1	0.982	19.	TJP1	0.741
10.	PRKAA2	0.982	20.	GCG	0.73

5.13.1Identification of 8 core targets from metabolitesand diabetes related targets

The SEA and STP databases for *Homosapiens* were also analyzed to look for the targets of the 27 metabolites identified above. Figure 75A shows that we were able to identify 805 targets from SEA and 654 targets from STP across all metabolites, with 266 of these targets serving as overlaps between the two databases. Between the GeneCards and DisgeNET databases for diabetic targets, a total of 2352 overlapping targets were found (Fig. 75B). Using a confidence threshold of 0.7 and narrowing the search to human beings, 132 overlapping targets were found between all metabolites and diabetes-related targets (Table 50) fromthe string web server (Fig. 75C). Eight core targets were selected (scores above 0.995) for the study in the further step.

Table 50 Overlapping target genes of human genome within direct network and their score through STRING sever

S. No.	Target	Score	S. No.	Target	Score
1.	CTSG	0.999	6.	MMP2	0.997
2.	PARP1	0.999	7.	SHBG	0.996
3.	MPO	0.999	8.	ALB	0.996
4.	CASP3	0.999	9.	EDNRA	0.994
5.	MMP14	0.997	10.	TTR	0.994

5.13.2. Protein-protein interaction network analysis

The protein-protein interaction **(**PPI) network consists of 8 nodes, 7 edges, and an 8.59e-06 enrichment p-value (Figure 75D) in the 8 core targets through the string web server. Based on the network map, CASP3, MPO, PARP1, and CTSG, the key targets, were defined as the highest target scores, followed by MMP14, MMP2, SHBG, and ALB. Further, these core targets were employed to verify the significant role of diabetes in molecular docking analysis.

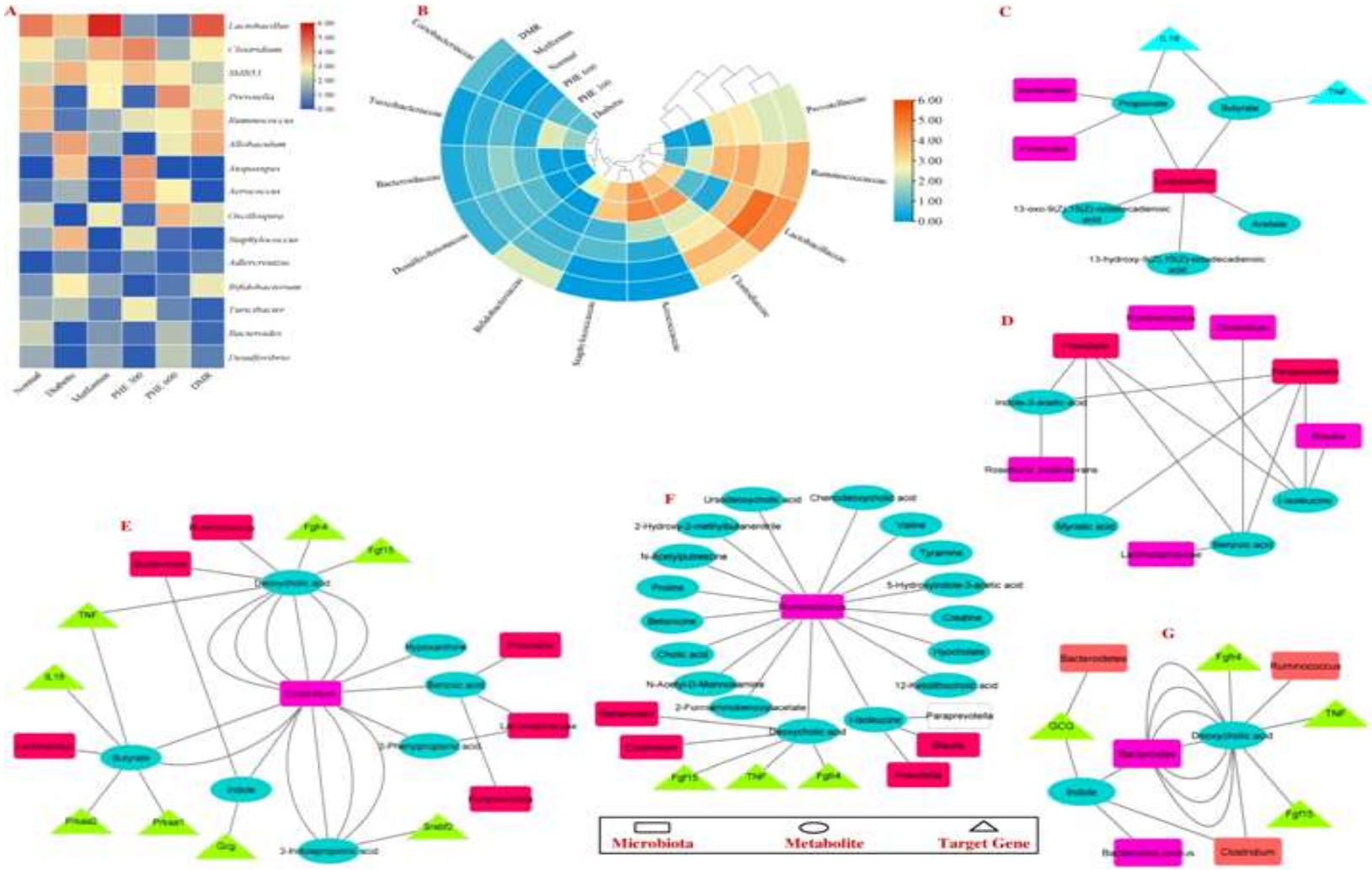

Figure 74 Heat maps of gut microbiota structures. A) Heat map of gut microbiota structures of all group rats at genus level, B) Cluster auto polar heat map of gut microbiota-family with enrichment of Prevotellaceae and Ruminococcaceae in the treatment groups. Gut microbiota-metabolite-target network. C) Lactobacillus, D) Prevotella, E) Clostridium, F) Ruminococcus, and G) Bacteroides

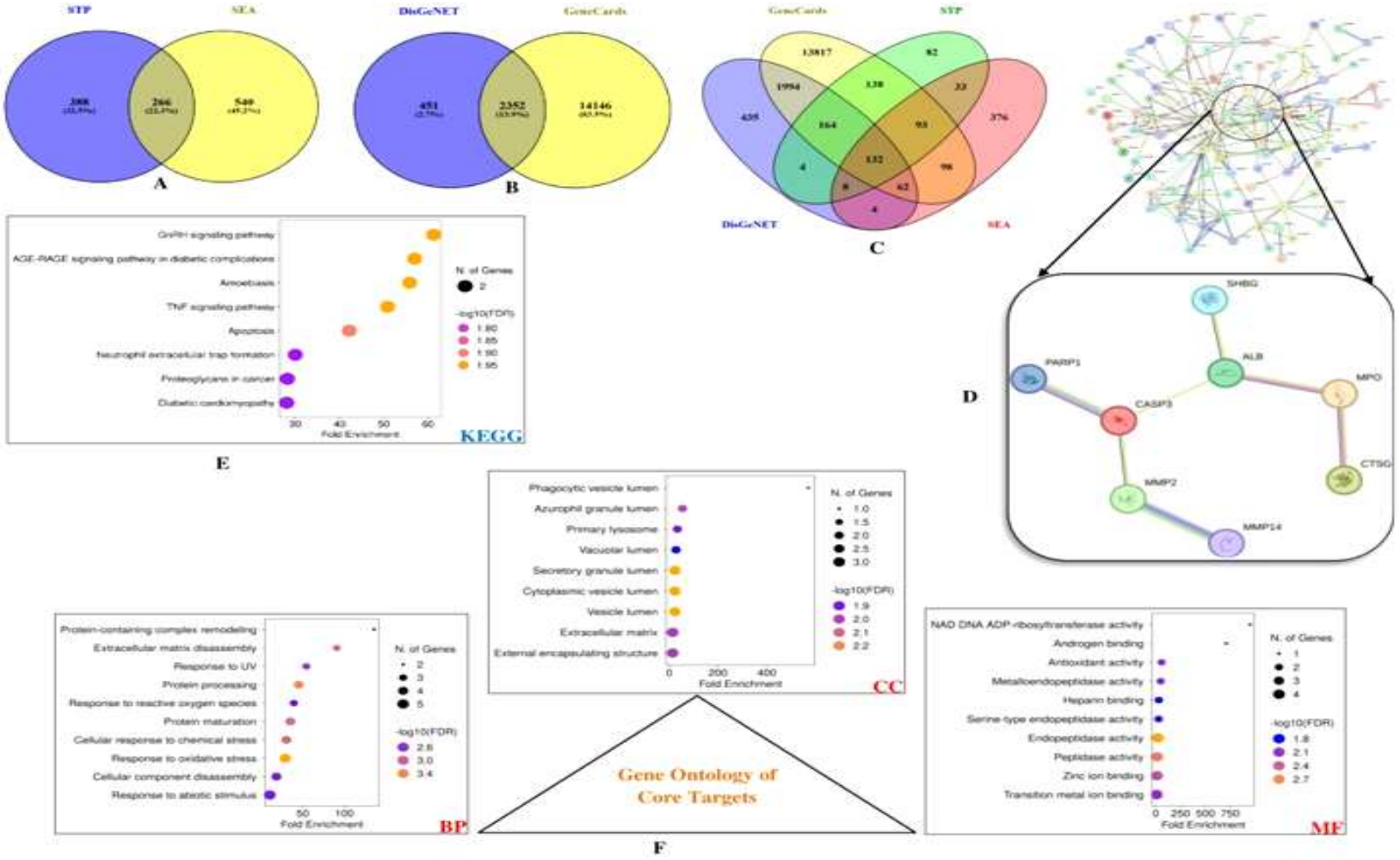

Figure 75 Venny overlapping images, PPI network, KEGG and gene ontology study of key targets in the present study. A) Identification of 266 key targets of all metabolites, B) 2352 Common targets of DM related genes, C) 132 key targets of metabolites and DM related genes, D) PPI network of 8 core target genes through String web server, E) Identification of enrichment of KEGG pathways through ShinyGo database, and F) Dotplot for 3 Functional component of core targets in gene ontology study

5.13.3Identification of the 3 Kyoto encyclopedia of genes and genomes pathway enrichments and gene ontology enrichment analysis of the 3 components

KEGG pathways and GO enrichment were used to look at eight main targets to learn more about how gut metabolites work in the treatment of diabetes. There was an emphasis on signaling pathways in the KEGG pathway enrichment study. Figure 75E shows the three most enriched signaling pathways from the KEGG database. The 56.99-fold enrichment value of the AGE-RAGE signaling pathway in complications of diabetes suggests that it may act as a strong inhibitory pathway for DM (Fig. 76). As shown in Figure 75F, there were three parts to the GO enrichment analysis: MF, BP, and CC, involved in explaining pharmacological activity in the treatment of DM.

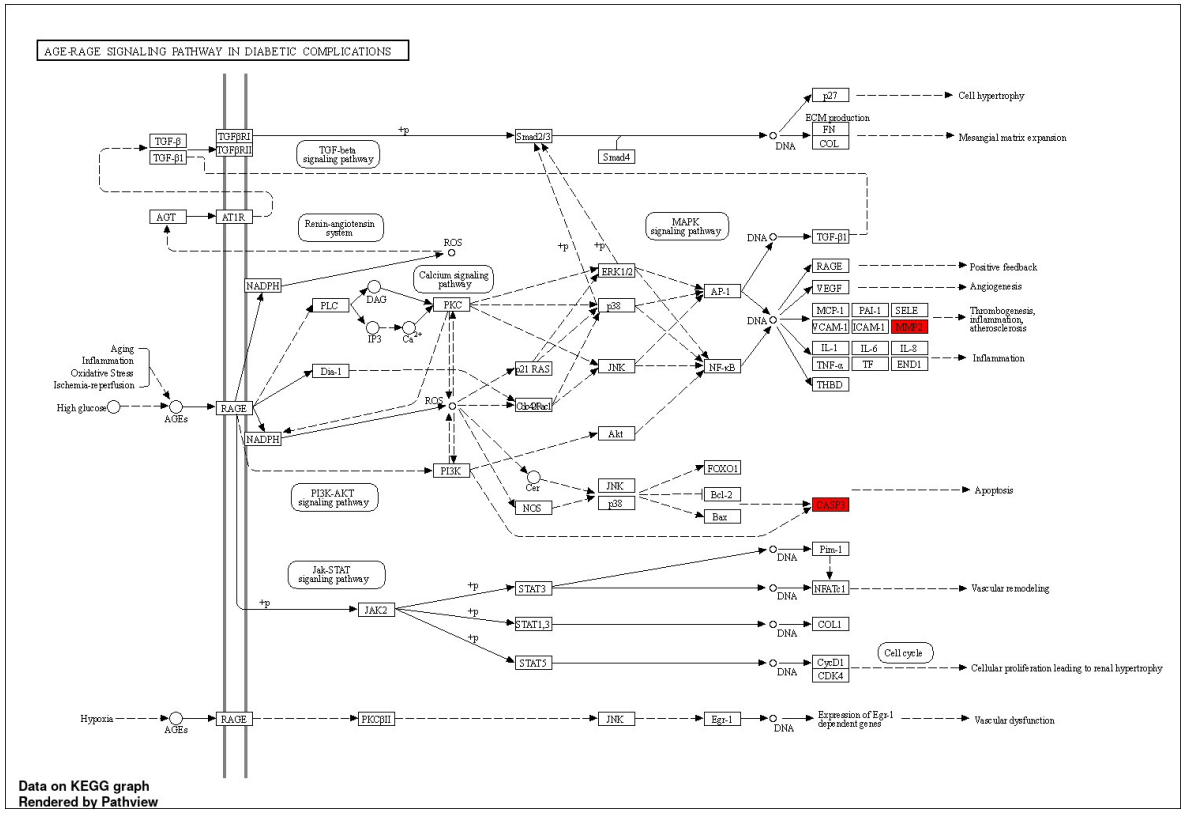

Figure 76 Enrichment of the core genes in KEGG AGE-RAGE signaling pathway in diabetic complications

5.13.4Molecular docking test

A total of 9 metabolites out of 27 of the above 6 genus of gut microbiome were enriched in the gut of both species (mouse and humans) by the gutMgene database. These nine metabolites (acetate, butyrate, propionate, l-isoleucine, proline, creatine, ursodeoxycholic acid, 3-phenyl propionic acid, and 3-indole propionic acid) were found to work well in the gut, and their enrichment might be the best way to treat diabetes. Moreover, the 9 metabolites and 3 key targets (MMP2, CASP3, and MMP14) linked to both the signaling pathways explained earlier (AGE-RAGE in diabetic complications and TNF) were identified via KEGG fold enrichment. Table 51 shows the results of a molecular docking test (MDT), which was used to confirm the molecular binding affinities of all complexes. The stability of the complex involving the ligand and protein increases with an increasing negative docking score. Ursodeoxycholic acid (UDCA), one of the nine metabolites found in the gut, has a stable molecular structure with eight targets in the human genome and four targets in the rat genome. The stable complexes were MMP2-UDCA (− 10.06 kcal/mol; Fig. 77A), CASP3-UDCA (− 8.69 kcal/mol; Fig. 77B), and MMP14-UDCA (− 8.68 kcal/mol; Fig. 77C), for the human genome (Table 51), which showed close interactions of these genes as provided by string web server network analysis. The stable complexes for the rat genome were also observed for FGFR4 (− 10.44 kcal/mol), FGF15 (− 9.62 kcal/mol), and TNF (− 7.31 kcal/mol) with UDCA.

Table 51 Binding affinity score of metabolites for the core target genes

S.No.	Core genes (Human & Rats)	PDB ID	Gut metabolites molecular docking score (with negative value in kcal/mol)								
			Acetate	Butyrate	Propionate	l-Isoleucine	Proline	Creatine	Ursodeoxycholic acid (UDCA)	3-phenyl propionic acid (PPA)	3-indole propionic acid (IPA)
1.	CTSG	1kyn	4.48	4.85	4.66	4.95	4.37	4.07	9.17	6.70	7.95
2.	SHBG	1lhv	3.95	3.92	3.77	4.68	4.86	5.21	8.95	5.73	6.54
3.	MMP2	3ayu	4.78	5.01	4.88	4.80	5.06	5.93	10.06	6.93	7.77
4.	MPO	4ejx	4.89	4.78	4.81	5.10	4.90	4.35	10.09	5.24	6.51
5.	CASP3	4jqz	4.80	5.13	5.02	4.82	4.90	4.87	8.69	5.66	6.40
6.	MMP14	4qxu	3.57	4.14	3.75	4.22	4.46	4.34	8.68	5.71	6.67
7.	PARP1	5ha9	3.66	4.27	4.03	5.78	4.95	4.94	8.30	5.65	6.42
8.	ALB	6m4r	4.23	4.60	4.31	4.47	4.99	4.82	9.32	6.14	7.76
9.	TNF	1u5z	4.36	4.14	4.16	4.89	4.81	4.82	7.31	5.98	6.65
10.	FGF15	2p23	4.21	5.07	4.49	4.63	4.53	4.80	9.62	5.45	5.77
11.	FGFR4	4xcu	4.68	5.14	4.88	5.02	5.07	5.19	10.44	6.74	7.58
12.	FAS	6rop	3.96	4.67	4.36	4.45	5.23	5.09	8.42	5.31	5.91

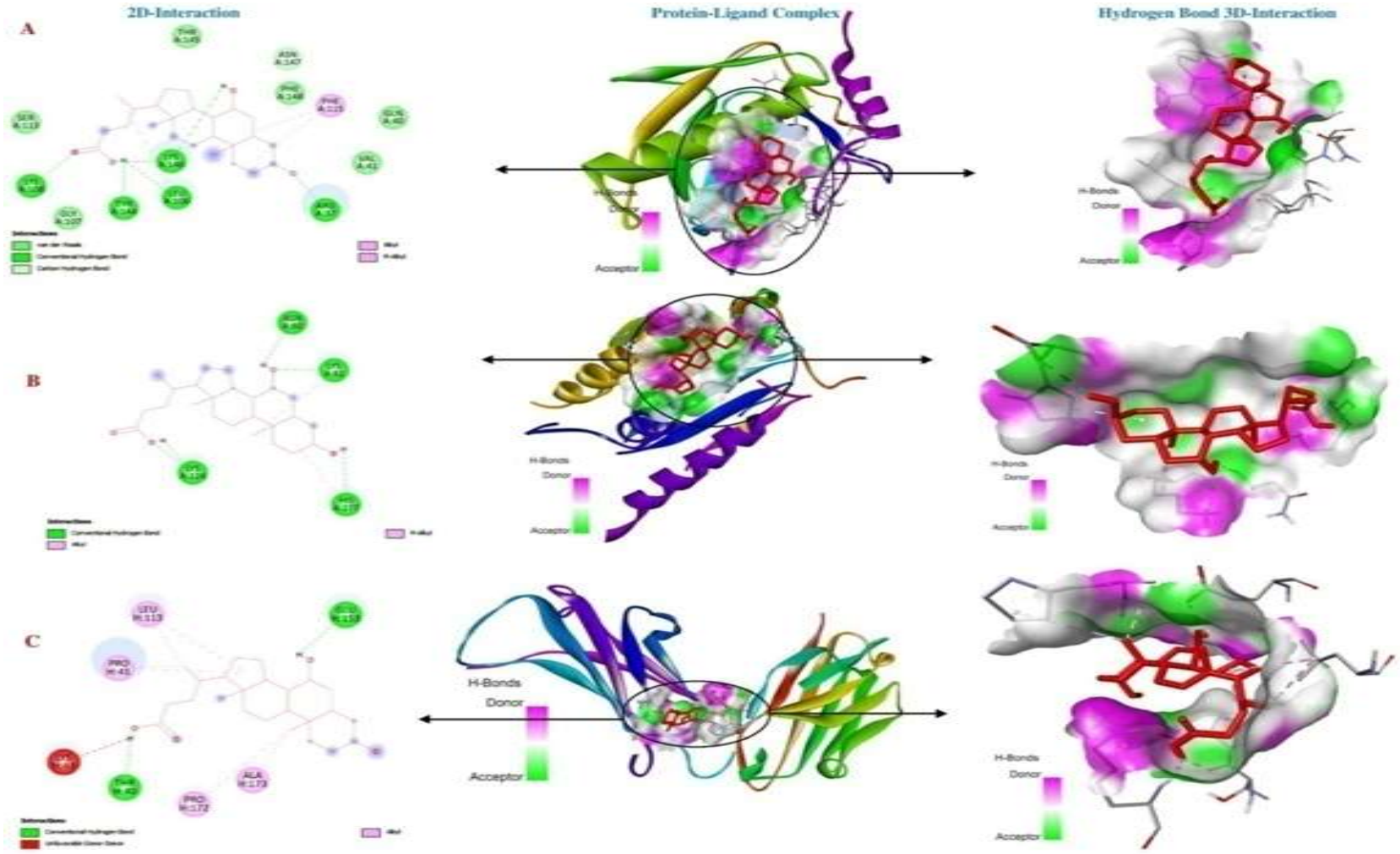

Figure 77 The molecular docking test on core targets of AGE-RAGE signaling pathway in diabetic complications and TNF signaling pathways with metabolites of gut microbiota. A) Ursodeoxycholicacid-MMP2 (PDB ID: 3AYU), B) Ursodeoxycholic acid-CASP3 (PDB ID: 4JQZ) and C) Ursodeoxycholic acid-MMP14 (PDB ID: 4QXU).